STEPS TOWARDS THE IMPLEMENTATION OF ERT FOR MONITORING OF TRANSIENT HYDROLOGICAL PROCESSES

By

Alexander Furman

A Dissertation submitted to the Faculty of the

DEPARTMENT OF HYDROLOGY AND WATER RESOURCES

In Partial Fulfillment of the Requirements
For the Degree of

DOCTOR OF PHILOSOPHY
WITH A MAJOR IN HYDROLOGY

In the Graduate College

THE UNIVERSITY OF ARIZONA

2003

THE UNIVERSITY OF ARIZONA ®
GRADUATE COLLEGE

As members of the Final Examination Committee, we certify that we have read the dissertation prepared by Alexander Furman entitled "Steps Towards the Implementation of ERT for Monitoring of Transient Hydrological Processes" and recommend that it be accepted as fulfilling the dissertation requirement for the degree of Doctor of Philosophy

Paul "Ty" A. Ferré	10-22-03 Date
Arthur W. Warrick	10-22-03 Date
Shlomo P. Neuman	10/22/03 Date
Mary M. Poulton	10/22/03 Date
Peter J. Wierenga	10/22/03 Date

Final approval and acceptance of this dissertation is contingent upon the candidate's submission of the final copy of the dissertation to the Graduate College.

I herby certify that I have read this dissertation prepared under my direction and recommend that it be accepted as fulfilling the dissertation requirement.

Dissertation director: Paul "Ty" A. Ferré	10-22-03 Date

STATEMENT BY THE AUTHOR

This dissertation has been submitted in partial fulfillment of requirements for an advanced degree at The University of Arizona and is deposited in the University Library to be made available to borrowers under rules of the Library.

Brief quotations from this dissertation are allowable without special permission, provided that accurate acknowledgment of source is made. Requests for permission for extended quotation from or reproduction of this manuscript in whole or in part may be granted by the head of the major department or the Dean of the Graduate College when in his or her judgment the proposed use of the material is in the interests of scholarship. In all other instances, however, permission must be obtained from the author.

SIGNED: 

ACKNOWLEDGMENTS

The work presented here could not have been completed without the help of many, and I apologize to all those that are not personally mentioned here.

First, I thank my advisors, Art Warrick and Ty Ferré. This paragraph is short of describing how each in his own way contributed to my studies. Perhaps the main thing is that both Art and Ty allowed me to feel as a part of a team, and I think a good one.

I also thank my other committee members, Mary Poulton, Peter Wierenga, and Shlomo Neuman, for providing continuous support. I specially thank Shlomo for the great opportunity to work together on a unique contribution to the analytic element method, resulting in one of the papers presented here, and for his patience during this research.

I would like also to thanks the USDA-NRI competitive grants program, and SAHRA (Sustainability of Semi-Arid Hydrology and Riparian Areas), for the generous financial support during my studies.

Finally, I would like to thank my supporting family, Tamar and Iddo (and of course, Danna), which each in his own way made this period a great experience and a time of joy.

TABLE OF CONTENTS

TABLE OF CONTENTS (Continued)

LIST OF ILLUSTRATIONS

LIST OF ILLUSTRATIONS (Continued)

LIST OF ILLUSTRATIONS (Continued)

LIST OF TABLES

ABSTRACT

The adaptation of the electrical resistivity tomography (ERT) for monitoring of subsurface hydrological processes is the focus of this research. Specifically, the increase in the method's accuracy, expressed by its spatial and temporal resolution, is sought.

A spatial sensitivity analysis of the ERT method is presented. This sensitivity analysis is conducted by a perturbation approach, and is making extensive use of the analytic element method (AEM) to compute potentials in the subsurface. Presented are sensitivity maps for individual typical and atypical arrays. Also presented are sensitivity maps for surveys comprised of a single array type and for mixed surveys, and guidelines for array selection for the detection of a localized target. Results indicate superiority of wide arrays over small arrays, and the relatively poor performance of the double dipole array type.

Several optimality criteria are discussed for the selection of an optimal survey, including optimality of individual arrays to individual subsurface targets (locally optimal), and global optimality, achieved through the use of genetic algorithms. In both cases results show superiority of mixed surveys.

The method presented here, for optimal ERT configuration, opens the way for implementation of the method for a wide variety of hydrological applications.

In addition to the main focus of this dissertation, a complementary work was completed to extend the AEM to compute transient processes. This unique solution uses the Laplace transform to bring the flow equation to a linear, time independent form. The resultant

modified Helmholtz equation is then solved using the AEM, and the result is numerically transformed to the time domain.

INTRODUCTION

General

Accurate monitoring of subsurface properties, conditions, and processes, and in particular those that place in the vadoze zone, is crucial for a wide variety of applications. Examples may range from the estimation of recharge as the basis for sustainable development (e.g. *Harrington et al.*, 2002; *Cook and Robinson*, 2002), to monitoring of remediation processes (*Lowe at al.*, 2002), to monitoring biological activity (e.g. *Suarez and Rifai*, 2002). Monitoring in the subsurface is a challenging task for both technical and economical reasons. The construction of monitoring wells, the most standard technique in subsurface hydrology, is feasible, especially for shallow saturated regions of the subsurface, yet relatively expensive. In the unsaturated zone, suction lysimeters can allow for limited water monitoring.

Very few properties of the subsurface can be measured directly. In most cases, another property is measured and an association is made to the desired property. An example is the measurement for the weight and bulk density of a soil sample, and the calculation of volumetric water content based on these measurements. In other cases, the response of the subsurface to a stress is monitored, and a mathematical association to subsurface properties is constructed, with pumping tests being the most common example of this approach.

The available instrumentation for monitoring hydrological processes in the vadoze zone has seen quite extensive development in the last few decades. Instruments are capable of

through association with other properties (e.g. time domain reflectometry, TDR, measurements of dielectric permittivity). However, most of these instruments are only capable of measuring soil properties at the scale of a few 100's to a few 1000's of cubic cm.

At the other extreme, remote sensing techniques, and especially airborne and space-borne methods, are capable of monitoring water content (and other properties) at varying scales, starting at meters to 100 km. However, these techniques typically provide surface information only and are not capable of providing detailed information regarding the relatively shallow subsurface (*Huisman et al.*, 2002).

There is clearly a need for a monitoring technique that will allow for the measurement of water content, or a related physical property, at an intermediate to large scale, with depth penetration. Ideally the monitoring method will also be inexpensive, non-destructive and non-invasive, and will allow short measurement times.

Recent technological advancement allows the accommodation of techniques that were associated with large scale geological exploration. New instrumentation is being developed and accommodated routinely for hydrological and environmental purposes. Among the techniques that were accommodated from the field of geosciences are seismic surveys (e.g. *Perker* et al., 1993); magnetic anomalies (e.g. *Babu*, 1991); electromagnetic explorations (e.g. *Buselli and Lu*, 2001); gravity methods (e.g. *Pool and Eychaner*, 1995; *Rodell and Famiglietti*, 2002), and various electromagnetic methods.

The subject of this dissertation is an examination of low frequency (or direct current) electrical resistivity methods including resistivity sounding, induced polarization, and electrical resistivity tomography. Detailed descriptions of the different methods are given by *Telford et al.*, 1990. The use of direct current, the non-destructive and non-invasive nature of the method, and the advancement of sensors to detect relatively low currents and potential differences make ERT attractive for use in field conditions. The availability of commercial hardware and software have allowed expansion of the use of the method in recent years (e.g. *Michot et al.*, 2003; *Glass et al.*, 2002)

The fundamentals of the ERT method are described in the first paper of this dissertation and a more complete description of the method can be found in *Telford et al.* (1990). A detailed description of the application of ERT to hydrological monitoring is provided later in this introductory section. In general, in the ERT method current is applied to the soil through two electrodes and the potential is measured between two other electrodes. The electrodes may be placed at different locations to tailor the spatial sensitivity of the measurement. Making measurements with many different electrode combinations (typically 10's to 1000's) creates a large data-set. Then, inversion methods (e.g. Occam's, *LeBrecque et al.*, 1996) can be used to generate a detailed resistivity map of the subsurface.

For hydrological purposes, this resistivity map can be manipulated further and the components of the bulk electrical resistivity can be inferred through relationships such as that developed by *Archie's* (1942). Specifically, the effects of spatial variations in

volumetric water content pore water salinity, and electrical conductivity of the soil solids can be determined from the bulk electrical conductivity. This separation can be challenging, but it is not the subject of this research. Rather, we assume that such a separation can be achieved and will be improved if estimates of the bulk electrical conductivity distribution are improved.

Although ERT is being used widely, a few major problems still need to be addressed for its optimal application. These include the relatively low accuracy of the method, and low spatial and temporal resolution. Some of these problems result from the non-uniqueness associated with inversion. Some improvement may be achieved by the advancement of measurement equipment, allowing, for example, the measurement of potential at more than one location for a single location of current application (e.g. AGI, 2002). Improved equipment may also reduce measurement time. However, the reduction here may be limited by the charge time associated with the soil and the electrodes (see *Dahlin*, 2000).

Our primary goal in this research is to accommodate ERT for measurement of subsurface hydrological conditions (i.e. water content) with higher accuracy and with improved spatial and temporal resolution. This will ultimately allow tracking of the transient processes of infiltration and recharge.

Research hypothesis

The general hypothesis of this research is that the quality of the resistivity image obtained by an ERT system can be improved by optimal selection of the arrays composing an ERT survey. That is, the measured quantities can be improved with little or no prior knowledge of the subsurface structure. An improved resistivity image leads to an increased uniqueness of the inverted image, and therefore increased confidence in the results. This may later lead to increased spatial resolution, and improved temporal resolution, primarily by allowing fewer measurements, thereby allowing for repeated acquisition of images in short times.

ERT for hydrological monitoring

The application of ERT to hydrological monitoring is comprised of three major components: measurement, inversion, and conversion. Figure 1 describes the relations among the three components.

Measurement stage

The first component is measurement. Current, I, is applied to the subsurface through two current electrodes, C_1 and C_2. The difference in potentials between two other potential electrodes, P_1 and P_2, ΔV, is measured. The measured potential is recorded as apparent resistivity, ρ_a, calculated as

$$[1] \qquad \rho_a = \frac{G\Delta V}{I}$$

where G is a geometric factor, $G = f(C_1, C_2, P_1, P_2)$. For a homogeneous subsurface, the apparent resistivity and the actual resistivity are the same. For a heterogeneous subsurface, the geometric factor may be viewed as a weighting factor. The apparent resistivity measured is then a function of the resistivity distribution and of the electrode array configuration

$$[2] \qquad \rho_a = f(\rho(x, y, z), I, C_1, C_2, P_1, P_2)$$

An ERT survey is comprised of a few 10's to a few 1000's of measurements, which differ in the location of one or more of the electrodes. That is, the above process is repeated many times for each survey.

The result of the measurement stage of the hydrological implementation of ERT is an array of apparent resistivities, each a result of measurement using a unique electrode array. This apparent resistivities array is passed to the inversion module, including the generation data (i.e. electrode locations and applied current).

Inversion stage

The next stage is inversion. The apparent resistivities are used to calculate a model resistivity structure of the subsurface, ρ^M. Many inversion schemes exist for ERT applications (e.g. *Loke and Barker*, 1996; *LeBrecque et al.*, 1996), but all operate on similar principals. The inversion module includes a foreword simulation tool that allows

it to simulate the flow of current in a model resistivity structure. Using this foreword model and the apparent resistivities measured in field, including the electrode locations and the applied currents, an array of model apparent resistivities, ρ_a^M is calculated. The next step is to adjust the model resistivity, ρ^M, so that the differences between the measured and the model apparent resistivities will be minimized

$$[3] \qquad Z = MIN\left(\overline{\rho_a} - \overline{\rho_a^M}\right)$$

where Z is an objective function. The result of the inversion stage is then a model-based detailed description of the subsurface electrical resistivity, ρ^M, that is primarily a function of the measured apparent resistivities and their associated electrode array configurations

$$[4] \qquad \rho^M = f\left(\overline{\rho_a}, \overline{I}, \overline{C_1}, \overline{C_2}, \overline{P_1}, \overline{P_2}\right)$$

where the overbar indicates an array, the length of which is equal to the number of ERT arrays in a survey.

Conversion stage

The final stage for hydrological implementation of ERT is the conversion of electrical resistivity values to hydrological properties. This is typically done using the empirical relationships developed by *Archie* (1942) or similar empirical relations (e.g. *Glover et al.*, 2000). These relationships correlate the bulk electrical resistivity of a medium with the

porosity, ϕ, the degree of saturation, S, the electrical resistivity of the pore water, ρ_w, and empirical fitting parameters a, m, and n :

$$[5] \qquad \rho = a\phi^{-m}S^{-n}\rho_w .$$

The bulk electrical resistivity depends on three major components – the electrical conductivity of the soil solids, the water content, and the concentration of electrolytic solutes. In addition, the porosity affects the bulk electrical conductivity, but relatively small errors are associated with this effect. In non-clay soils, surface electrical conductivity is also minimal. The other two components are harder to obtain. In many applications one of the two can be found externally, by prior knowledge of hydrological conditions (e.g. when monitoring in aquifers), providing the ability to convert electrical resistivity directly to the other property (e.g. solute concentration). In other cases, one of the two (water content and solute concentration) can be assumed constant through time, and changes in the other can be calculated. For example, when monitoring infiltration, the solute concentration in the water can be assumed stable in time, hence the only parameter that changes between two concessive measurements will be the water content. It is important to note that in this case only changes in the property can be monitored, not the actual value.

In all other cases, the separation between water and solute contents is more difficult, and external supporting measurements are needed. The water content can be obtained as a function of the electrical resistivity, and the parameters of Archie's law

[6] $$\theta = f\left(\rho^M, \phi, a, m, n, \rho_w\right)$$

for the case that all parameters, including solute concentration, are known, and as

[7] $$\Delta\theta = f\left(\Delta\rho^M, \phi, a, m, n\right)$$

for other cases.

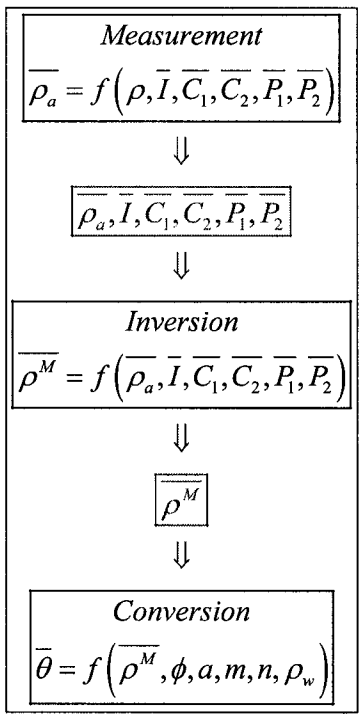

Figure 1: Schematic description of stages involved in the application of ERT for hydrological purposes

Research perspective

As described above, the implementation of ERT for hydrological purposes is made of three major stages: measurement stage, inversion stage, and conversion stage. The first two stages (measurement and inversion) are common to hydrological and non hydrological purposes, with a unique property of the first in hydrological implementation (i.e. that it may be time constrained). The third block (conversion) is also used widely in other fields, such as petroleum exploration, but it is of particular interest in hydrological implementation.

The aim of this research is to improve the applicability of ERT for hydrological implementation through the improvement of the first block, namely the measurement stage. That is, to improve the data collection through the wise location of the electrodes for each electrode array, and by selecting the electrode arrays that will maximize the quality of the data gathered in each survey. This will be achieved both in general and specifically for time-constrained surveys. This optimization is performed before the survey is conducted, and therefore cannot use information obtained through the inversion process, such as the partial derivative matrix that is the heart of most inversion routines. Measurement optimization is achieved primarily through a sensitivity analysis of the measured signal (potential) to the subsurface structure. In mathematical terms, this is a perturbation analysis, but unlike previous sensitivity perturbation analyses (e.g. *Knight*, 1992; *Kluitenberg and Knight*, 2003), it is performed here numerically. A short explanation of the numerical perturbation analysis is given below.

The most important point is that the survey optimization and the sensitivity analysis are initially performed with minimal knowledge of the actual electrical resistivity structure of the subsurface. Therefore, we concentrate on conducting sensitivity analyses for a homogeneous background. However, the availability of external information (e.g. layered structure, results from previous

ERT survey) can, and should, be used to conduct the background simulation. This is a future addition to this line of research.

It is important to note that further improvement to the measured quantities can be made through technical improvement of the instrumentation and that further improvement to the overall result (i.e. of monitoring of hydrological properties) may be reached through improvement of inversion and conversion algorithms. This research is focused in the measurement stage, and throughout this research we do not make any changes to the other parts of the process, inversion and conversion. The underlying assumption is that the improvement to the measurement stage is translated, though not linearly, through the inversion and conversion stages to the final result. However, we do suggest that improvement to inversion algorithms may be obtained by weighting the inputs to the algorithm (i.e. apparent resistivities) according to the data worth they represent, as obtained from our sensitivity analysis.

Numerical perturbation analysis

Consider the DC potentials in the subsurface due to a sink and source couple located at the surface. The potentials throughout the subsurface, and particularly at the surface itself, are described by the solution to Laplace's equation

$$[8] \qquad \frac{\partial}{\partial x}\left(K\frac{\partial V}{\partial x}\right)+\frac{\partial}{\partial y}\left(K\frac{\partial V}{\partial y}\right)=0$$

with appropriate boundary conditions to represent the surface. K is the electrical conductivity, V is the electrical potential, and x and y are spatial directions.

The electrical conductivity may be viewed as a perturbed sum

$$[9] \qquad K = K_0(x,y) + K_1(x,y)$$

with subscripts 0 and 1 indicating background and perturbed conductivities, respectively. The potential distribution can be viewed as a perturbed sum

$$[10] \qquad V = V_0(x,y) + V_1(x,y)$$

where V_0 is the potential due to the background conductivity, K_0, and V_1 is the potential due to the perturbed domain.

Taking the first order spatial numerical derivative of the potential with respect to the perturbed electrical conductivity result in

$$[11] \qquad \left.\frac{\partial V}{\partial K_1(x_0,y_0)}\right|_{(x_0,y_0)} \approx \left.\frac{V - V_0}{\Delta K}\right|_{(x_0,y_0)} = \left.\frac{V_1}{\Delta K}\right|_{(x_0,y_0)}$$

Note that the equality in equation [11] is valid in general, but due to the boundary-less nature of the computational method used (i.e. analytic element method), it is also valid from the computational point of view. The interaction between the perturbation and the background domain is captured through the coefficients of the perturbation solution (see paper 1). It is also important to note that quantities indicated by index 0 are not necessarily due to homogeneous subsurface, although we demonstrate our solution as such (i.e. homogeneous).

All four papers are presented as submitted, or as published. Stylistic changes were made to bring all papers to a single format. In papers that were already published, only typographical errors were corrected. For continuity reasons, all figures and tables were renumbered to include the paper's number.

A reference list is included at the end of each paper. A complete reference list (including references to the introductory part) is given at the end of this dissertation.

PRESENT STUDY

Dissertation structure

The dissertation presented here is composed of three original papers submitted or accepted for publication in *Vadose Zone Journal*, and in addition, a fourth original paper accepted for publication in *Advances in Water Resources*. The first three papers include the material directly related to the dissertation title, and the fourth paper presents an improvement to one of the mathematical modeling techniques used.

The papers included are (status at time of the dissertation defense):

1. A. Furman, A.W. Warrick, T.P.A. Ferré, 2002. Electrical Potential Distributions in Response to Applied Current in a Heterogeneous Subsurface: Solution for Circular Inclusions, *Vadose Zone Journal*, 1: 273-280. (Published).
2. A. Furman, T.P.A. Ferré, A.W. Warrick, 2003. A Sensitivity Analysis of Electrical-Resistance-Tomography Array Types Using Analytical Element Modeling, *Vadose Zone Journal*, 2: 416-423. (Published).
3. A. Furman, T.P.A. Ferré, A.W. Warrick, 2003. Optimization of ERT surveys for monitoring transient hydrological events using perturbation sensitivity and genetic algorithms, *Vadose Zone Journal*. (In review).
4. A. Furman, S.P. Neuman, 2003. Laplace-Transform Analytic Element Solution of Transient Flow in Porous Media, *Advances in Water Resources*. (In press).

Summary of papers

Accepting the above hypothesis, we assume that the method for evaluating the quality of the individual measurements (i.e. arrays) is the sensitivity of an array to the subsurface electrical conductivity. We therefore define the sensitivity of an array as its response to a change in the subsurface conductivity. Specifically, the sensitivity will be defined as the response to a small change of the electrical conductivity (by one conductivity unit) in a finite subsurface volume. This finite volume is referred through the text as perturbation, or inhomogeneity. Furthermore, we will assume that the direction of the sensitivity (i.e. increased or decreased potential) does not matter, but only its magnitude. A formal definition of array sensitivity is given in paper 1. At this point we conduct the sensitivity analysis over a homogeneous domain.

A mathematical method is desired for the computation of the above definition of sensitivity, for very large numbers of arrays and locations of the perturbation. The analytical element method provides such a method. The mathematical details of this method, with specific application for a circular inhomogeneity are given in paper 1, including some simple results for the flow through a conductivity perturbation. Finally, included in paper 1 are guidelines for the selection of the ERT arrays that are most sensitive to a single location (target) in the subsurface.

Paper 2 starts by presenting the spatial sensitivity of a few typical and atypical arrays. This is performed by numerous solutions of the electrical flow problem, with the location of our conductivity perturbation changing among solutions. By plotting the sensitivity at

the location of the perturbation we obtain a detailed sensitivity map for every type of array. We further define the sample volume as the volume in which most of the sensitivity of an array resides. While the sample volume has no physical meaning, it is a useful tool for array comparison.

Comparison of array types shows clear disadvantages of arrays of the double dipole type (see definitions of array and survey types in papers 1 and 2). Arrays of the partially overlapping type seem to have advantage over the Wenner and the Schlumberger types.

An ERT survey is typically composed of 10's to 1,000's of arrays. The sensitivity of a single array therefore has very little meaning. The contribution of each measurement to the inverted resistivity image depends to a large extent on the resistivity structure. In other words, since the inversion process (which is not discussed in this research) is a highly non-linear process, the relative weight of each array in the solution varies. As an initial approach, we evaluate the sensitivity of a whole survey by assuming that all arrays are weighted, on the average, the same. Using this assumption sensitivity maps are drawn and compared for some typical and a-typical mono-type (i.e. composed of a single type of arrays, e.g. Wenner) surveys. The sensitivity of a survey at each spatial location is defined simply as the summation of the sensitivities of all contributing arrays to that location. A comparison is also made to a survey that is composed of different types of arrays, each of which is most sensitive to a certain location in the subsurface.

Comparison of survey types (for a specific set of electrodes) gives similar conclusions as the comparison of array types. The double dipole array seems to be disadvantageous,

while the partially overlapping survey seems to carry advantages over the typical surveys of the Wenner and the Schlumberger types. A comparison to the locally optimal survey suggests that an optimal survey will be composed of more than one array type.

The idea that the optimal survey is not comprised of a single array type, and the understanding that under field conditions the time frame for measurement and the equipment may vary between different applications, lead to the search for a technique that will allow the identification of an optimal survey. That is, given equipment characteristics (e.g. number of electrodes, single measurement time), and monitored process characteristics (e.g. time scale, required investigation depth), this optimization technique will seek the set of arrays that will lead to an optimal acquisition of data.

Given the large number of arrays to choose from, and the even larger number of possible surveys, we choose to make use of genetic algorithms for this optimization process. In Paper 3 the basics of genetic algorithms are introduced. Details of specific gene and chromosome structures used are listed. Several definitions for survey optimality criteria are explored, and a comparison is made between traditional surveys and optimal surveys on the basis of the cumulative sensitivity maps.

Throughout the three papers extensive use is made of the analytic element method (AEM). Specifically, a solution for the Laplace equation in a semi-infinite generally homogeneous domain that includes a sink / source pair and a single perturbation is applied to determine the effects of an electrical conductivity perturbation. This solution is then repeated for many perturbation locations and many arrays. This is a classic

example of exploiting this numerical method to compute values at a limited number of locations (i.e. at the locations of the potential electrodes). This shows a distinct advantage over finite element methods that must solve for the potential at every point in the domain even though this information is not necessary for analysis. The analytical element method can be used for much more complex problems. However, it is currently limited to steady state problems (i.e. solutions to the Laplace equation, or the Helmholtz equation).

The fourth paper introduces an important extension to the AEM. Using the Laplace transform, the transient diffusion equation becomes the time independent modified Helmholtz equation. This equation can be solved in the Laplace domain by means of the AEM. The solution then can be inverted (numerically) back into the time domain. The fourth paper presents development of two elements for the modified Helmholtz equation, namely a well and a circular inhomogeneity. The paper describes the general methods for creation of new elements, and presents an example solution for an aquifer that contains a well and a conductivity / storage inhomogeneity. The solution accuracy is examined for a few cases in comparison to other known solutions and found to be very high.

FUTURE WORK

The work presented here provides a complete method for the application of optimized ERT for an electrically pseudo-homogeneous two-dimensional subsurface. Real life, however, is slightly more complex. We see the main need for further development in the directions of complex heterogeneity, addition of the third dimension, and the incorporation of the method presented in this research with hydrological modeling. In addition to theoretical development, there is a need to ground truth the method under laboratory and field conditions.

A simplified description for the way we see the use of our methodology in the framework of hydrological monitoring is shown in Figure 2. The electrical resistivity structure of the subsurface is used as a basis for hydrological modeling, which will result in both an estimation of the time frame allowed for the ERT survey, and the expected electrical conductivity structure of the subsurface at the end of the next time step. Using these parameters sensitivity maps can be calculated for the different possible ERT arrays, and the genetic algorithm (or direct solution if applicable) can be used to define the optimal survey. Once an optimal survey has been detected, a full ERT survey is conducted. Results from this survey are inverted, for both electrical resistivity and hydrological properties. The whole process can now be repeated for the next time step.

As discussed above, the main steps needed to complete for this application are the development of the ERT sensitivity code for three dimensional heterogeneous structure

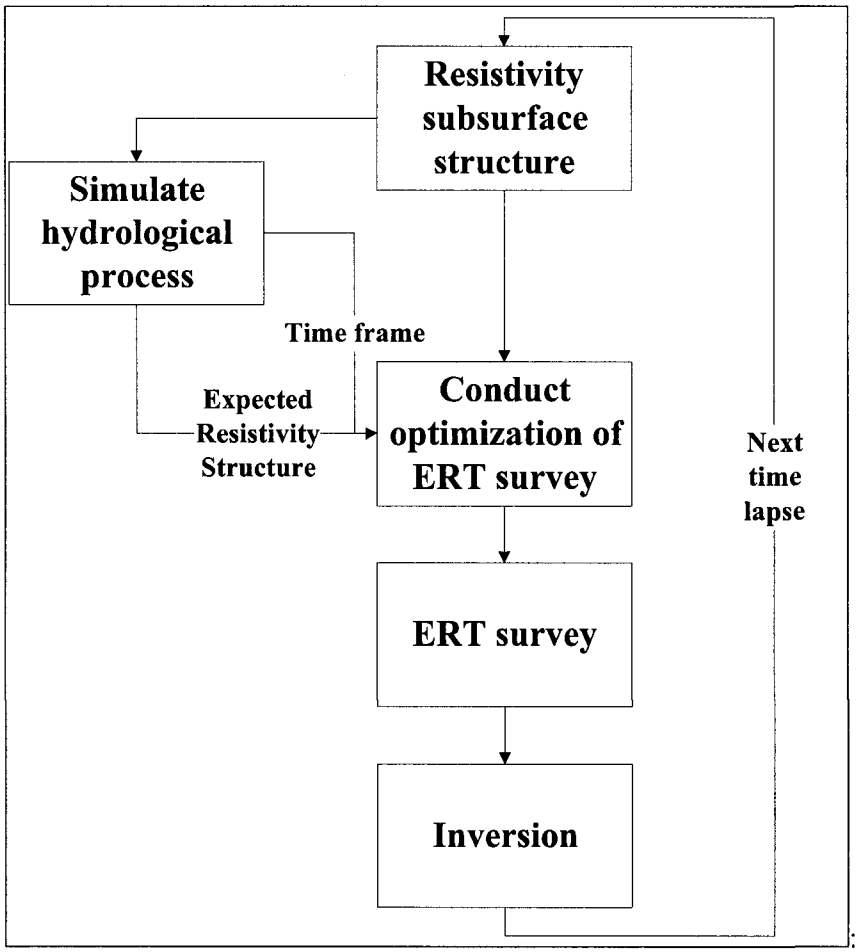

Figure 2: framework for coupled optimized ERT - hydrological modeling.

The frame of hydrological implementation is one option, but in general the algorithm presented above may be also used to improve measurement results, but re-optimization of electrode locations based on the increased understanding of the subsurface structure obtained from initial survey.

REFERENCES

Abramowitz, M., I.A. Stegun (editors), 1964. Handbook of mathematical functions, *National Bureau of Standards.*

AGI – Advanced Geophysics Inc., 2000. RES2DINV user manual, Austin, Texas.

Archie, G.E. 1942. The electric resistivity log as an aid in determining some reservoir characteristics. *Trans. Am. Inst. Min. Metall. Pet. Eng.*, 146: 54-62.

Babu, H.V.R, N.K. Rao, V.V. Kumar, 1991. Bedrock topography from magnetic anomalies – an aid to groundwater exploration in hard-rock terrains. *Geophysics*, 56(7): 1051–1054.

Baker, J. M. and R. J. Lascano, 1988. The spatial sensitivity of time domain reflectometry. *Soil Science*, 147(5):378-384.

Bakker, M., 2003. Transient analytic elements for periodic Dupuit-Forchheimer flow, submitted for publication in to *Advances in Water Resources*.

Bakker, M., A.I. Anderson, T.N. Olsthoorn, O.D.L. Strack, 1999. Regional groundwater modeling of the Yucca mountains site using analytic elements, *J. of Hydrology*, 226 (3-4): 167-178.

Bakker, M., V. Kelson, W.J. Zaadnoordijk, 2002. The TIM project, http://www.engr.uga.edu/~mbakker/tim.html, accessed Dec. 2002.

Bakker, M., O.D.L. Strack, 2003. Analytic elements for multi aquifer flow, *J. of Hydrology*, 271: 119-129.

Barker, R., J. Moore, 1998. The application of time-lapse electrical tomography in groundwater studies, *The Leading Edge*, pp. 1454-1458.

Barnes, R., Janković, I., 1999. Two-dimensional flow through large number of circular inhomogeneities, *J. of Hydrology*, 226:204-210.

Bateman, H., 1954. Tables of integral transforms, Volume 1, *McGraw-Hill.*

Binley, A., S. HenryPoulter, B. Shaw, 1996. Examination of solute transport in an undisturbed soil column using electrical resistivity tomography. *Water Resources Research*, 37(4):763-769.

Buselli, G., K. Lu, 2001. Groundwater contamination monitoring with multichannel electrical and electromagnetic methods, *Journal of Applied Geophysics*, 48: 11-23.

Carslaw, H.S., J.C. Jaeger, 1959. Conduction of heat in solids, second edition, *Clarendon Press, Oxford.*

Coley, D.A., 1999. An introduction to genetic algorithms for scientists and engineers, *World Scientific.*

Cook, P.G., Robinson, 2002. N.I. Estimating groundwater recharge in fractured rock from environmental super 3H and super 36Cl, Clare Valley, South Australia. *Water Resources Research*, 38(8), doi:10.1029/2001WR000772.

Crump, K.S., 1976. Numerical inversion of Laplace transforms using a Fourier series approximation, *J. of the Association for Computing Machinery*, 23(1): 89-96.

Dahlin, T., 2000. Short note on electrode charge-up effects in DC data acquisition using multi-electrode array, *Geophysical Prospecting*, 48: 181-187.

Dahlin, T., M.H. Loke, 1998. Resolution of 2D Wenner resistivity imaging as assessed by numerical modeling, *Journal of Applied Geophysics*, 3: 237-249.

De Gery, J.C., G. Kunetz, 1956. Potential and apparent resistivity over dipping beds, *Geophysics*, 21:780-793.

De Glee, G.J., 1930. Over groundwaterstromingeen bij wateronttrekking door middel van putten. Thesis. J. Waltmena, *Delft* (The Neterlands), 175 pp.

De Hoog, F. R., J. H. Knight, and A. N. Stokes, 1982. An improved method for numerical inversion of Laplace transforms. *S.I.A.M. J. Scientific and Statistical Computation*, 3: 357-366.

De Lange, W.J., and O.D.L. Strack, 1999. Introductory comments. *J. of Hydrology*, 226: 127.

Edlefsen, N.E., and A.B.C. Anderson. 1941. The four-electrode resistance method for measuring soil-moisture content under field conditions. *Soil Science*, 51: 367-376.

Evjen, H.M., 1938. Depth factor and resolving power of electrical measurements, *Geophysics*, 3:78-95.

Ferré, P.A., J.H. Knight, D.L. Rudolph, and R.G. Kachanoski, 2000. A numerically based analysis of the sensitivity of conventional and alternative time domain reflectometry probes. *Water Resources Research*, 36(9):2461-2468.

Ferré, P.A., J.H. Knight, D.L. Rudolph, and R.G. Kachanoski, 1998. The Sample area of conventional and alternative time domain reflectometry probes. *Water Resources Research*, 34(11):2971-2979.

Ferré, P.A., D.L. Rudolph, and R.G. Kachanoski, 1996. Spatial averaging of water content by time domain reflectometry: implications for twin rod probes with and without dielectric coatings. *Water Resources Research*, 32(2):271-279.

Furman, A., T.P.A. Ferré, A.W. Warrick, 2003. A Sensitivity Analysis of Electrical-Resistance-Tomography Array Types Using Analytical Element Modeling, *Vadose Zone Journal*, 2: 416-423.

Furman, A., A.W. Warrick, T.P.A. Ferré, 2002a. Using numerical perturbation analysis to optimize electrode arrays for rapid subsurface monitoring, SAGEEP 2002, Las Vegas, Feb. 10-14. *EEGS*, Denver, CO.

Furman, A., A.W. Warrick, T.P.A. Ferré, 2002b. Electrical potential distributions in response to applied current in a heterogeneous subsurface: solution for circular inclusions, *Vadose Zone Journal*, 1:273-280.

Glass, R.J., M.J. Nicholl, A.L. Ramirez, and W.D. Daily, 2002. Liquid phase structure within an unsaturated fracture network beneath a surface infiltration event: Field experiment, *Water Resources Research*, 38(10), 1199, doi:10.1029/2000WR000167.

Glover, P.W.J., M.J. Hole, J. Pous, 2000. A modified Archie's law for two conducting phases, *Earth and Planetary Science Letters*, 180(3-4): 369-383.

Gradshteyn, I.S., I.M. Ryzhik, 2000. Table of integrals, series, and products, Sixth edition, *Academic Press*.

Grifiths, D.H., R.D. Barker, 1993. Two-dimensional resistivity imaging and modeling in areas of complex geology, *Journal of Applied Geophysics*, vol. 29, pp. 211-226.

Haitjema, H.M., 1995. Analytic element modeling of groundwater flow. *Academic Press*.

Haitjema, H.M., O.D.L. Strack, 1985. An initial study of thermal energy storage in unconfined aquifers, Final report to *Battelle Pacific-Northwest laboratory*.

Harrington, G.A., Cook, P.G., A.L. Herczeg, 2002. Spatial and Temporal Variability of Ground Water Recharge in Central Australia: A Tracer Approach. *Groundwater*, 40(5): 518-528.

Holland, J.H., 1975. Adaptation in natural and artificial systems, *Univ. of Michigan press*, Ann Arbor.

Hollenbeck, K.J., 1998. INVLAP.M: A matlab function for numerical inversion of Laplace transforms by the De Hoog algorithm, available at http://www.isva.dtu.dk/staff/karl/invlap.htm, accessed Dec. 2002.

Huisman, J.A., J.J.J.C. Snepvangers, W. Bouten, G.B.M. Heuvelink, 2002. Mapping spatial variation in surface soil water content: comparison of ground-penetrating radar and time domain reflectometry. *J. of Hydrology*, 269: 194-207.

Jacob, C.E., 1946. Radial flow in a leaky artesian aquifer, *Transactions, American Geophysical Union*, 27(11): 198-205.

Janković, I., 2002. http://www.civil.buffalo.edu/Faculty/jankovic.html, accessed Dec. 2002.

Janković, I., 2002. Split. v.2.4. Available at http://www.groundwater.buffalo.edu (cited June 2002; verified 6 Sept. 2002). *University of Buffalo* Groundwater Research Group, Buffalo, NY.

Janković, I., R. Barnes, 1999. Three-dimensional flow through large number of spheroidal inhomogeneities, *J. of Hydrology*, 226: 224-233.

Janković, I., R. Barnes, 2000. Analytic-based Solution for Three-dimensional Transient Groundwater Flow Near Partially Penetrating Wells Under Unconfined Conditions, *2000 AGU Fall Meeting, San Francisco, CA.*

Janković, I., R.J. Barnes, R. Soule, 2001. Local Modelling of Groundwater Flow Using Analytic Element Method Three-dimensional Transient Unconfined Groundwater Flow With Partially Penetrating Wells and Ellipsoidal Inhomogeneities, *2001 AGU Fall Meeting, San Francisco, CA.*

Keller, G.V., F.C. Frischknecht, 1966. Electrical methods in geophysical prospecting, *Pergamon Press*, New York.

Kluitenberg, G.J., J.H. Knight, 2003. Sensitivity of heat-pulse methods to spatial variations in soil thermal properties, *SSSA Annual Meeting*, Denver, CO, Nov. 2-6, 2003.

Knight, J. H., 1992. Sensitivity of time domain reflectometry measurements to lateral variations in soil water content. *Water Resources Research,* 28(9):2345-2352.

Knight, J.H., P.A. Ferré, D.L. Rudolph, and R.G. Kachanoski. 1997. The response of a time domain reflectometry probe with fluid-filled gaps around the rods. *Water Resources Research*, 33(6):1455-1460.

Koefoed, O., D.T. Biewinga, 1976. The application of electromagnetic frequency sounding to groundwater problems. *Geoexploration*, 14(3-4): 229-241.

LeBrecque, D.J., M. Miletto, W. Daily, A. Ramirez, and E. Owen, 1996. The effects of noise on Occam's inversion of resistivity tomography data, *Geophysics*, 61: 538– 548.

Loke, M.H. 2000. Electrical imaging surveys for environmental and engineering studies: A practical guide to 2-D and 3-D surveys [Online]. Available at http://www.agiusa.com (modified 30 July 2002; verified 6 Sept. 2002). *Advanced Geosciences*, Austin, TX.

Loke M.H., R.D. Barker, 1996. Rapid least-squares inversion of apparent resistivity pseudosections using a quasi-Newton method. *Geophysical Prospecting*, 44: 131-152.

Lowe, K.S., F.G. Gardner, R.L. Siegrist, 2002. Field Evaluation of In Situ Chemical Oxidation Through Vertical Well-to-Well Recirculation of NaMnO4. *Ground Water Monitoring and Remediation*, 22(1): 106-115.

Michot, D., Y. Benderitter, A. Dorigny, B. Nicoullaud, D. King, and A. Tabbagh, 2003. Spatial and temporal monitoring of soil water content with an irrigated corn crop cover using surface electrical resistivity tomography, *Water Resources Research*, 39(5), doi:10.1029/2002WR001581.

Moon, P., D.E. Spencer, 1961. Field theory handbook, *Springer-Verlag*.

Parker Jr, J.C., J.R. Pelton, M.E. Dougherty, 1993. A versatile shotgun source for engineering and groundwater seismic surveys. *Geophysics*, 58(10): 1511–1516.

Pool, D.R., J.H. Eychaner, 1995. Measurements of aquifer-storage change and specific yield using gravity surveys, *Groundwater*, 33(3): 425-432.

Ritz, M., H. Robain, E. Pevago, Y. Albouy, C. Camerlynck, M. Descloitres, A. Mariko, 1999. Improvement to resistivity pseudosection modeling by removal of near-surface inhomogeneity effects: application to a soil system in south Cameroon, *Geophysical Prospecting*, 47: 85-101.

Rodell, M., J. S. Famiglietti, 2002. The potential for satellite-based monitoring of groundwater storage changes using GRACE: the High Plains aquifer, Central US. *J. of Hydrology*, 263(1-4): 245-256.

Roy, A., A. Apparao, 1971. Depth of investigation in direct current methods, *Geophysics*, 36: 943-959.

Roy, A., 1972. Depth of investigation in Wenner, three-electrode, and dipole-dipole DC resistivity methods, *Geophysical Prospecting*, 20: 329-340.

Savic, D.A., G.A. Walters, 1997. Genetic algorithms for least-cost design of water distribution systems, J. of Water Resources Planing and Management, 123: 67-77.

Schapery, R.A., 1961. Approximate method of transform inversion for viscoelastic stress analysis. *Proceedings of the fourth U.S. National Congress of Applied Mathematics*, pp. 1075-1085.

Seigel, H.O., 1959. Mathematical formulation and type curves for induced polarization, *Geophysics*, 29: 547-565.

Spies, B. R., 1989. Depth of investigation in electromagnetic sounding methods. *Geophysics*, 54: 872-888.

Sternberg, Y.M., 1969. Flow to wells in the presence of radial discontinuities, *Groundwater*, 7: 17-20.

Storz, H., W. Storz, F. Jacobs, 2000. Electrical resistivity tomography to investigate geoelectrical structure of the earth's upper crust, *Geophysical Prospecting*, 48: 455-471.

Strack, O.D.L., 1989. Groundwater mechanics. *Prentice Hall*, Upper Saddle River, NJ.

Strack, O.D.L., 2003. Theory and applications of the analytic element method, Review of *Geophysics*, 41(2), doi:10.1029/2002RG000111.

Suarez, M.P., H.S. Rifai, 2002. Evaluation of BTEX Remediation by Natural Attenuation at a Coastal Facility. *Ground Water Monitoring and Remediation*, 22(1): 62-77.

Sun, N-Z. 1994. Inverse problems in groundwater modeling, *Kluwer Academic Publishers*, pp. 337.

Telford, W.M, L.P. Geldart, R.E. Sheriff, 1990. Applied geophysics (second edition), *Cambridge*, UK.

Theis, C.V., 1935. The relation between the lowering of the piezometric surface and the rate and duration of discharge of a well using groundwater storage, *Transactions, American Geophysical Union*, 2: 519-524.

The MathWorks. 1998. Matlab. *The MathWorks, Inc.*, Natick, MA.

Vozoff, K., 1958. Numerical resistivity analysis: horizontal layers, *Geophysics*, 23: 536-566.

Vozoff, K., 1960. Numerical resistivity interpretation: general inhomogeneity, *Geophysics*, 25: 1184-1194.

Wang, M., C. Zheng, 1998. Ground water management optimization using genetic algorithms and simulated annealing: Formulation and comparison, *Journal of the American Water Resources Association*, 34(3): 519-530.

Wardlaw, R.,M. Sharif, 1999. Evaluation of Genetic Algorithms for Optimal Reservoir System Operation, *Journal of Water Resources Planning and Management*, 125(1): 25-33.

Warrick, A.W., J.H. Knight, 2002. Two-dimensional unsaturated flow through circular inclusion, *Water Resources Research*, 38(7), DOI 10.1029/2001WR001041.

Yadav, G.S., P.N. Singh, K.M. Srivastava, 1997. Fast method of resistivity sounding for shallow groundwater investigations, *Journal of Applied Geophysics*, 36: 45-52.

Zaadnoordijk, W.J., 1988. Analytic elements for transient groundwater flow. PhD thesis, *University of Minnesota.*

Zaadnoordijk, W.J., 1998. Transition from Theis wells to steady Thiem wells. *Hydrological Sciences J.*, 43(6): 859-873.

Zaadnoordijk, W.J., O.D.L. Strack, 1993. Area sinks in the analytic element method for transient groundwater flow. *Water Resources Research*, 29(12): 4121-4129.

Zhadanov, M.S., G.V. Keller, 1994. The geoelectrical methods in geophysical exploration, *Elsevier*, New York.

Zhou, Q.Y., J. Shimada, A. Sato, 2001. Three-dimensional spatial and temporal monitoring of soil water content using electrical resistivity tomography. *Water Resources Research*, 37(2): 273-285.

Zhou, W., B. Beck, A. Adams, 2002. Selection of electrode array to map sinkhole risk areas in karst terrenes using electrical resistivity tomography, *Proceedings of SAGEEP 2002*, EEGS, Las Vegas.

APPENDIX A: ELECTRICAL POTENTIAL DISTRIBUTIONS IN A HETEROGENEOUS SUBSURFACE IN RESPONSE TO APPLIED CURRENT: SOLUTION FOR CIRCULAR INCLUSIONS

Alex Furman, A.W. Warrick, and Ty P.A. Ferré

Vadose Zone Journal, 1: 273-280 (2002)

Abstract

An analytic solution to the Laplace equation for potential distribution in response to current flow in a heterogeneous, two-dimensional semi-infinite domain is studied. Circular heterogeneities of varying sizes and electrical conductivities are considered. We investigate the response of the stream function, the potential field, and in particular the potential at the top boundary relative to the background as function of the size, location, and electrical conductivity of circular inclusions taken singly or multiply. The analytic solution sets the basis for the application of sensitivity analysis to the electrical resistance tomography (ERT) method, as an initial step towards improving the application of the method to tracking rapid hydrological processes.

Introduction

One of the greatest limitations to monitoring vadose zone processes is the effect of the measuring device on the hydrologic processes under investigation. Standard methods (gravimetric sampling, tensiometers, neutron probes, time domain reflectometry) are invasive and/or destructive, potentially disturbing geological bedding, flow regimes, etc.

Non-invasive geophysical methods provide a possible means to improve vadose zone monitoring.

In the electrical resistance tomography (ERT) method, current is injected into the ground through two current electrodes and simultaneously measured with two potential electrodes. A series of apparent electrical resistance measurements are made using sets of four electrodes placed at the ground surface. By simultaneously interpreting the response of electrode arrays with differing electrode separations, it is possible to form a two- or three-dimensional image of the subsurface electrical conductivity distribution. This method is becoming popular in vadose zone hydrology because the strong dependence of the electrical conductivity on the volumetric water content and salinity allows for rapid, non-intrusive monitoring through electrical conductivity mapping. Instruments have developed rapidly, allowing for automated measurement of large numbers of electrode arrays with off-the-shelf systems. However, this ease of use has the potential for misapplication of the method if users do not fully appreciate the response of each ERT measurement to subsurface conditions or the manner in which multiple measurements are combined to form a single image of the subsurface electrical conductivity distribution.

Any single ERT measurement represents the steady state response of the system to a fixed electrical source and sink. Therefore, the response of an array to a given subsurface electrical conductivity distribution can be determined numerically with readily available analysis packages. However, given the large number of measurements used in a typical

ERT survey, the sensitivity of the system response to the domain size, and the high spatial resolution necessary to model small heterogeneities, numerical solutions can be cumbersome and time consuming. This is compounded greatly if ERT is to be applied to the study of transient processes.

We present a powerful analytical method that can be used to efficiently predict the response of a set of ERT measurements to isolated subsurface heterogeneities. The results can be presented as electrical flow nets, which lead to improved understanding of the sensitivity of ERT measurements to single and multiple subsurface bodies such as voids, ore bodies, clay lenses, and regions of relatively high water content or salinity. The solution can be used for the forward simulation of current flow in general, or as part of the inversion used to determine medium properties from ERT measurements. In addition, the method can be used to identify appropriate targets for ERT surveys and to optimize the ERT surveys for expected target properties.

Background

The Electrical Resistance Tomography Method

Each single ERT measurement is based on a measurement of the electrical potential between two electrodes (P1 and P2 in Figure A-1, commonly referred as M and N in the geophysics literature) due to a constant current applied through two other electrodes (C1 and C2 in Figure A-1, A and B in the geophysics literature). The apparent electrical conductivity is calculated as the ratio of the applied current to the measured potential, with a correction applied for the geometrical effects of the electrode spacings. This

apparent electrical conductivity is some weighted average of the electrical conductivities of the subsurface regions through which current flows. However, an infinite number of electrical conductivity distributions can give rise to the same apparent electrical conductivity. To resolve this non-uniqueness problem, a large number of overlapping measurements are made and interpreted simultaneously.

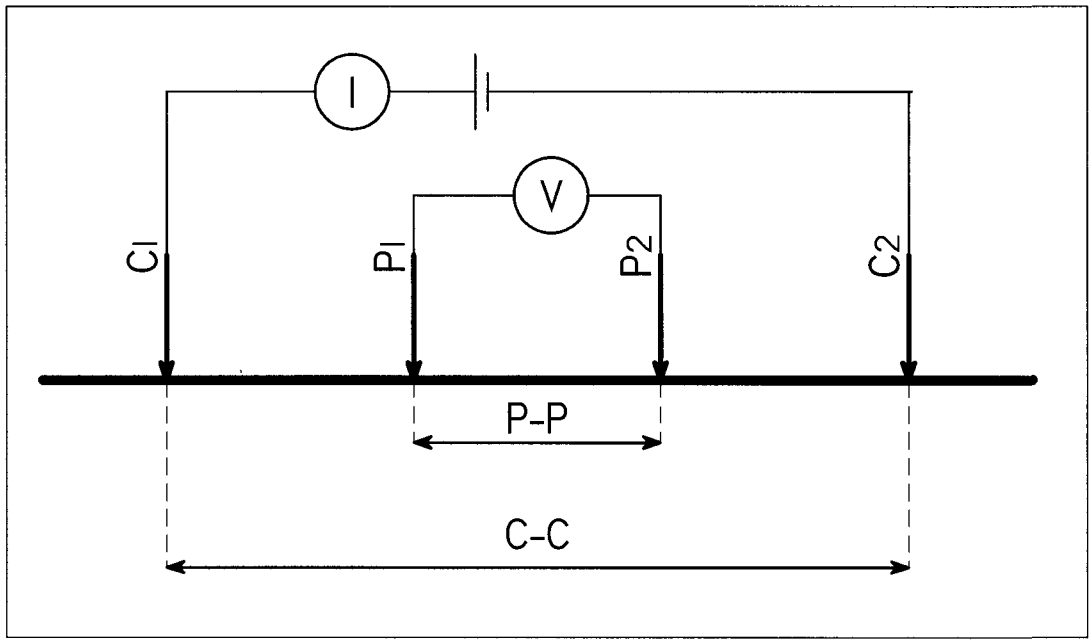

Figure A-1: Schematic diagram of electrical resistance tomography system.

All combinations of four electrodes may be classified as one of four array types (Table A-1). Typical ERT surveys use one of three classical array types: Wenner, Schlumberger, or double dipole. Schlumberger arrays center the potential electrode pair between the current electrodes. A Wenner array is a specific Schlumberger array with equal spacing between all adjacent electrodes. C-P-P-C arrays include the common Wenner and Schlumberger arrays as well as a large number of arrays that do not center

the current electrodes and potential electrodes at the same location. We refer to these arrays as Wenner/Schlumberger type arrays. To form a double dipole array, the current and potential electrode pairs do not overlap. Commonly these arrays have equal spacing between the current electrodes and the potential electrodes. P-P-C-C (or C-C-P-P) arrays include the common double dipole arrays as well as a large number of arrays that have different C-C and P-P separations. For simplicity, we refer to these as double dipole arrays. We classify P-C-C-P arrays as "inverse" in that the location of the current electrodes is opposite to the Wenner and Schlumberger arrays. P-C-P-C (and C-P-C-P) arrays are referred to here as "partially overlapping". For a more detailed description of array types and their associated geometric factors, see *Telford et al.* (1990) and *Loke* (2000).

Table A-1: Definition of four array types

Type	Configuration	Typical Array
A	C-P-P-C	Wenner, Schlumberger
B	P-C-C-P	inverse
C	C-C-P-P or P-P-C-C	double dipole
D	C-P-C-P or P-C-P-C	partially overlapping

The uniqueness of the final interpretation of a set of ERT measurements depends upon the signal to noise ratio of the measurements, the properties of the inversion routine used, and the degree to which each region of the subsurface is sampled by multiple measurements. This last condition depends on the number of measurements, their locations and array types, and the size and location of the subsurface heterogeneities. The method presented below allows for a more precise investigation of the spatial

sensitivity of any given ERT array, which is critical in designing a set of ERT measurements that will lead to a unique interpretation of the subsurface electrical conductivity distribution.

The Analytic Element Method

The Analytic Element (AE) method is based on the superposition of suitable closed-form analytic functions (*Strack*, 1989). It is essentially based on solution for each element in the flow regime, superposition of the components, and matching potential and flow at interfacial boundaries. Among the advantages of this method are the high solution accuracy near interfaces, stability, and automatic solution of the stream function that can be expressed through the use of complex variables. Among the disadvantages of the AE method are that the inclusion must be of relatively simple geometry (here we use circles), time dependence can not be considered directly, and there is a very limited number of available models (e.g. Split (*Janković*, 2002)).

For a brief description of the AE method and a history of complex variable methods see the introductory chapter of *Strack* (1989). *Barnes and Janković* (1999), and *Janković and Barnes* (1999) recently showed the use of this method for domains including a large number (10^5) of two- or three-dimensional inclusions. Among possible uses are the accurate simulation of water flow in the subsurface, and the tracking of the exact route of particles through soil. Two major applications of the analytic element method to groundwater modeling are the Dutch (The Netherlands) National Groundwater Model

(NAGROM), and the Metropolitan Groundwater Model of the Minneapolis / Saint Paul, Minnesota (*De Lange and Strack*, 1999).

Theory

We present a two-dimensional analysis of the electrical potential distribution in response to a paired source and sink of electrical current applied at the ground surface, with electrodes located at $[x, y] = [-s, 0]$, and $[x, y] = [s, 0]$. Figure A-2 illustrates the solution domain, including heterogeneities and images. A detailed development of the analytic element approach is presented in the appendix. The current electrodes have a separation of $2s$.

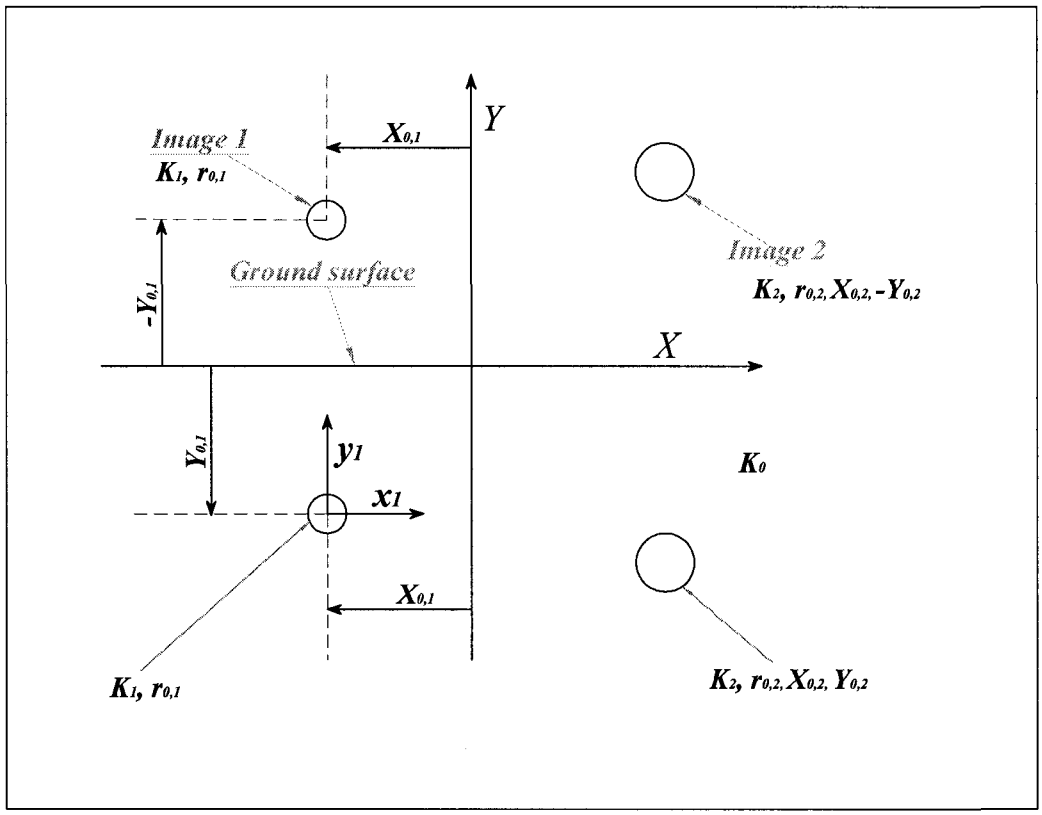

Figure A-2: Schematic diagram of the solution domain including heterogeneities and images

Following *Barnes and Janković* (1999), who applied the analytic element method to the study of steady-state water flow, we define a complex electrical potential Ω by

$$[1] \qquad \Omega(z) = \Phi(z) + i\Psi(z)$$

where $z = x + iy$ a complex variable, and Φ is the flux potential, $\left[\mathrm{MLV^{-1}T^{-3}}\right]$, which is equal to the electric potential, V [V], multiplied by the electrical conductivity K $\left[\mathrm{MLV^{-2}T^{-3}}\right]$. Ψ is the stream function $\left[\mathrm{MLV^{-1}T^{-3}}\right]$. The complex potential distribution due to the applied current is

$$[2] \qquad \Omega_B = \frac{q}{2\pi} \ln\left[\frac{z-s}{z+s}\right] + Const.$$

where q $\left[\mathrm{MLV^{-1}T^{-3}}\right]$ is the source strength, which is equal to twice the current applied to the soil through the source electrode, and the subscript, B, denotes the homogeneous background condition.

We now consider J isolated cylindrical heterogeneities with centers at $[x_{0,j}, y_{0,j}]$, with radii of $r_{0,j}$, and with electrical conductivities, K_j, that contrast with the background electrical conductivity, K_0. These localized heterogeneities may represent clay lenses, conduits, or roots, depending on the scale of investigation. The perturbation of the electric potential due to each of these heterogeneities, defined in terms of the local dependent variable $z_j = x_j + iy_j$, is

$$[3] \qquad \Omega_j = \Omega_j^+ = \sum_{n=0}^{N} a_{n,j} \left(\frac{z_j}{r_{0,j}}\right)^n \quad |z_j| \le r_{0,j}$$

or

$$[4] \qquad \Omega_j = \Omega_j^- = -\sum_{n=1}^{N} \bar{a}_{n,j} \left(\frac{z_j}{r_{0,j}}\right)^{-n} \quad |z_j| > r_{0,j}$$

where Ω_j^+ refers to the region within the heterogeneity, for which $|z_j| < r_{0,j}$, and Ω_j^- applies to the region outside of the heterogeneity $|z_j| > r_{0,j}$. N is the number of components in the series; the solution is exact as N approaches infinity. Image cylinders

are added symmetrically (with respect to the ground surface) above the ground surface to simulate the zero electrical conductivity air. The potential contribution due to each of these images is

$$[5] \qquad \Omega_{I,j} = -\sum_{n=1}^{N} \overline{a}_{n,j} \left(\frac{z_{I,j}}{r_{0,j}} \right)^{-n}$$

with $z_{I,j}$ measured from the center of the image. For our case, as images are above ground, we eliminate the need for separate equations for potentials within the images. The combined potential is

$$[6] \qquad \Omega = \Omega_B + \sum_{j=1}^{J} \left(\Omega_j + \Omega_{I,j} \right)$$

The above solution satisfies stream (current) continuity everywhere because Ψ is continuous. However, at the interface of each inclusion, there is a discontinuity in the flux potential, Φ. For the entire domain, Φ is related to the electric potential ϕ by $\Phi = K\phi$, with K corresponding to the local electrical conductivity.

For computational purposes, it is convenient to compute Φ in a dimensionless form of Φ/q and to use the coordinates $X = x/s$, $Y = y/s$. For these coordinates we also define $R_0 = r_0/s$. The dimensionless stream function Ψ/q will vary from 0 to π assuming Ψ is defined to be 0 along y = 0 and $-s \leq x \leq s$. With $x_{0,j}$ and $y_{0,j}$ the global coordinates of the center of each inclusion, relative coordinates $x_{1,j}$ and $y_{1,j}$ are related to global coordinates x and y by

$$x_{1,j} = x - x_{0,j} \quad y_{1,j} = y - y_{0,j}$$

Further details of the solution are given in the appendix.

Results and examples

Potential Distribution

Our goal is to describe the effects of the location, relative electrical conductivity, and size of cylindrical subsurface inhomogeneities on the electric potential measured at the ground surface. We consider cylinders that are oriented such that they can be represented as circles in a two-dimensional cross-section. Understanding of the voltage distribution in the presence of those heterogeneities represents the first step towards identifying preferred electrode arrays to locate subsurface objects of contrasting electrical conductivity.

All computations were conducted using Matlab (*The MathWorks*, 1998), with M (number of matching points) set to 100, and N (number of parameters in series) set to 20. Iterations were continued until no parameter was changed by more than 10^{-10}.

We first examine the flow net formed by lines of equal ϕ and Ψ created by application of our analytic element method to a single inhomogeneity. For ease of comparison, values of Φ, ϕ, and Ψ are normalized as Φ/q, ϕ/q, and Ψ/q. The electrical conductivity of the background domain, K_0, is one. Figure A-3 shows flow nets for a portion of the homogeneous domain (0), and for the same portion of the domain for two cases of single circular inhomogeneities. Figures A-3d and A-3e give more detailed views of the regions

immediately surrounding the heterogeneities. The properties of the two heterogeneities are identical except for the relative electrical conductivity, which is set to $K = 10$ for the first case (*I*), and to $K = 0.1$ for the second (*II*). The properties for these perturbations and for those used in later examples are listed in Table A-2.

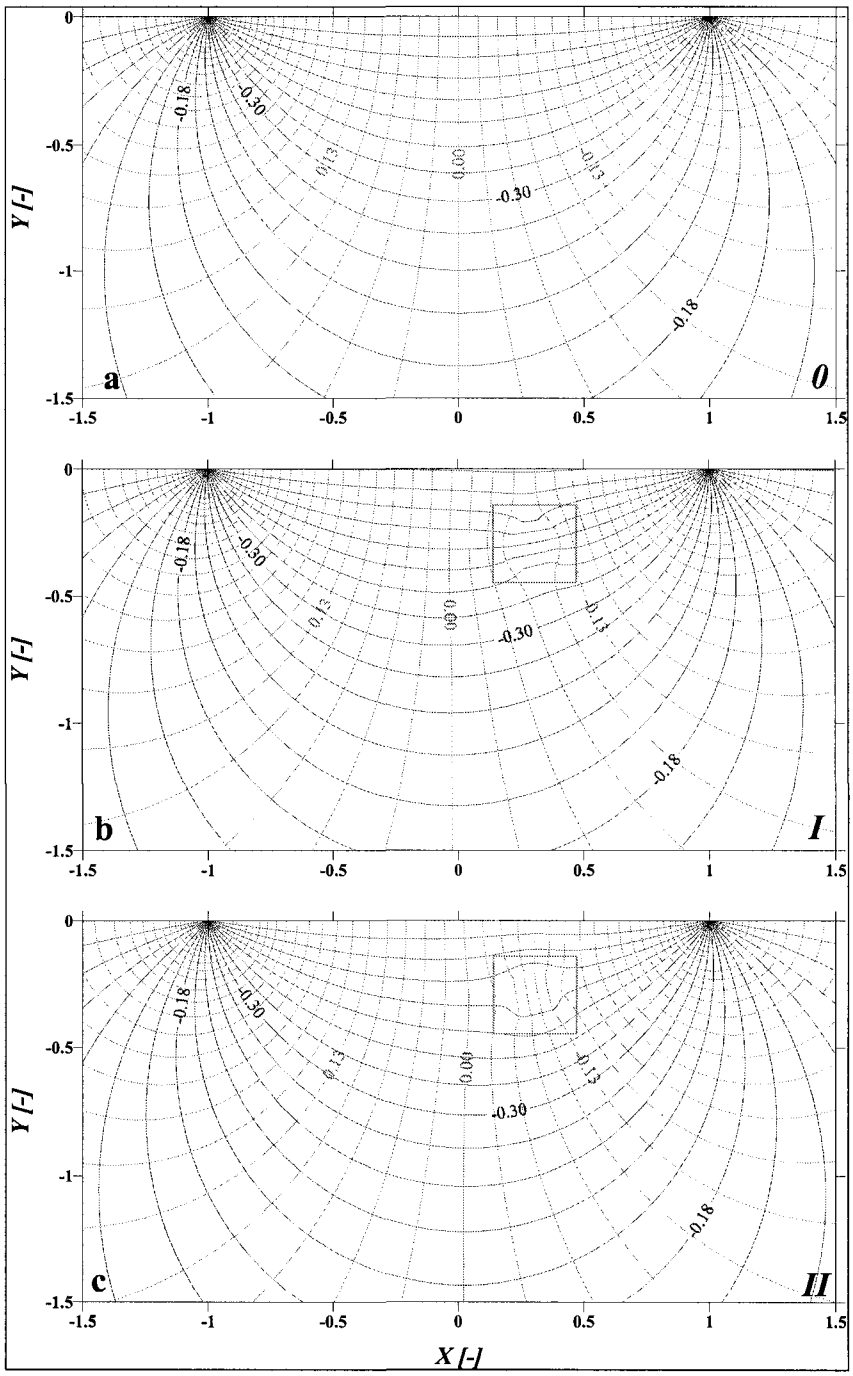

Figure A-3: Electrical flow nets for: a) a homogeneous medium; b) a single circular inclusion at [0.3, -0.3] with $K_1 = 10$ and $R_0 = 0.1$ (I); c) a single circular inclusion at [0.3, -0.3] with $K_1 = 0.1$ and $R_0 = 0.1$ (II). Current is applied at [-1, 0] and [1, 0].

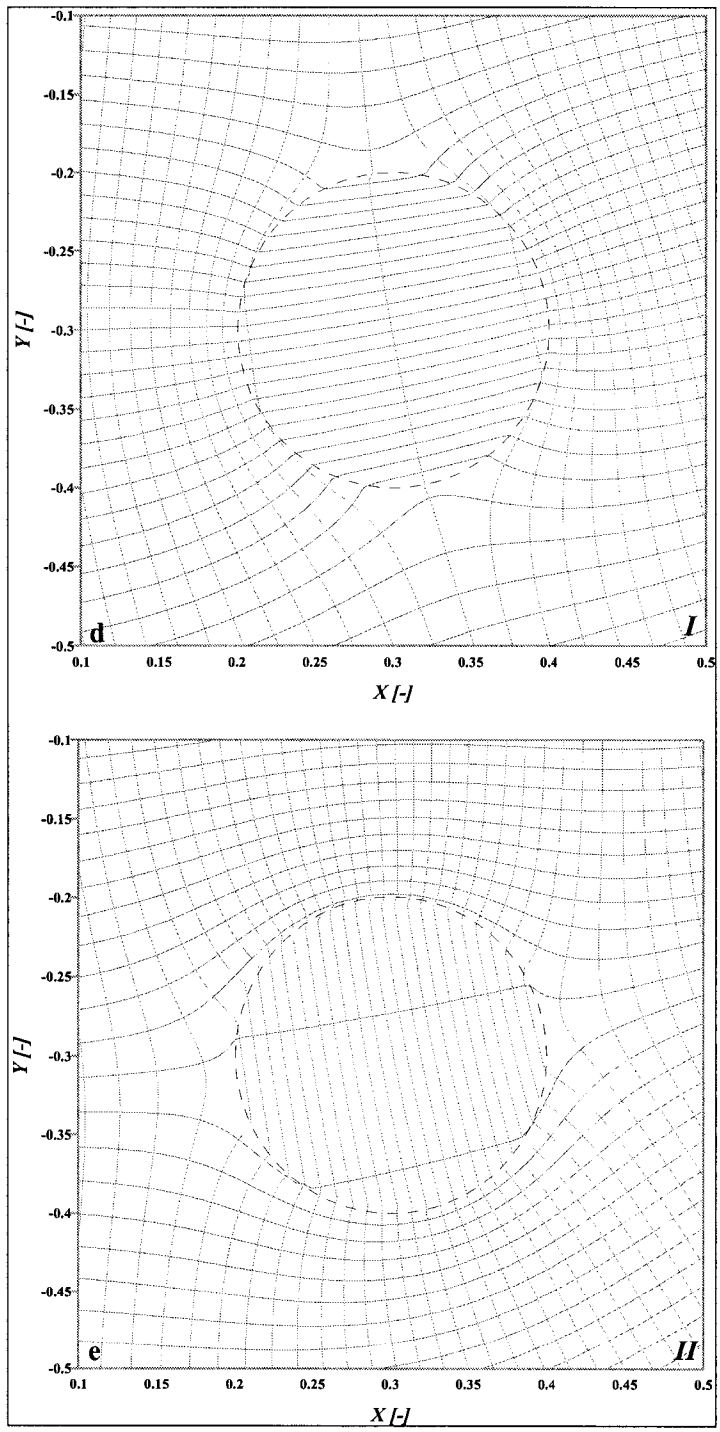

Figure A-3 (continued): Electrical flow nets for: d) a detailed view of inclusion I; e) a detailed view of inclusion II.

Table A-2: Background and inclusion properties for examples

Type	Configuration	Typical Array
A	C-P-P-C	Wenner, Schlumberger
B	P-C-C-P	inverse
C	C-C-P-P or P-P-C-C	double dipole
D	C-P-C-P or P-C-P-C	partially overlapping

As expected, a conductive heterogeneity (*I*, Figures A-3b and A-3d) causes convergence of flow, while a resistive body (*II*, Figures A-3c and A-3e) causes flow divergence. That is, the conductive body shows reduced potential gradients within the inhomogeneity and an increased gradient in the upstream (left) and downstream (right) directions. There are decreased gradients above and below the body as flow is diverted from these regions into the inhomogeneity. The effect is reversed for the low conductivity body. To better visualize the effects of the perturbation throughout the domain, the potential change due to the addition of the heterogeneity is plotted in Figure A-4 for the two heterogeneities shown above. Positive changes show increased potential at a given location compared to the homogeneous background case; negative changes show a decreased potential.

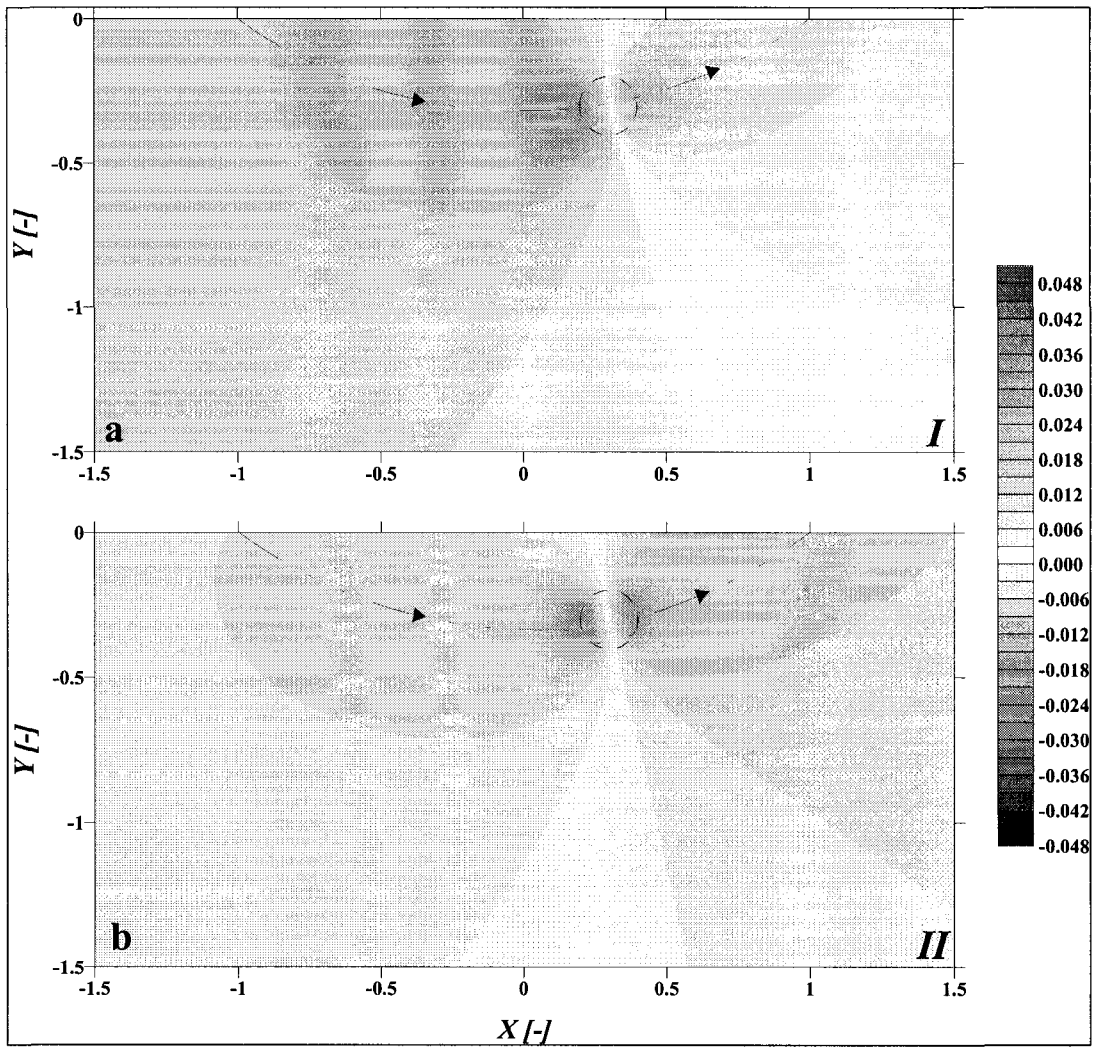

Figure A-4: Change of potential from that in a homogeneous domain due to a single inclusion at [0.3, -0.3] with $R_0 = 0.1$ for a) $K_1 = 10$ (I) and b) $K_1 = 0.1$ (II). Current is applied at [-1, 0] and [1, 0]. The streamline passing through each inhomogeneity illustrates the direction of flow.

Although the responses to the two heterogeneities differ slightly, they have many common features. For both cases, the potential is perturbed throughout the domain as a result of an isolated heterogeneity. The line of zero change runs through the center of the heterogeneity, but is not normal to the ground surface. Finally, comparison with Figures

A-3b and A-3d show that the regions of greatest impact are located along a stream line that initially runs through the location of the center of the inclusion. These features are seen for all single perturbations regardless of their location, size, or relative electrical conductivity, as shown in Figure A-5. In general, the impact of a body is determined by the fraction of the total flow rate that flows through the body. For example, a large, deep, conductive perturbation shows a very high increase in the potential adjacent to the heterogeneity, but due to its depth, the potential change at the ground surface is quite small. Similarly, a conductive perturbation that is not located between the source and sink (e.g. body e, Figure A-5c) has a relatively small impact on the electrical potential at the ground surface because a small fraction of the total flow passes through the body.

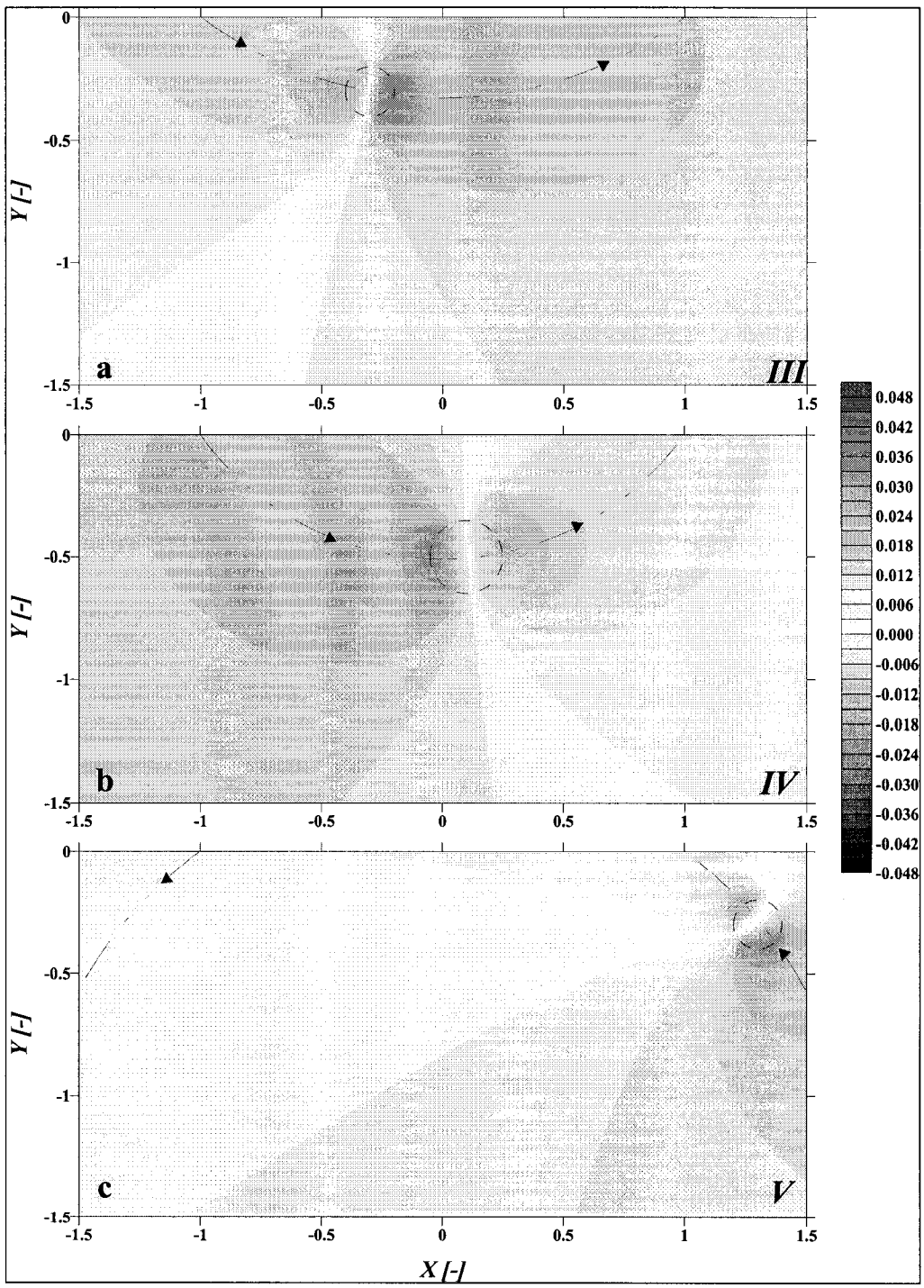

Figure A-5: Change of potential, compared with a homogeneous domain, resulting from a) Inclusion III, b) Inclusion IV, c) Inclusion V. The streamline passing through each inhomogeneity illustrates the direction of flow. See Table A-2 for inclusion properties.

Given that a single perturbation impacts the potential distribution throughout the domain, we expected that the combined effect of multiple heterogeneities would give rise to a complex potential distribution. To examine this, we begin with anomalies (*I*) (Figures A-3b, A-3d, and A-4a) and (*III*) (Figure A-5a). The combined effect of these perturbations is a region of large decrease of potential between the bodies (Figure A-6a). Physically, this is due to the focusing effect of body (*I*) combined with the diversion caused by body (*III*). The potential changes outside of the two bodies are reduced. The further addition of body (*IV*) essentially "captures" flow from body (*III*, Figure A-6b). As a result, the increased potential difference to the right of body (*III*) is restored, and the location of the most negative potential change moves to the region between bodies (*III*) and (*IV*). This is a good demonstration of the advantage of the analytic element method. Solution of such a problem using finite difference or finite element methods would require a very large number of nodes/elements to avoid numerical problems resulting from the locally steep gradients. For the analytic element method the only cost is a slight increase in the number of iterations needed for convergence.

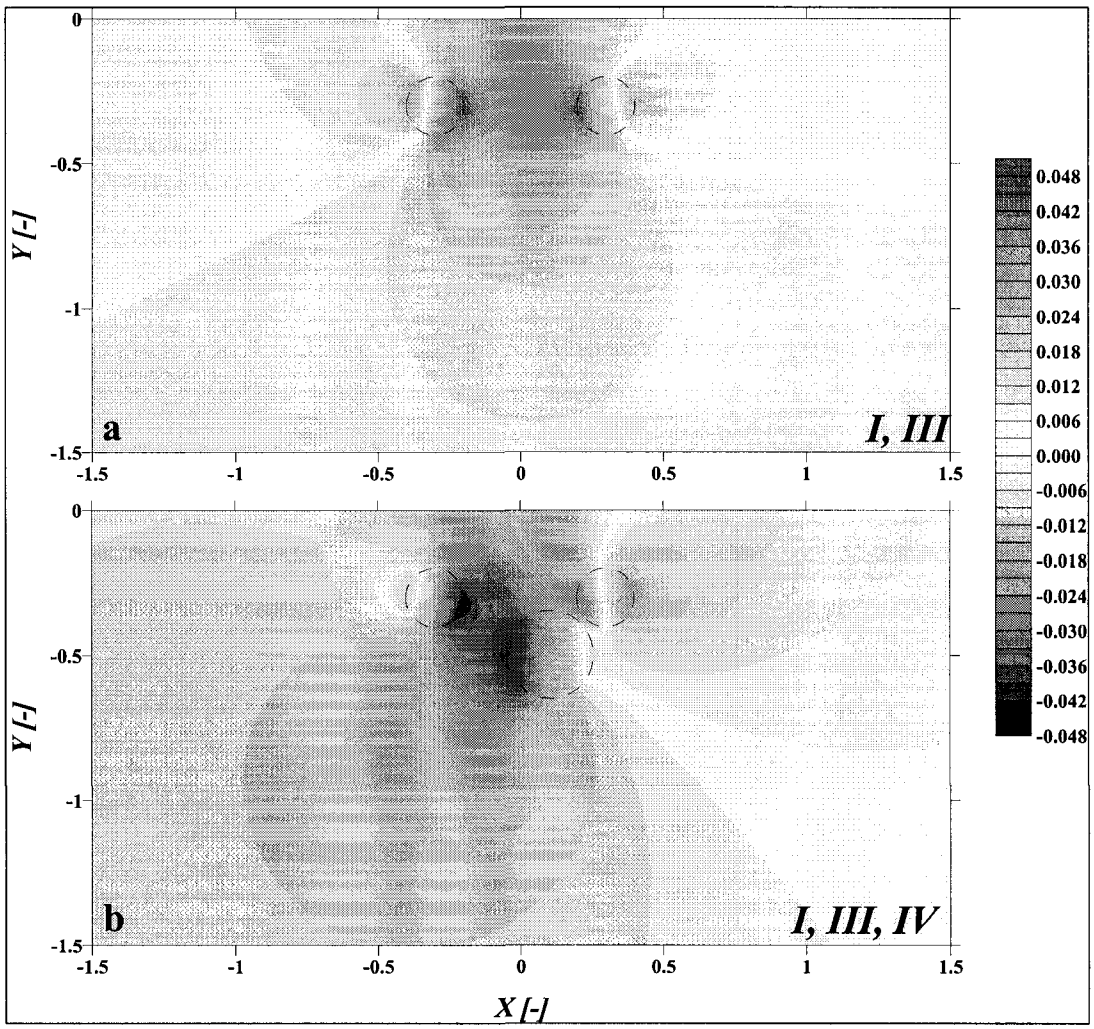

Figure A-6: Change of potential, compared with a homogeneous domain, resulting from a) two inclusions (I, III) and b) three inclusions (I, III, and IV). See table A-2 for inclusion properties.

Sensitivity

To use the analytic element method to examine the performance of an ERT system, we define the sensitivity, *S*, of a single ERT array to a conductivity perturbation, as the absolute change in measured potential between the two potential electrodes:

[7] $$S = |\Delta V - \Delta V_B|$$

Single perturbations were centered on square grid nodes, with the grid spacing equal to the electrode separation, and with the electrodes located above grid nodes. We use a 21 electrode linear system (numbered and located at X = -10 through X = 10, at the ground surface). A total of 35,910 different four electrode arrays can be formed from these electrodes; only a small fraction of these are standard Wenner, Schlumberger, or double dipole arrays. Our perturbation location grid extends to twice the width of the electrode system (X = -20 to X = 20. The maximum perturbation depth considered is 20. In all calculations the perturbation has a relative conductivity of K = 2, and a radius of r_0 = 0.5, such that the perturbation diameter is equal to the minimal electrode separation.

Table A-3 lists the sensitivitie calculated for some arrays to a single perturbation located at [X, Y] = [0, -2]. For this anomaly, most of the arrays that have high sensitivities are not one of the classic array types (i.e. Wenner, Schlumberger, or double dipole).

The method presented here can be used to identify the array that has the highest relative sensitivity to any given perturbation. However, in practice, the ability to sense a perturbation depends on the signal to noise ratio of the ERT system. Assuming that the system noise is constant, the absolute value of the sensitivity of the most sensitive array can be used as an indicator of the signal to noise ratio of the most sensitive array. Therefore, before considering the characteristics of the most sensitive arrays, we present the absolute sensitivity of the most sensitive arrays (Figure A-7). The results show that even if the most sensitive array is selected ERT systems will always be better able to

characterize shallow subsurface properties within the span of the electrodes. The results presented in Figure A-7 can be used as a measure of the confidence of the conclusions made below. That is, the analysis of the optimal array is more applicable in regions of higher absolute sensitivity of the most sensitive array.

Table A-3: Performance of most sensitive arrays and some standard arrays in response to a perturbation centered at [0, -2]

Type	Configuration	Typical Array
A	C-P-P-C	Wenner, Schlumberger
B	P-C-C-P	inverse
C	C-C-P-P or P-P-C-C	double dipole
D	C-P-C-P or P-C-P-C	partially overlapping

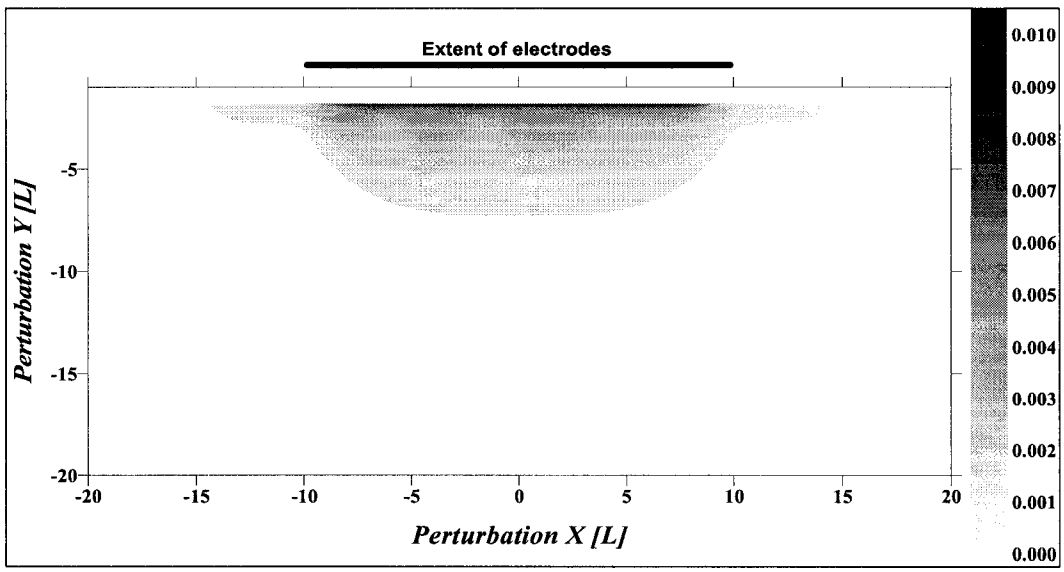

Figure A-7: The absolute sensitivity of the most sensitive arrays to a conductive perturbation plotted at the location of the perturbation.

Figure A-8 describes the characteristics of the most sensitive array for a single perturbation located at each grid node. Figure A-8a shows the C-C separation of the array and Figure A-8b shows the P-P separation. Figure A-8c shows the offset, defined

here as the horizontal distance between the array center (i.e. average location of all electrodes) and the perturbation (where a positive offset indicates that the center of the array is to the right of the perturbation). Figure A-8d shows the opening, defined here as the distance between the center of the current electrodes and the center of the potential electrodes. For example, for a perturbation located at [0, -1] the most sensitive array has C-C separation of 3, a P-P separation of 3, an offset of 0, and an opening of 1. This is a partially overlapping array with the current electrodes located at [-1, 0] and [2, 0] the potential electrodes placed at [-2, 0] and [1, 0]. The C-C separations of the most sensitive arrays tend to be equal to or slightly larger than the P-P separation. In comparison with the classic arrays, double dipole arrays have equal C-C and P-P separations, Wenner arrays have a C-C separation that is three times their P-P separation, and Schlumberger arrays typically have even larger C-C to P-P ratios. For the region beneath the electrodes, the most sensitive array tends to be centered directly above the investigated perturbation. However, for deeper perturbations and perturbations located outside of the span of the electrodes, wider arrays are required to deliver current to the perturbation. Given the limited span of electrodes available, it was not possible to form a wide array that is centered above the perturbation. As a result, the offset is larger. With few exceptions, the opening tends to be minimal. That is partially overlapping arrays are preferred over double-dipole arrays.

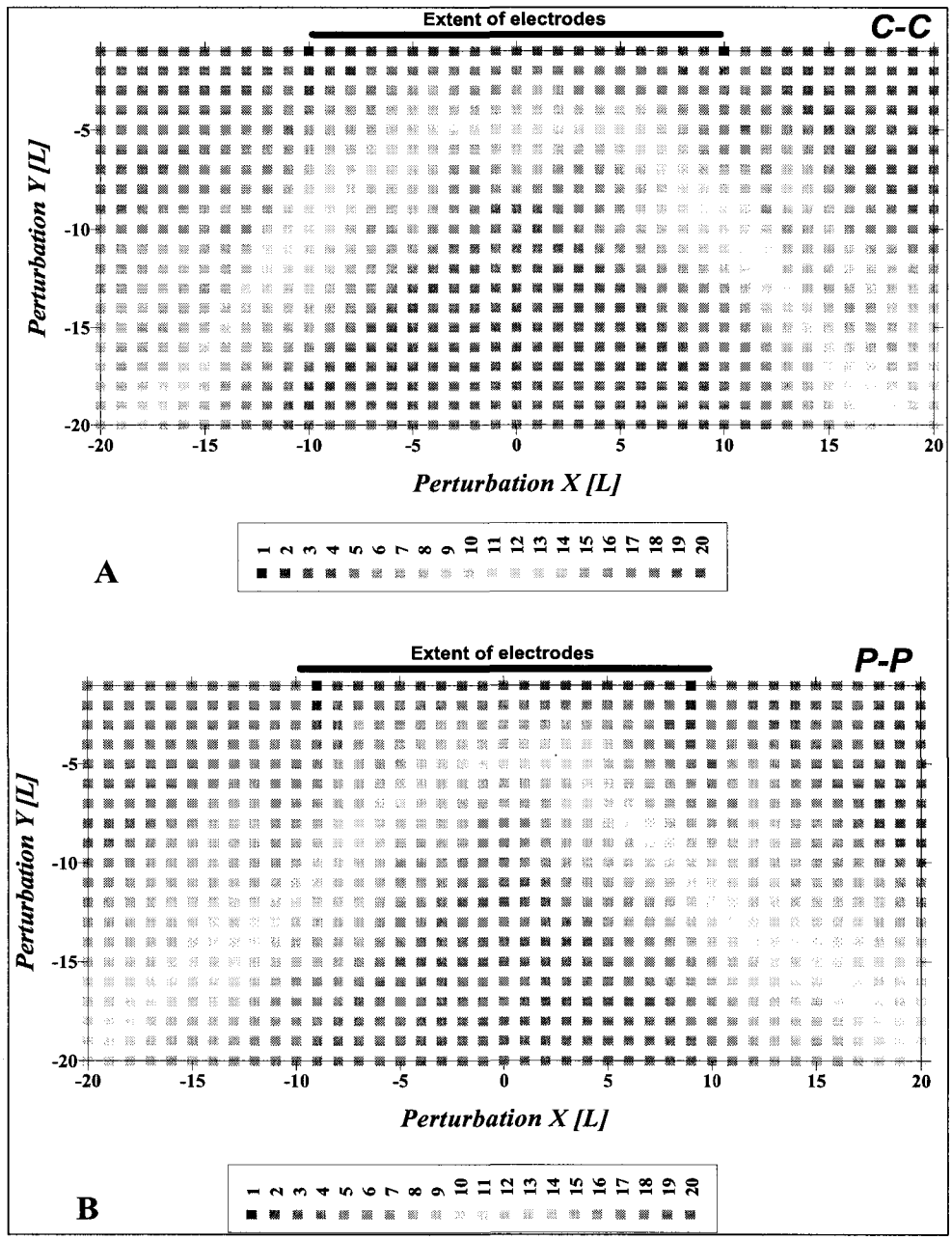

Figure A-8: The C-C (A) and P-P (B) separations for the arrays showing the highest sensitivity to a conductive perturbation plotted at the location of the perturbation.

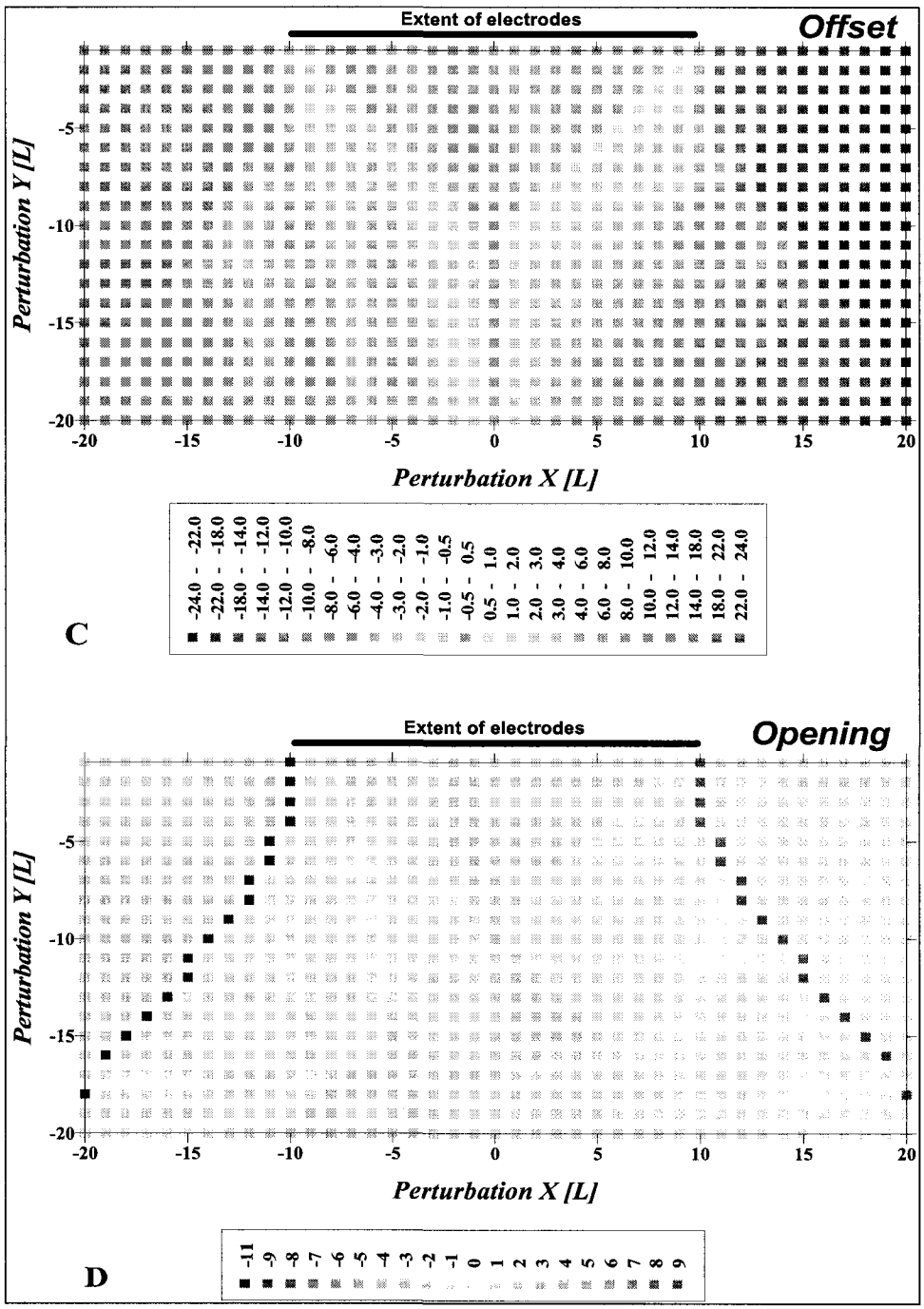

Figure A-8 (continued): The offset (C) and opening (D) of the arrays showing the highest sensitivity to a conductive perturbation plotted at the location of the perturbation.

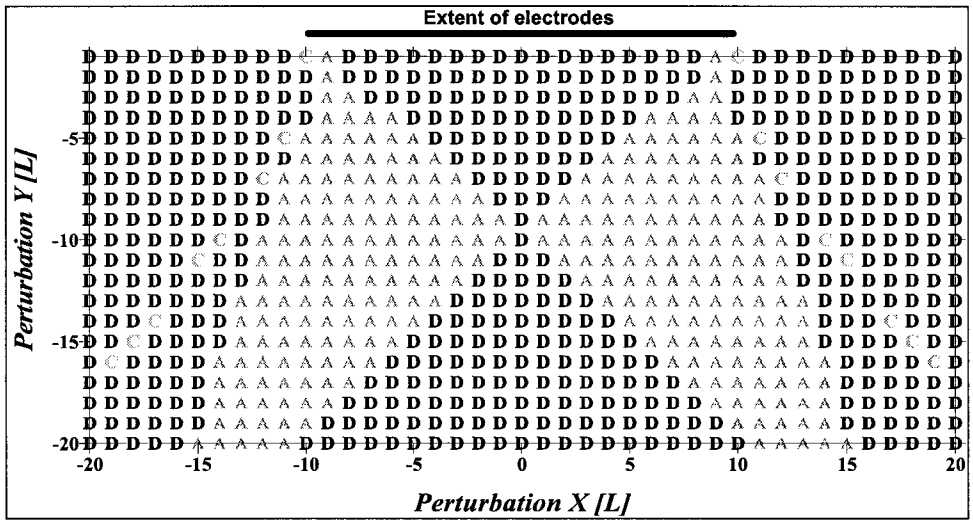

Figure A-9: The array type (see table A-1 for definitions) of the arrays showing the highest sensitivity to a conductive perturbation plotted at the location of the perturbation.

Discussion

The arrays showing the highest sensitivity to a single perturbation are identified according to the descriptions in Table A-1 in Figure A-9. There is no region in which an inverse array shows the highest sensitivity to a perturbation. Most of the domain is dominated by partially overlapping or Wenner / Schlumberger arrays, with a limited region in which double dipole arrays show the highest sensitivity. Typically, electrodes are placed such that the subsurface region of interest lies within a triangle or trapezoid located directly beneath the electrode set (e.g. *Loke*, 2000). This area coincides with the region of greatest absolute sensitivity shown in Figure A-7. Surprisingly, this region is dominated by the seldom-used partially overlapping arrays, with the margins preferring the more commonly used Wenner / Schlumberger arrays.

The following general rules describe the array that is most sensitive to a single perturbation:

1. For perturbations located under the electrode set in the area of greatest absolute method sensitivity, the array tends to be a partially overlapping array centered above the perturbation with equal current and potential electrode separations. Generally, the optimal separation (C-C and P-P) can be determined as Electrode Separation = 3 + 2 (Perturbation Depth – 1). The opening in this case would be minimal (one).

2. For perturbations located outside of the electrode set, both the current and potential electrode separations tend to be as large as possible (the maximal C-C and P-P separations possible) provided both separations are equal. This results in a partially overlapping array with an opening of one. In this case the array tends to be centered about the electrode-set center ($X = 0$), such that the maximal current density is generated near the perturbation. The absolute sensitivity to these perturbations is small. As a result, measurement made with these arrays will have a relatively low signal to noise ratio.

3. A large transitional zone (Figure A-9) exists between the previous two regions, in which the optimal array is characterized by a type A (Wenner / Schlumberger like) configuration for most cases. The P-P separation tends to be as large as possible, but smaller that the C-C separation. The opening in this region tends to be zero, making the array symmetric (i.e. a wide Schlumberger).

4. The small transitional zone between regions 2 and 3 is characterized by double dipole like arrays. The arrays are asymmetric and the C-C and P-P separations increase with the depth of the perturbation.

Summary and conclusions

An analytical solution to the Laplace equation is applied for a semi-infinite isotropic domain containing circular, non-overlapping inhomogeneities in an otherwise homogeneous background. Electric flow in a vertical plane is considered. The circular inhomogeneities may represent roots, gopher holes, conduits, or, in large number, the heterogeneous composition of the subsurface. The analytical solution is better suited to analysis of this problem than numerical methods because it offers higher accuracy that is not resolution dependent (*Janković and Barnes*, 1999), greater ease of solution, and a lack of boundary effects. Using this solution, we investigate the effects of a local subsurface inhomogeneity on potential distributions throughout the domain. The highly accurate solution and the simultaneous solution for stream functions allow for better insight into the effects of strongly contrasting bodies and multiple heterogeneities. Initial investigation of the sensitivity of ERT arrays identifies the subsurface region in which the signal to noise ratio is expected to be relatively high. The results show that the seldom-used partially overlapping array has the highest sensitivity to perturbation in this region. A general rule for choosing the optimal array in this region is defined. This rule can be used directly to choose optimal arrays for ERT investigations of isolated bodies such as

for archeological, infrastructure, and geological surveying. Furthermore, this represents a first step toward improving the ERT method for quantitative applications to subsurface hydrology.

Appendix

Further details on the analytic element model for electrical flow through a circular inhomogeneity in a vertical half space

Consider an isolated cylindrical heterogeneity with center at $x_{0,1}$, $y_{0,1}$, and with an electrical conductivity, K_1, that contrasts with the background electrical conductivity, K_0. As previously mentioned, This localized heterogeneity may represent a clay lens, conduit, or root, depending on the scale of investigation. The perturbation of the electric potential component due to this heterogeneity, defined in terms of the local dependent variable $z_1 = x_1 + iy_1$, is

$$[\text{A-1}] \quad \Omega_1^+ = \sum_{n=0}^{N} a_{n,1} \left(\frac{z_1}{r_{0,1}} \right)^n \qquad |z_1| \le r_{0,1}$$

or

$$[\text{A-2}] \quad \Omega_1^- = -\sum_{n=1}^{N} \bar{a}_{n,1} \left(\frac{z_1}{r_{0,1}} \right)^{-n} \qquad |z_1| > r_{0,1}$$

where Ω_1^+ refers to the region within the heterogeneity, for which $|z_1| < r_{0,1}$, and Ω_1^- applies to the region outside of the heterogeneity $|z_1| > r_{0,1}$. N is the number of components in the series; the solution is exact as N approaches infinity. An image

cylinder is added above the ground surface to simulate the zero electrical conductivity air. The contribution due to this image is

$$[A\text{-}3] \quad \Omega_{I,1} = -\sum_{n=1}^{N} \overline{a}_{n,1} \left(\frac{z_{I,1}}{r_0} \right)^{-n}$$

with $z_{I,1}$ measured from the center of the image.

Additional heterogeneities may be taken with centers at $[x_{0,j}, y_{0,j}]$, with radii $r_{0,j}$ and with electrical conductivities of K_j. For this preliminary analysis we assume the inclusions are not overlapping. A second heterogeneity is shown in Figure A-2 along with its image centered at $[x_{0,2}, y_{0,2}]$. The contribution due to the jth heterogeneity is by equations [3] and [4]. The contribution from the image for the j^{th} inclusion is by equation [5], with the combined potential by [6]. The solution satisfies stream (current) continuity everywhere because y is continuous. However, at the interface of each inclusion, there is a discontinuity in the flux potential F. For the entire domain, Φ is related to the electrical potential f by $\Phi = K\phi$, with K corresponding to the local electrical conductivity. Therefore, to assure continuity of the potential at each interface Φ must satisfy

$$[A\text{-}4] \quad \frac{\Phi^+}{K_j} = \frac{\Phi^-}{K_0} \qquad j = 1,...J$$

with K_0 the background electrical conductivity and K_j the electrical conductivity within the inclusion, j = 1,2,...J. Combining [6] and [A-4] leads to

$$[A\text{-}5] \quad K_j \Phi_j^- - K_0 \Phi_j^+ = \left(K_0 - K_j \right) \Phi_{R,j}$$

with a remainder $\Phi_{R,j}$ given by

$$[A\text{-}6] \quad \Phi_{R,j} = \Phi_{I,j} + \Phi_B + \sum_{p=1,p\neq j}^{J} \left(\Phi_p + \Phi_{I,p}\right)$$

Substitution for the relative electrical conductivity of the inclusion, k_j, defined as K_j/K_0, gives

$$[A\text{-}7] \quad k_j\Phi_0^- - \Phi_0^+ = \left(1-k_j\right)\Phi_{R,j}$$

This expression is comparable to Eq. [12] of *Barnes and Janković* (1999) for steady state water flow.

Solution for $a_{n,j}$

The coefficients that satisfy [A-4] can, in principle, be found directly. However, it is simpler to find them by sequential approximation. This is accomplished by first considering (following *Barnes and Janković*, 1999, eqs. [17], and [18])

$$[A\text{-}8] \quad a_{0,j}^u = \frac{\left(k_j-1\right)}{M}\sum_{m=0}^{M-1}\Phi_{R,j}^{u-1}$$

$$[A\text{-}9] \quad a_{n,j}^u = \frac{2\left(k_j-1\right)}{M\left(k_j+1\right)}\sum_{m=0}^{M-1}\left[\Phi_{R,j}^{u-1}\cdot e^{-in\theta_m}\right]$$

where u denotes iteration number, and $i=\sqrt{-1}$.

The values of qm are control points on $|\,\mathrm{zj}\,| = r_{0,j}$ and may be chosen by $\theta_{m,j} = 2\pi m/M$, $m = 0,\ldots M\text{-}1$. The last two equations may be repeated with u = 1, 2, …, with $\Phi_{R,j}^0 = 0$,

and $\Phi^{u}_{R,j}$ computed using "old" values of $a_{n,j}$. The iteration is continued until the $a_{n,j}$ do not change significantly between iterations. For convenience, we choose θ_m to be the same for all of the inclusions.

Acknowledgments

This research was funded in part by SAHRA (Sustainability of Semi-Arid Hydrology and Riparian Areas) under the STC program of the National Science Foundation, agreement EAR-9876800. This research was also supported in part by Western Research Project W-155.

References

Barnes, R., and I. Janković, 1999. Two-dimensional flow through large number of circular inhomogeneities. *J. of Hydrology*, 226: 204–210.

De Lange, W.J., and O.D.L. Strack, 1999. Introductory comments. *J. of Hydrology*, 226: 127.

Janković, I., 2002. Split. v.2.4. Available at http://www.groundwater.buffalo.edu (cited June 2002; verified 6 Sept. 2002). *University of Buffalo Groundwater Research Group*, Buffalo, NY.

Janković, I., and R. Barnes, 1999. Three-dimensional flow through large number of spheroidal inhomogeneities. *J. of Hydrology*, 226: 224–233.

Loke, M.H. 2000. Electrical imaging surveys for environmental and engineering studies: A practical guide to 2-D and 3-D surveys [Online]. Available at http://www.agiusa.com (modified 30 July 2002; verified 6 Sept. 2002). *Advanced Geosciences*, Austin, TX.

Strack, O.D.L., 1989. Groundwater mechanics. *Prentice Hall*, Upper Saddle River, NJ.

Telford, W.M., L.P. Geldart, R.E. Sheriff, 1990. Applied geophysics. 2nd ed. Cambridge Univ. Press, Cambridge, UK.

The MathWorks. 1998. Matlab. *The MathWorks*, Inc., Natick, MA.

APPENDIX B: A SENSITIVITY ANALYSIS OF ELECTRICAL-RESISTIVITY-TOMOGRAPHY ARRAY TYPES USING ANALYTICAL ELEMENT MODELING

Alex Furman, Ty P.A. Ferré, and A.W. Warrick

Published in Vadose Zone Journal, 2: 416-423 (2003)

Abstract

The analytic element method is used to investigate the spatial sensitivity of different electrical resistivity tomography (ERT) arrays. By defining the sensitivity of an array to a subsurface location we are able to generate maps showing the distribution of the sensitivity throughout the subsurface. This allows us to define regions of the subsurface where different ERT arrays are most and least sensitive.

We compare the different arrays using the absolute value of the sensitivity and using its spatial distribution. Comparison is presented for three commonly used arrays (Wenner, Schlumberger, and double dipole), and for one atypical array (partially overlapping).

Most common monitoring techniques use a single measurement to measure a property at a single location. The spatial distribution of the property is determined by interpolation of these measurements. In contrast, ERT is unique in that multiple measurements are interpreted simultaneously to create maps of spatially distributed soil properties. We define the spatial sensitivity of an ERT survey to each location based on the sum of the sensitivities of the single arrays composing the survey to that location.

With the goal of applying ERT for time-lapse measurements, we compare the spatial sensitivities of different surveys on a "per-measurement" basis. Compared are three surveys based on the typical Wenner, Schlumberger, and double dipole arrays, one atypical survey based on the partially overlapping array, and one mixed survey built of arrays that have been shown to be optimal for a series of single perturbations. Results show the inferiority of the double dipole survey compared with other surveys. On a per-measurement basis, there is almost no difference between the Wenner and the Schlumberger surveys. The atypical partially overlapping survey is superior to the typical arrays. Finally, we show that a survey composed of a mixture of array types is superior to all of the single array type surveys.

By analyzing the spatial sensitivity of the single array, and most significantly the sensitivity of the ERT survey, we set the basis for quantitative measurement of subsurface properties using ERT, with applications to both static and transient hydrologic processes.

Introduction

Electrical Resistivity Tomography (ERT) is widely used for mapping shallow subsurface geological structure (*Storz et al.*, 2000), solute distribution (*Binley et al.*, 1996), water content (*Zhou et al.*, 2001), and other environmental, hydrological and engineering features (*Dahlin*, 2000). The method is based on the introduction of electrical current into the soil through two surface electrodes and the simultaneous measurement of the induced potential gradient with other surface electrodes. Each potential measurement

gives insight into the electrical properties of the subsurface materials. The inversion of multiple measurements made with overlapping electrode arrays allows for the interpretation of the two-dimensional distribution of electrical conductivity in the subsurface. The electrical conductivity distribution can then be related to the volumetric water content, concentration of electrolytic solutes in the pore water, and the surface conductivity of the subsurface materials.

Each ERT measurement represents some average of the heterogeneous subsurface electrical conductivities in the shallow subsurface. Given that the current is applied and the potential is measured at the surface, all ERT arrays are more sensitive to the properties of shallow subsurface materials than to deeper material properties. In general, arrays with larger electrode separations are assumed to have sample areas that extend deeper beneath the ground surface, while the sample areas of smaller arrays are limited to the shallow subsurface. To form a more unique image of the subsurface electrical conductivity distribution, the apparent resistivity is measured through many electrode combinations and interpreted simultaneously. In general, it is felt that the use of a large number of arrays with different array sizes will lead to a more accurate representation of the spatial structure of the subsurface electrical conductivity.

With modern field equipment, many electrodes can be installed and measurements can be made automatically using multiple electrode arrays. As a result, many thousands of combinations of electrodes can be formed using a standard set of 21 electrodes. However, caution should be used in choosing the arrays comprising a survey to minimize

soil charge time (*Dahlin*, 2000). The total time required to collect stacked measurements for each array is typically only about 15 seconds. However, the total measurement time can become impractical if too many arrays are used. Therefore, more efficient application of the ERT method requires the development of a quantitative method to define the most useful subset of ERT arrays to form an ERT survey.

The identification of an optimal ERT array set is even more critical when monitoring transient processes. The simultaneous inversion of multiple measurements is based on the underlying assumption that all measurements were made on an identical subsurface conductivity field. However, for many transient processes, such as water infiltration or solute transport, the subsurface electrical conductivity distribution can change rapidly with time. To use ERT to monitor these processes it is critical that all electrode arrays are measured within a time frame over which it is reasonable to assume that the conductivity field is unchanging. In practice, this time frame will be defined based on the expected rate of change of the subsurface electrical conductivity due to the transient process under study. The optimal use of ERT for monitoring transient hydrologic processes requires a careful choice of the number and distribution of electrode arrays to achieve maximum spatial resolution and maximum accuracy in the time available for measurement.

We hypothesize that a quantitative approach to determining the optimal choice of ERT arrays to form an ERT survey can be designed based on the spatial sensitivities of ERT arrays. This general concept is not new. In fact, it is common practice to combine arrays

of different electrode spacings to form an ERT survey, with the implicit assumption that the depth of penetration increases with increasing array width. This practice is based on definitions of the depth of penetration of arrays, such as "The maximum depth at which a buried half-space can be detected by a measurement system at a particular frequency" (*Spies*, 1989). Similarly, *Evjen* (1938) and *Roy and Apparao* (1971) define the depth of investigation as the depth at which a thin horizontal layer of ground contributes the maximum amount to the total measured signal at the ground surface. Using this definition *Roy and Apparao* (1971) and *Roy* (1972) calculate the depth of investigation for many array types. These analyses are aimed, primarily, at determining the depth investigation of arrays, with no consideration of the distribution of array sensitivity throughout the subsurface. As a result, there is no consideration of the cumulative sensitivity distribution of the arrays that comprise a survey. We present a more complete method of analysis of the spatial distribution of ERT spatial sensitivity leading to a more complete definition of the optimal set of arrays to meet specific monitoring objectives.

The objective of this investigation is to apply the analytic-element solution for a circular perturbation in a homogeneous field, presented by *Furman et al.* (2002b) to investigate the sensitivity of the electrical potential at the ground surface to electrical heterogeneities distributed throughout the subsurface. This allows for the definition of the spatial sensitivity of any given electrode array and the development of a quantitative measure of the contribution of that array to the cumulative response of an ERT survey. Based on this definition, we identify the basis on which to choose an optimal survey set, which minimizes survey time while maximizing the useful information for inferring subsurface

properties. Development of an optimization method based on this description of sensitivity distribution may be used to improve the capabilities of ERT for quantitative monitoring of static and transient subsurface hydrologic processes.

Theory

A unique description of the contribution of each ERT measurement to the definition of the distributed subsurface electrical conductivity requires an understanding of the spatial sensitivity of each ERT measurement. Understanding of the spatial sensitivity of indirect measurement methods is most advanced for time domain reflectometry (TDR). *Baker and Lascano* (1988) used direct measurements of the response of TDR probes to small perturbations to describe the spatial sensitivity of TDR probes. *Knight* (1992) developed an analytical expression defining the response of TDR probes to small changes from a uniform distribution of dielectric permittivity in the plane transverse to a TDR probe. *Ferré et al.* (1996) extended this to consider special cases of heterogeneous dielectric permittivity distributions. *Knight et al.* (1997) introduced numerical approaches to allow for fully heterogeneous distributions. Finally, *Ferré et al.* (1998, 2000) used these definitions to uniquely define the spatial sensitivities and sample areas of TDR probes. The approaches used in these investigations can be used to describe the spatial sensitivity of any instrument that measures the steady state distribution of energy potentials at the point at which the energy is applied to the medium, such as TDR, a well used for a slug/bail test, or an air permeameter. However, the method is not directly amenable to the interpretation of a method for which energy is applied at one location and measured at another location, such as ERT. To date, the spatial sensitivity of ERT measurements has

only been discussed to a limited extent (*Loke*, 2000). There has been no attempt to rigorously define the spatial sensitivity of individual ERT measurements, which is necessary to optimize the design of an ERT survey.

Solution for flow through an inhomogeneity

To investigate the sensitivity of an ERT system, one needs an efficient way to describe the spatial distribution of electric potential in the subsurface, and in particular at the ground surface, in response to the applied electric current and as a function of the subsurface geo-electric structure. An efficient approach is necessary because of the large number of four electrode arrays that can be formed even with a limited number of electrodes. For example, for a system of 50 electrodes, almost 1.5 million different four electrode arrays can be formed. The small current applied requires that the potential at the ground surface be calculated with high accuracy. This, together with the need for rapid solutions, makes using finite element or finite difference numerical methods less attractive.

Many models have been developed to predict the distribution of electrical potential in the subsurface due to current applied at, or below, the surface. Of these models, most have been developed for homogeneous domains (e.g. *Keller and Frischknecht*, 1966), layered strata (e.g. *Vozoff*, 1958), and dipping beds (e.g. *De Gery and Kunetz*, 1956). *Keller and Frischknecht* (1966) present a model, partially based on the work of *Vozoff* (1960) for the potential at the surface due to applied current and an arbitrarily shaped inhomogeneity. *Zhadanov and Keller* (1994) present an analytical solution, based on *Siegel* (1959), for

the response of electrode array to a spherical inhomogeneity. The method presented captures much of the principles used for the analytic element solution presented by *Barnes and Janković* (1999), but uses Legendre polynomials instead of the variable separated power series used *by Barnes and Janković* (1999). *Seigel* (1959) presents a series of dimensionless response curves for specific arrays. The solution presented by *Zhadanov and Keller* (1994) may well be suited for our purpose, however we choose to use the readily available two-dimensional solution through the analytic element method.

Based on *Barnes and Janković* (1999), *Furman et al.* (2002b) presented an analytic element based solution for the problem of steady-state flow in a semi-infinite vertical domain composed of cylindrical inhomogeneities in a otherwise homogeneous subsurface. This solution can be written as

$$[1] \qquad V = \frac{\Phi_B + \Phi_P + \Phi_I}{K}$$

$$[2] \qquad \Phi_B = \frac{q}{4\pi} \ln\left(\frac{(x-s)^2 + y^2}{(x+s)^2 + y^2}\right)$$

$$[3] \qquad \Phi_{P|I} = \sum_{n=0}^{N} \lambda \left(\frac{r}{r_0}\right)^{\lambda \cdot n} \left[A_n \cos(\theta \cdot n) + B_n \sin(\theta \cdot n)\right]$$

$$[4] \qquad \lambda = \begin{cases} 1 & r \le r_0 \\ -1 & r > r_0 \end{cases}$$

where V is the electric potential [V]; Φ is the flux potential [$V\Omega^{-1}m^{-1}$], equal to the electric potential multiplied by the electrical conductivity, K [$\Omega^{-1}m^{-1}$], which varies by location; x and y are the horizontal and vertical location coordinates; q is the source strength [A], which is equal to twice the current, I [A], applied to the soil through the source electrode; r and r_0 are the distances from the cylinder (or its image) center and the cylinder (or its image) radius, respectively [m]; and θ is the angle from the horizontal [-]. The subscript B represents the background (homogeneous) solution, P represents the perturbation solution, and I represent the image cylinder solution, which is needed to accurately simulate the zero conductivity of the above-surface air. Figure B-1 illustrates the locations and properties of two cylinders and their two images. The flux potential is calculated for each inhomogeneity in the subsurface (marked P), and for each corresponding image inhomogeneity (marked I). A_n and B_n are coefficients to be determined by matching the electrical potential at M points on each of the cylinder interfaces.

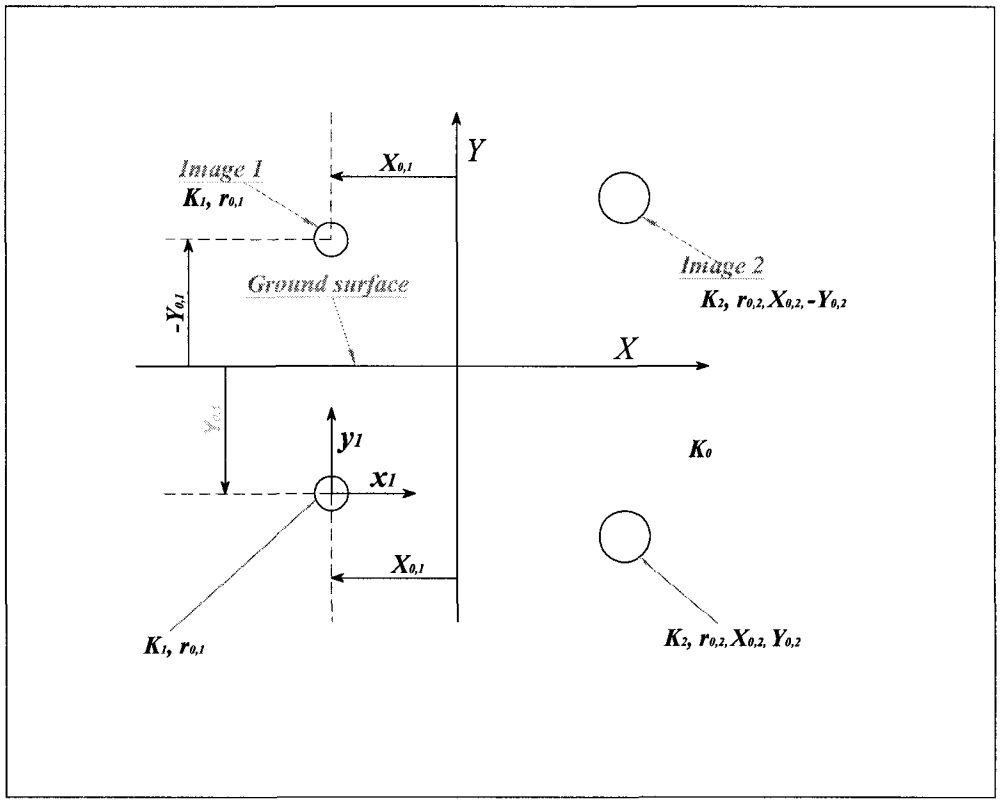

Figure B-1: Schematic diagram of solution domain including two heterogeneities and corresponding images.

The sensitivity of an ERT array to a conductivity perturbation

To form the most efficient set of ERT arrays, we begin by defining the contribution that each array makes to a unique definition of the subsurface properties. One approach is to identify the set of arrays that has the greatest sensitivity to a single perturbation placed at a number of fixed locations in the subsurface. Another approach is to identify those arrays that have the greatest cumulative sensitivity within regions of the subsurface. Both approaches begin with the definition of a response function that is based on the response of an array to a perturbation in an otherwise homogeneous subsurface (*Furman et al.*,

2002a). This response function can then be used directly, or it can be integrated over subsurface regions to define a relative sensitivity index (*SI*).

We use a two-dimensional analytic solution for electrical flow through a vertical cross section from two surface line sources through a subsurface that contains a single electrical heterogeneity that is circular in cross section. This solution defines the response of any ERT array to a small perturbation. The response function (R) is then defined as the difference between the apparent resistivity (ρ_a, [Ω·m]) calculated for the array with (ρ_a) and without ($\rho_a{}^{H}$) the inclusion normalized by the applied current, I:

$$[5] \qquad R = \frac{\left(\rho_a - \rho_a^H\right) I}{G}$$

The geometric factor, G [m], is specific to each ERT array [m]. It is defined such that the ratio of the potential difference measured between the potential electrodes, ΔV, to the current applied through the current electrodes, I, is equal to the true resistivity of a homogeneous subsurface, ρ^H, (*Telford et al.*, 1990).

$$[6] \qquad \rho_a^H = \frac{\Delta V^H}{I} G$$

Note that a factor of 2π is embedded in G. If the same current is applied to this array in a heterogeneous medium, the apparent resistivity will be:

$$[7] \qquad \rho_a = \frac{\Delta V}{I} G$$

Combining equations [5] through [7] gives:

[8] $$R = \Delta V - \Delta V^{H}$$

R is therefore the change in the potential measured between the potential electrodes for a given array with a fixed applied current that is caused by a single, small subsurface perturbation. Due to the relative locations of current application and potential measurements, a region of increased electrical conductivity can cause either an increase or a decrease in the measured potential difference, depending upon the perturbation location. To reduce the complications due to this polar response, we define the sensitivity, S [V], of an array to a single perturbation as the magnitude of the response:

[9] $$S(P) = |R|$$

where P is a vector describing the perturbation properties (i.e. location, size, and relative electrical conductivity).

Results and discussion

Single array sensitivity maps

A map of the distribution of measurement sensitivity can be constructed based on the sensitivity of different arrays to single conductivity perturbations located throughout the subsurface. These maps show the distribution of the array sensitivity to the location of a perturbation. This procedure may be repeated using different perturbations (i.e. of different size or relative conductivity). The spatial sensitivity distribution is a property of

the array and will not change with the perturbation properties; only the magnitude of the response function will change. The polarity of the response function will change if the polarity of the perturbation changes, but the sensitivity function will remain unchanged and positive. Throughout this paper we use a circular perturbation with a diameter of one (i.e. equal to the smallest electrode separation), and a relative electrical conductivity of two (i.e. twice the electrical conductivity of the background).

The cumulative sensitivity, CS, is calculated by

$$[10] \qquad CS = \frac{\sum_{i=1}^{J} S}{\sum_{i=1}^{N} S}$$

where i is a rank index, equal to one for the most sensitive perturbation and equal to N for the least sensitive one, and J is a summation limit.

Figure B-2 shows example sensitivity maps for Wenner, Schlumberger, and double dipole arrays and for an atypical array that has partially overlapping current and potential electrode pairs. All 21 electrodes are shown in each figure for ease of comparison. The electrodes used for each array are identified with long red arrows for current electrodes and short blue arrows for potential electrodes. The contours are filled with colors to represent the smooth variation of the sensitivity function with location. While it is difficult to determine the value of sensitivity at any location on these maps, these absolute values are not as important as the distribution of sensitivity throughout the subsurface. To show this distribution more clearly, contours for CS = 25, 50, 75, and

90% are shown. These contours are defined such that, for example, the 25% contour includes the regions of highest sensitivity whose cumulative sensitivity is 25% of the total sensitivity of the array. In other words, only 10% of the measurement sensitivity of the array lies outside of the 90% sample area contour. We use the 90% contour to define the measurement area of an array. The lower percentile contours show the distribution of sensitivity within the sample area. The more closely spaced these contours, the more spatially concentrated the sensitivity within the sample area.

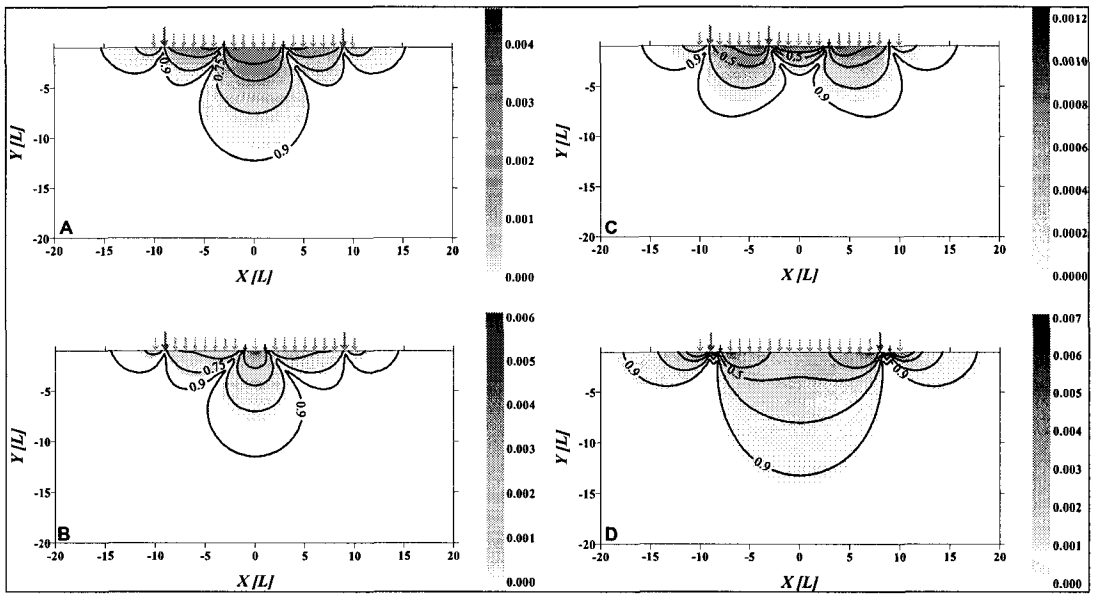

Figure B-2: Sensitivity maps for A) Wenner; and B) Schlumberger; C) double dipole; and D) partially overlapping arrays. Contours of cumulative sensitivity relative to the total sensitivity are shown. All of the electrodes used in simulations for this study are shown as arrows. Long red arrows show current electrode locations and short blue arrows show potential electrodes for specific array for which sensitivity is shown. Note that the sensitivity scale differs among arrays.

Although the sensitivity distribution is similar for all of the arrays, some significant differences exist. The major difference is the magnitude of the sensitivity. The sensitivity of the double dipole array is much lower than those of the other arrays. The partially overlapping array shows the highest sensitivity. These results apply not only to the four specific arrays analyzed. Rather, they are based on observations of simulations of many different arrays of each array type. We have shown results for arrays with similar dimensions to allow for the most direct visual comparisons. Table B-1 presents the percentage of the subsurface area enclosed within the 25, 50, 75, and 90% sample areas (i.e. the CS = 25, 50, 75, and 90% contours) for each array shown in Figure B-2. Note that in addition to having a higher total sensitivity, the partially overlapping array has larger sample areas than the Wenner, Schlumberger, and double dipole array types.

Table B-1: Percentage of domain needed to cover percentile of the total sensitivity for arrays shown in Figure B-2

% of total sensitivity	25%	50%	75%	90%
Wenner	1.1%	3.2%	8.6%	20.4%
Schlumberger	0.5%	2.3%	6.9%	17.6%
Double dipole	1.1%	3.1%	7.6%	17.9%
Partially overlapping	1.9%	5.9%	13.8%	28.1%

Time constrained survey configuration

Because ERT measurements are rapid and nondestructive, the method can be ideal for monitoring transient hydrologic processes. However, this application introduces another constraint on the identification of an optimal survey design. That is, the total number of measurements may be limited. The simplest approach to reducing the number of arrays

used in a survey, based on the sensitivity analysis presented in *Furman et al.* (2002b), is to reduce the discretization of the subsurface, thereby reducing the number of single perturbations used to identify the optimal array set. Another approach, which is commonly employed in designing traditional ERT surveys, is to arbitrarily reduce the electrode arrays considered for inclusion (e.g. only considering Wenner arrays). However, the subset of arrays identified in this manner will, of necessity, be less sensitive at many points than the set that includes all array types. A third approach is to determine which array type gives the most evenly distributed, highest sensitivity on a per measurement basis. Although the arrays identified using this approach will not match the maximum sensitivity at each point in the subsurface, this approach can be used to design a survey that gives a higher overall sensitivity using a fixed, smaller number of measurements. This approach also has the advantage of assessing the distribution of sensitivity of the entire survey, rather than only considering the sensitivity of individual arrays.

None of these approaches is best for all applications. In this study, we compare the results of optimizing ERT arrays based on identifying the locally optimal arrays for a reduced number of subsurface points to the traditional method of limiting the survey to a include only a single array type.

Survey sensitivity maps

The analysis leading to Figure B-2 shows how sensitivity maps can be generated for a single array. To compare different surveys, we need a way to describe the cumulative

spatial sensitivity of all of the arrays comprising an ERT survey. To create such a map, we average the sensitivity at each location [*X*, *Y*], over all of the arrays that comprise a single survey. For example, if a Wenner survey is composed of 63 arrays, the sensitivity at point [*X*, *Y*] = [2, -5] on all the 63 sensitivity maps will be summed and divided by 63.

$$[11] \qquad \bar{S}(X,Y) = \frac{1}{N_A}\sum_{i=1}^{N_A} S_i(X,Y)$$

where i in this case is index for the single array, and N_A is the total number of arrays in a single survey. Cumulative sensitivity contours are calculated for the resulting map as was done for the single arrays shown on Figure B-2.

Designing a survey based on sensitivities to a single perturbations

Furman et al. (2002b) presented a methodology for determining which array is most sensitive to a single conductivity perturbation. As a first approximation, this method may be used to identify the most efficient set of ERT arrays to sample the subsurface with well-distributed sensitivity. Specifically, the subsurface is divided into a finite number of cells. Then, the array that is most sensitive to a perturbation in each cell is found. These arrays are combined to form the ERT survey. For the case presented by *Furman et al.* (2002b), the subsurface was divided into 820 cells. All four-electrode combinations that could be formed using 21 electrodes were analyzed. Thus, the maximum number of arrays used (820) was a small fraction of the total number of possible arrays (35,910). In practice, some arrays showed the highest sensitivity to multiple perturbation locations,

reducing the number of arrays used to 262. However, even this number of measurements may be too large for monitoring some transient events.

The case shown by *Furman et al.* (2002b) was chosen to create detailed coverage of the entire subsurface. Here, we restrict the number of perturbations used to match an arbitrary time requirement. For this example we assume that the monitored process requires that a survey be completed every half-hour. If each measurement takes 15 seconds, this allows for a maximum of 120 measurements per survey. We now locate 120 perturbations evenly through the investigated domain (Figure B-3), and use the locally optimal array approach of *Furman et al.* (2002b).

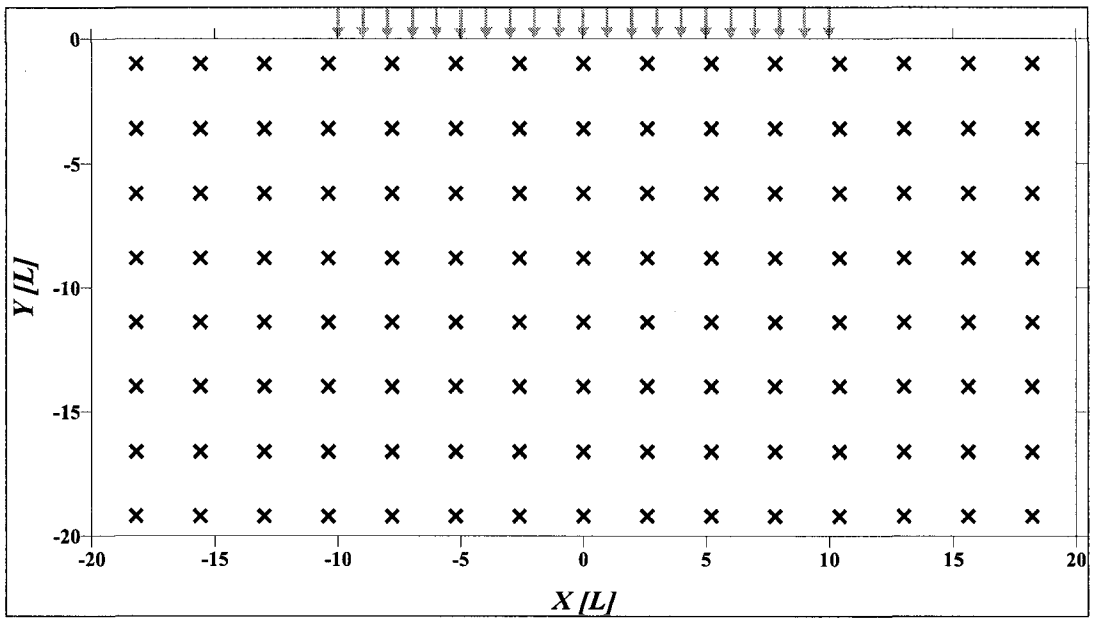

Figure B-3: Location of perturbations used to create survey set based on the locally optimal array. All of the electrodes used in simulations for this study are shown as arrows.

In practice, 120 perturbations identify fewer than the optimal 120 arrays, as shown above. In our case, only 49 arrays were identified because some arrays are the optimum choice for more than one heterogeneity location. More perturbation locations could be added to identify 120 optimal arrays. But, this introduces an arbitrary choice into the survey design. Therefore, we use only the 49 arrays identified for further analysis. We then form a cumulative sensitivity for the survey by summing the sensitivities of all 49 arrays at each point in the subsurface. This sum is then normalized by the total number of arrays (i.e. 49 in this case). The result (Figure B-4) is a map of the average sensitivity distribution of this survey on a per measurement basis.

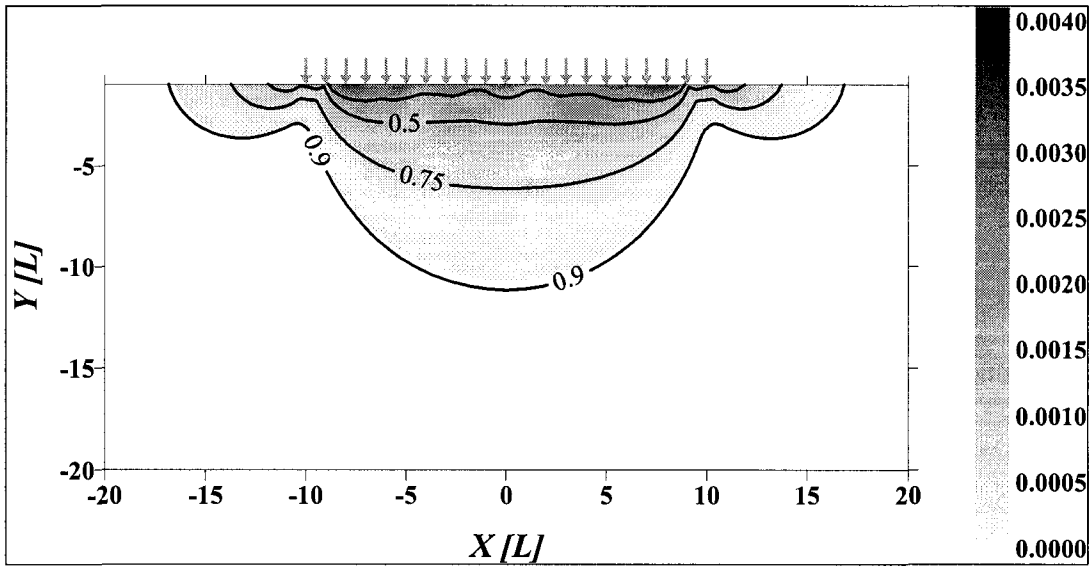

Figure B-4: Normalized cumulative sensitivity map for locally optimal survey set. Contours of percentile contribution to the sensitivity are shown. All electrodes used are shown.

Other survey types

While the local optimization approach is appealing because it is conceptually simple and because it ensures that each location will be sampled with some sensitivity, it is not obvious that this approach will identify the arrays that lead to a survey with the highest or with the most evenly distributed sensitivity. This is because each array is not sensitive to only one location; it has some sensitivity distribution. For example, Figure B-5 shows the sensitivity of a single array that was identified as most sensitive to a single perturbation located ay [*X*, *Y*] = [-5.2, -8.8] (marked by *). The array sensitivity at that point is $2.72 \cdot 10^{-4}$ volts. But, the same array has a sensitivity of $7.55 \cdot 10^{-3}$ volts to the point [*X*, *Y*] = [2.2, -1.0]. Therefore, while this array was chosen based on consideration of its sensitivity at only one location, it may have a much greater impact on the average sensitivity at other locations in the subsurface. Given that ERT measurements are

processed simultaneously to generate a map of electrical conductivity, it would seem that a better approach to identifying the optimal array set would be based on considerations of the cumulative survey sensitivity distribution. A simple criterion for identifying the optimal survey is that which gives the highest cumulative sensitivity per measurement and the largest sample areas, generally leading to a more well distributed spatial sensitivity.

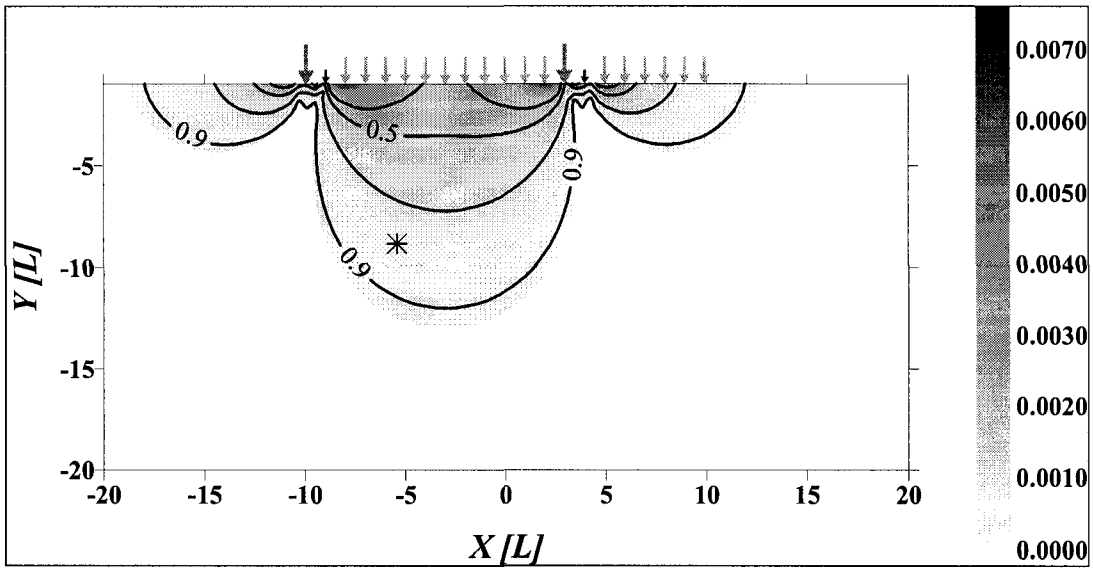

Figure B-5: Sensitivity map for partially overlapping arrays that is the most sensitive to the location marked by *. Contours of cumulative sensitivity relative to the total sensitivity are shown. All of the electrodes used in simulations for this study are shown as arrows. Long red arrows show current electrode locations and short blue arrows show potential electrodes for specific array for which sensitivity is shown.

To demonstrate the cumulative sensitivity approach to designing an ERT survey, we consider ERT surveys comprised of only one array type. To compare the cumulative sensitivity of different array types, we begin by summing the sensitivity of many single

arrays for each type. Different numbers of unique arrays can be made with a fixed number of electrodes for different array types. For example, using the 21 electrodes shown on previous figures, 63 Wenner, 171 partially overlapping, 172 Schlumberger, and 297 double dipole arrays can be constructed. To avoid biasing the results by arbitrarily choosing among arrays, we used all of the possible arrays of a given type and then normalized the cumulative sensitivity by the number of arrays used. The result (Figure B-6) shows the average spatial sensitivity of each array type on a per measurement basis. Table B-2 lists the percent of the subsurface area within each sample area contour. We add to table B-2 the same parameters obtained from the locally optimal survey, as shown in Figure B-4, for comparison.

Table B-2: Percentage of domain needed to cover percentile of the total sensitivity for survey sets shown in Figure B-4 and Figure B-6

% of total sensitivity	25%	50%	75%	90%
Wenner	0.8%	2.3%	6.1%	14.6%
Schlumberger	0.8%	2.4%	6.3%	15.0%
Double dipole	0.9%	2.5%	6.4%	15.8%
Partially overlapping	1.2%	3.3%	8.5%	19.4%
Locally Optimal	1.6%	4.5%	11.4%	24.8%

The Wenner and the Schlumberger type surveys show almost identical sensitivity distributions. This is not entirely unexpected, as almost one third of the Schlumberger arrays are also Wenner arrays. On a per measurement basis, the Wenner survey seems slightly superior to the Schlumberger survey. Therefore, of the two, the Wenner survey should be preferred when survey time is a limitation.

The double dipole survey shows smaller sample areas than the other arrays. Its sensitivity distribution is relatively shallow and the absolute values of the sensitivity are orders of magnitude smaller than those of the other surveys. The atypical partially overlapping survey type shows the largest sample area and the highest average sensitivity (value of $1.3 \cdot 10^{-4}$ volts compared with $7.06 \cdot 10^{-5}$, $6.19 \cdot 10\text{-}^{5}$, and $1.33 \cdot 10^{-5}$ volts for Wenner, Schlumberger, and double dipole surveys, respectively). These results suggest that, on average, a survey comprised of only partially overlapping arrays is preferred to surveys comprised of Wenner, Schlumberger, or double dipole arrays. These results support the conclusions of *Furman et al.* (2002b) who found that the partially overlapping arrays were preferred, based on their maximum sensitivity to individual subsurface perturbations, for most regions of the subsurface.

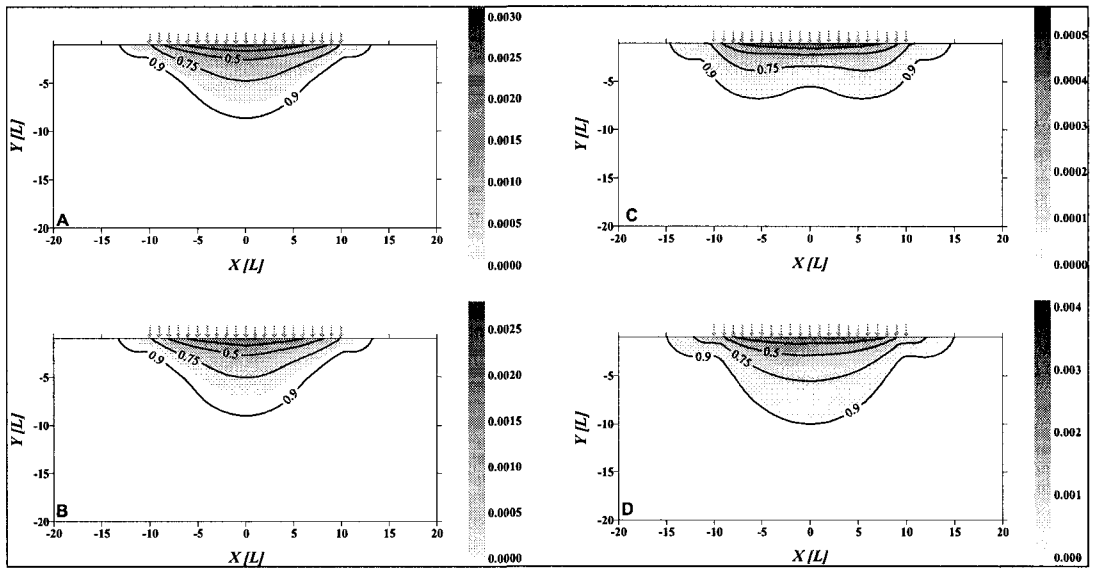

Figure B-6: Normalized survey sensitivity maps for A) Wenner; B) Schlumberger; C) double dipole; and D) partially overlapping arrays. Contours of cumulative sensitivity relative to the total sensitivity are shown. All of the electrodes used in simulations for this study are shown as arrows. Note that the sensitivity scale differs among arrays.

Further examination shows that the survey configuration based on the locally optimal approach shows higher average sensitivity values ($7.48 \cdot 10^{-3}$, almost twice that of the partially overlapping survey) and larger sample areas than the single array type surveys. This demonstrates that the inclusion of multiple array types was more important than the analysis of survey sensitivity in identifying the optimal survey design.

Conclusions

The use of analytic element methods allows for the rapid, accurate analysis of the sensitivity of many ERT arrays to single subsurface electrical conductivity perturbations. Based on these analyses, *Furman et al.* (2002a) defined the sensitivity of ERT arrays to single perturbations and used this definition to identify a set of arrays that gives the

greatest sensitivity to point locations within the subsurface. We extend this analysis to define the spatial sampling areas and sensitivity distributions of three common array types (Wenner, Schlumberger, and double dipole) and the atypical partially overlapping array. The results show that the double dipole array has small sample areas with sensitivity concentrated near the ground surface. The Wenner and Schlumberger arrays have very similar sample areas and sensitivities that are more sensitive to deeper materials than the double dipole array. The partially overlapping array has a sensitivity distribution that is similar to the Wenner and Schlumberger array types, but shows higher absolute sensitivities.

Unlike point measurement methods, the sensitivity of the ERT method should be defined for a whole survey that is composed of measurements made with many individual ERT arrays. This analysis is extended to consider the specific sensitivity of surveys comprised of only Wenner, Schlumberger, double dipole, or partially overlapping arrays, as well as to the locally optimal survey set as defined by *Furman et al.* (2002b). The results show that of the surveys composed of only one array type, the survey composed of partially overlapping arrays gives higher, more evenly distributed sensitivity than those formed with the other, more typical array types. This supports and extends the conclusion of *Furman et al.* (2002a) who identified the partially overlapping array as preferred based on its maximum sensitivity to a larger number of individual subsurface locations. Furthermore, for the case examined, the locally optimal approach to designing a survey was found to be superior to the traditional approach of limiting a survey to one array type (e.g. Wenner). While it is not known whether this approach is best for all time-limited

ERT applications, it serves as a very good starting point for identifying a global approach to survey optimization for monitoring transient hydrologic processes with ERT.

Acknowledgments

This research was funded in part by SAHRA (Sustainability of Semi-Arid Hydrology and Riparian Areas) under the STC program of the National Science Foundation, agreement EAR-9876800. This research was also supported in part by Western Research Project W-188.

References

AGI – *Advanced Geophysics Inc.*, 2000. RES2DINV user manual, Austin, Texas.

Baker, J. M. and R. J. Lascano, 1988. The spatial sensitivity of time domain reflectometry. *Soil Science*, 147(5): 378-384.

Barnes, R., Janković, I., 1999. Two-dimensional flow through large number of circular inhomogeneities, *J. of Hydrology*, 226: 204-210.

Binley, A., S. HenryPoulter, B. Shaw, 1996. Examination of solute transport in an undisturbed soil column using electrical resistivity tomography. *Water Resources Research*, 37(4): 763-769.

Dahlin, T., 2000. Short note on electrode charge-up effects in DC data acquisition using multi-electrode array, *Geophysical Prospecting*, 48: 181-187.

De Gery, J.C., G. Kunetz, 1956. Potential and apparent resistivity over dipping beds, *Geophysics*, 21: 780-793.

Evjen, H.M., 1938. Depth factor and resolving power of electrical measurements, *Geophysics*, 3: 78-95.

Ferré, P.A., J.H. Knight, D.L. Rudolph, and R.G. Kachanoski, 2000. A numerically based analysis of the sensitivity of conventional and alternative time domain reflectometry probes. *Water Resources Research*, 36(9): 2461-2468.

Ferré, P.A., J.H. Knight, D.L. Rudolph, and R.G. Kachanoski, 1998. The Sample area of conventional and alternative time domain reflectometry probes. *Water Resources Research*, 34(11): 2971-2979.

Ferré, P.A., D.L. Rudolph, and R.G. Kachanoski, 1996. Spatial averaging of water content by time domain reflectometry: implications for twin rod probes with and without dielectric coatings. *Water Resources Research*, 32(2): 271-279.

Furman, A., A.W. Warrick, T.P.A. Ferré, 2002a. Using numerical perturbation analysis to optimize electrode arrays for rapid subsurface monitoring, SAGEEP 2002, Las Vegas, Feb. 10-14. *EEGS*, Denver, CO.

Furman, A., A.W. Warrick, T.P.A. Ferré, 2002b. Electrical potential distributions in response to applied current in a heterogeneous subsurface: solution for circular inclusions, *Vadose Zone Journal*, 1: 273-280.

Keller, G.V., F.C. Frischknecht, 1966. Electrical methods in geophysical prospecting, *Pergamon Press*.

Knight, J. H., 1992. Sensitivity of time domain reflectometry measurements to lateral variations in soil water content. *Water Resources Research*, 28(9): 2345-2352.

Knight, J.H., P.A. Ferré, D.L. Rudolph, and R.G. Kachanoski. 1997. The response of a time domain reflectometry probe with fluid-filled gaps around the rods. *Water Resources Research*, 33(6): 1455-1460.

Loke, M.H., 2000. Electrical imaging surveys for environmental and engineering studies: A practical guide to 2-D and 3-D surveys (Found at http://www.agiusa.com).

Roy, A., A. Apparao, 1971. Depth of investigation in direct current methods, *Geophysics*, 36: 943-959.

Roy, A., 1972. Depth of investigation in Wenner, three-electrode, and dipole-dipole DC resistivity methods, *Geophysical Prospecting*, 20: 329-340.

Seigel, H.O., 1959. Mathematical formulation and type curves for induced polarization, *Geophysics*, 29: 547-565.

Spies, B. R., 1989. Depth of investigation in electromagnetic sounding methods. *Geophysics*, 54: 872-888.

Storz, H., W. Storz, F. Jacobs, 2000. Electrical resistivity tomography to investigate geoelectrical structure of the earth's upper crust, *Geophysical Prospecting*, 48: 455-471.

Telford, W.M, L.P. Geldart, R.E. Sheriff, 1990. Applied geophysics (second edition), *Cambridge*.

Vozoff, K., 1958. Numerical resistivity analysis: horizontal layers, *Geophysics*, 23: 536-566.

Vozoff, K., 1960. Numerical resistivity interpretation: general inhomogeneity, *Geophysics*, 25: 1184-1194.

Zhadanov, M.S., G.V. Keller, 1994. The geoelectrical methods in geophysical exploration, *Elsevier*.

Zhou, Q.Y., J. Shimada, A. Sato, 2001. Three-dimensional spatial and temporal monitoring of soil water content using electrical resistivity tomography. *Water Resources Research*, 37(2): 273-285.

APPENDIX C: OPTIMIZATION OF ERT SURVEYS FOR MONITORING TRANSIENT HYDROLOGICAL EVENTS USING PERTURBATION SENSITIVITY AND GENETIC ALGORITHMS

Alex Furman, Ty P.A. Ferré, and A.W. Warrick

Submitted for publication in Vadose Zone Journal (2003)

Abstract

A simple yet powerful algorithm is presented for the optimal allocation of electrical resistivity tomography (ERT) electrodes to maximize measurement quality. The algorithm makes use of a definition of the sensitivity of an ERT array to a series of subsurface perturbations. An objective function that maximizes the average sensitivity of a survey comprised of large number of arrays is defined. A simple genetic algorithm is used to find the optimal ERT survey if there is a limited time allowed for survey. We further show that this approach allows for user definition of the sensitivity distribution within the targeted area.

Results show clear improvement in the sensitivity distribution. The total sensitivity of the optimized survey compared with typically used surveys composed of one array type. This improved sensitivity will allow for more accurate monitoring of static and transient vadose zone processes. Furthermore, the algorithm presented maybe fast enough to allow for real time optimization during time-laps surveys.

Introduction

Monitoring subsurface hydrologic processes, and particularly those that occur within the vadoze zone, is difficult and expensive. Many monitoring methods involve drilling for sampling or for access, which can disturb the process under investigation, and increase the cost of the monitoring. Alternatives typically include buried instrumentation (e.g. time domain reflectometry (TDR), thermocouples, or tensiometers). However, these point measurements provide limited spatial resolution because they require a separate probe for each measurement point. In contrast, non-destructive, non-invasive geophysical methods may offer high spatial and temporal resolution monitoring of shallow subsurface hydrological processes.

Electrical resistivity tomography (ERT) has long been seen as a promising non-invasive, non-destructive method (*Edlefsen and Anderson*, 1941). Recent advances in ERT instrumentation and inversion methods have increased the use of ERT for hydrologic investigations (*Barker and Moore*, 1998). Among these improvements are the use of multi-core cable, addressed electrodes, improved control and recording, and increased measurement accuracy, allowing for the use of very small currents (i.e. tens to hundreds of milliamps).

Despite the increased use of electrical geophysical methods, including ERT, applications are largely limited to monitoring static or very slowly changing conditions. Examples can be found for application of ERT to mineral exploration (e.g. *Griffiths and Barker*, 1993), geologic mapping (e.g. *Griffiths and Barker*, 1993; *Storz et al.*, 2000),

groundwater table location (e.g. *Yadav et al.*, 1997), and groundwater contamination mapping (e.g. *Buselli and Lu*, 2001). *Barker and Moore* (1998) showed that ERT could be used to monitor transient processes in the shallow subsurface. However, their examples are limited to processes that occur slowly, on the order of hours.

Increased accuracy can be achieved through noise reduction (*Ritz et al.*, 1999); improved inversion algorithms; assimilation of data obtained through other means (*Yeh et al.*, 2002); and optimized selection of arrays used to compose the survey (*Furman et al.*, 2003).

Improved monitoring of transient hydrologic processes requires improved measurement accuracy, and measurement that is more rapid. In addition, because ERT inversion is often ill posed (*Sun*, 1994), an increase in the number of measurements contributes to the overall ERT survey quality. Therefore, when monitoring a transient process, the number of measurements should be as large as time allows. Maximization of the number measurements can be achieved by reduction of the single measurement time, but this often causes an increase in the measurement error. Multi-channel monitoring equipment (e.g. *AGI*, 2002) can further increase the number of measurements. However, regardless of measurement rate, full survey optimization requires the choice of the optimal set of arrays to form a survey. We propose that improvements in instrumentation alone are not enough to allow for monitoring of more rapid processes with ERT. Rather, these improvements must be coupled with improved survey design to optimize data quality.

Although the time required for a single ERT measurement is dependent on many parameters, including the properties of the subsurface at the time of measurement, it can be treated as a constant (e.g. approximately 15 seconds). We consider that the time window available for completion of a survey is based on the physical process that is to be monitored. That is, all measurements comprising a survey must be made rapidly compared with the rate at which the electrical conductivity changes in the subsurface. The time window divided by the time required per measurement defines the maximum number of arrays in a survey, A. Furthermore, the rate of change of EC may change with time, leading to tightening or relaxation of the time frame, and a change in the number of arrays comprising a survey.

Typically, ERT surveys include only one type of array (e.g. Wenner arrays). *Zhou et al.* (2002) and *Furman et al.* (2003) suggest that a combination of different array types may increase ERT survey quality. *Furman et al.* (2003) showed that each ERT array is characterized by a unique sensitivity distribution, and that this sensitivity distribution can be used to compare arrays directly. We propose further that these sensitivity distributions can be used to design an ERT survey with a user-defined optimal sensitivity. This could then allow for the design of the optimal survey for specific monitoring needs. Specifically, we present a method to identify the optimal set of arrays to form an ERT survey composed of a fixed number of. The method makes use of Genetic Algorithms (GA) to identify the array set with the optimal cumulative survey spatial sensitivity based on user-defined criteria.

Theory

ERT as an optimization problem

A typical ERT survey is comprised of a set of four-electrode arrays. *Furman et al.* (2003) have shown that each array has a unique sensitivity and a unique sensitivity distribution. Therefore, sets of arrays can be chosen that give optimal cumulative sensitivity based on a user-defined total number of arrays and a user-defined preferred sensitivity distribution. The purpose of this investigation is to develop a method to identify these.

The sensitivity, S [V], of an array, a, to a finite circular perturbation at location, j, which has an electrical conductivity contrast with the background, ΔK [$\Omega^{-1}\cdot m^{-1}$], is defined here as the absolute change in apparent resistivity due to the perturbation, normalized by the geometric factor and the applied current (see *Telford et al.*, 1990). S_j^a can be calculated as:

$$[1] \qquad S_j^a = \left|\Delta V - \Delta V_H\right|,$$

where V [V] is the measured potential between the two potential electrodes, and H indicates the potential difference for the same applied current in a homogeneous subsurface. (Note all parameters used in this paper are listed and defined in Table C-1). Each array is associated with current electrodes located at C_1 [m] and C_2 [m], and

potential electrodes located at P_1 [m] and P_2 [m]. The perturbation location, j, is associated with a circular inhomogeneity centered at $[x, y] = [x_{0,j}, y_{0,j}]$.

The weighted cumulative sensitivity of an array can be defined as the weighted sum of the S_j^a values for a large number (J) of perturbations distributed throughout the subsurface:

$$[2] \qquad S_a = \frac{\sum_{j=1}^{J} \alpha_j S_j^a}{\sum_{j=1}^{J} \alpha_j}$$

where α [-] is a weighting factor. Through the use of these weighting factors, a common set of perturbation locations, distributed equally throughout the subsurface, can be used for all optimizations. Then, areas of the subsurface can be targeted by simply increasing the weighting factors in these regions.

The cumulative sensitivity of a survey, S_c, comprised of A [-] arrays can then be defined as:

$$[3] \qquad S_c = \sum_{a=1}^{A} S_a$$

It is convenient to normalize this survey cumulative sensitivity by the number of arrays to allow for more direct comparison of surveys with different numbers of arrays. The mean survey sensitivity is then defined as:

$$[4] \qquad \overline{S} = \frac{1}{AJ} \frac{\sum_{a=1}^{A} \sum_{j=1}^{J} \alpha_j S_j^a}{\sum_{j=1}^{J} \alpha_j}$$

If all perturbations are weighted equally, the mean survey sensitivity is:

$$[5] \qquad \overline{S} = \frac{1}{AJ} \sum_{a=1}^{A} \sum_{j=1}^{J} S_j^a$$

Consider, as an example, a survey that is designed to find the most representative average electrical conductivity (EC) of the subsurface using only 15 arrays. To achieve this, perturbations should be located evenly throughout the subsurface and weighted equally. Arrays with small electrode separations have sensitivities that are highly focused within the shallow subsurface. In contrast, wider arrays have moderate sensitivity over a much larger sample volume. As a result, it can be shown that wider arrays will have the highest cumulative sensitivities (*Furman et al.*, 2003). Therefore, as may be expected, a survey comprised of 15 wide arrays will give the best measure of the average electrical conductivity of the subsurface.

The optimization approach described above does not take into account the spatial distribution of sensitivity of the optimal survey. A similar approach can be designed to identify the survey that gives the best representation of the electrical conductivity of the subsurface while maintaining the most evenly distributed measurement sensitivity. This becomes increasingly important with increasing heterogeneity of the subsurface electrical

conductivity. To achieve greater uniformity of the cumulative sensitivity, a component is added to the objective function that states that the standard deviation of the normalized sensitivity values, σ_S, must be minimized as well as maximizing the mean survey sensitivity. The measure of performance of a survey, Z [-], is therefore based on two components: the survey average sensitivity and the survey standard deviation. The general form of the objective function, formatted to a maximization problem, is then:

$$[6] \qquad MAX(Z) = \beta\bar{S} - (1-\beta)\sigma_S$$

where β [-] is a weighting factor that can be used to adjust the relative weights of the survey sensitivity and the sensitivity distribution in the optimization. The optimal survey has the maximum Z. Setting β to one returns the survey with the highest cumulative sensitivity, as discussed above. As β decreases, the cumulative sensitivity of the optimal array will be lower, but more evenly distributed. The identification of the optimal survey for the case of β equal one is trivial: all of the possible arrays can be ranked in order of decreasing average sensitivity. Then, the 15 most sensitive can be chosen to form the survey. However, if β is not one, the optimization requires a more sophisticated approach.

In general, weights (i.e. α, β) may be used to tailor a survey to achieve a specific desired distribution of the survey sensitivity. However, if a lesser degree of freedom is required in the design of a survey (i.e. no specific target in the subsurface is considered) it is convenient to use a normalized offset instead of the sensitivity. Considering all arrays

that can be formed from a given set of electrodes, one array will have the maximum sensitivity to a perturbation at location, j, as described by *Furman et al.* (2002a). The sensitivity of this array is referred to as S_j^{MAX}. We define the offset, e_j^a [-], of array a to a perturbation centered at point, j, as the difference between the sensitivity of array a and S_j^{MAX}, normalized by S_j^{MAX}:

$$[7] \qquad e_j^a = \left(\frac{S_j^{MAX} - S_j^a}{S_j^{MAX}} \right).$$

The use of the offset in the optimization objective function is identical to the use of the sensitivity in equations [2] through [5]. We use the notations E_a and E_c for array and survey cumulative offset as the equivalents of S_a, and S_c, respectively, and the mean survey offset, $\overline{E}$, in equivalence to $\overline{S}$. The objective function, Z, is defined in this case as:

$$[8] \qquad MAX(\mathrm{Z}) = 1 - \left[\beta \overline{E} + (1-\beta)\sigma_E \right]$$

As the offset is a normalized quantity, the standard deviation of the offset may be omitted, resulting in a simplified objective function:

$$[9] \qquad MAX(\mathrm{Z}) = 1 - \overline{E}$$

The solution to the optimization problem in this case is simply the selection of the A arrays showing the lowest array offset, E_a.

Genetic algorithm for solution of the ERT optimization problem

In general, an ERT survey can be described as an 4 by A matrix, F, where the four rows store the locations of the current (C_1, C_2) and potential (P_1, P_2) electrodes, respectively. The A columns of the matrix represent the A arrays that comprise the ERT survey. Given the large number of four-electrode combinations that can be formed with as few as 21 arrays (35,910), the number of possible surveys that can be formed using only 15 arrays is enormous (approximately $2 \cdot 10^{68}$). Therefore, an efficient and robust optimization method is needed to define the optimal survey.

Genetic algorithms have been applied previously in the field of water resources to find the optimal design of water distribution systems (e.g. *Savic and Walters*, 1997), optimal reservoir operation (e.g. *Wardlaw and Sharif*, 1999), and optimal groundwater management (e.g. *Wang and Zheng*, 1998). Genetic algorithms can be described as numerical optimization methods that simulate the evolutionary process (*Holland*, 1970). Specifically, a population is defined as a number of different chromosomes. In the case of ERT, several surveys are defined using different combinations of arrays; each survey is a chromosome. Each chromosome is comprised of a number of genes. (Most genetic algorithms use binary or scalar variables to represent genes). We introduce the use of a vectored description of electrode locations, with four numbers representing the electrode numbers used as the two current and two potential electrodes, as the gene. The optimization marches forward through successive generations until the objective function is satisfied within some convergence criterion. The population begins with N initial

guesses. For ERT, the initial population may be chosen at random or based on some combination of Wenner, Schlumberger, double dipole, or partially overlapping (*Furman et al.* 2002a) arrays. Alternatively, the approach of *Furman et al.* (2003) can be used to define the locally optimized survey as an initial guess. Following the optimization procedure outline above, the surveys comprising the initial guess are ranked in order of their performance, *Z*. Mimicking natural selection, only the strongest (highest performance) chromosomes are carried forward into the next generation as an elite group (*Coley*, 1999). The remaining chromosomes are subject to a range of regeneration processes, or mutations, based on their relative fitness.

We distinguish between several mechanisms that may create (mutate) new chromosomes to enter the active "chromosome pool". Figure C-1 illustrates the different mechanisms by which new chromosomes are created. The gray regions represent parts that are altered during the evolutionary process. A gray column indicates complete gene replacement. A gray rectangle indicates a single electrode that was replaced. The rate at which the GA will converge towards the global optimum is primarily determined by the rate that new chromosomes are created through these mechanisms.

The genetic algorithm optimization approach is well suited to finding optimal ERT surveys for two reasons. First, its evolutionary nature, with multiple regeneration processes, allows for identification of the global optimum without full analysis of the error surface. Second, unlike most techniques, genetic algorithms allow for the simultaneous use of more than one initial guess (*Coley*, 1999). In contrast, most

optimization techniques (e.g. conjugate gradient, steepest descent, etc.) use a single starting point to initiate the optimization process. For these approaches, much attention is paid to the selection of this starting point, as it is crucial for the performance of the optimization method.

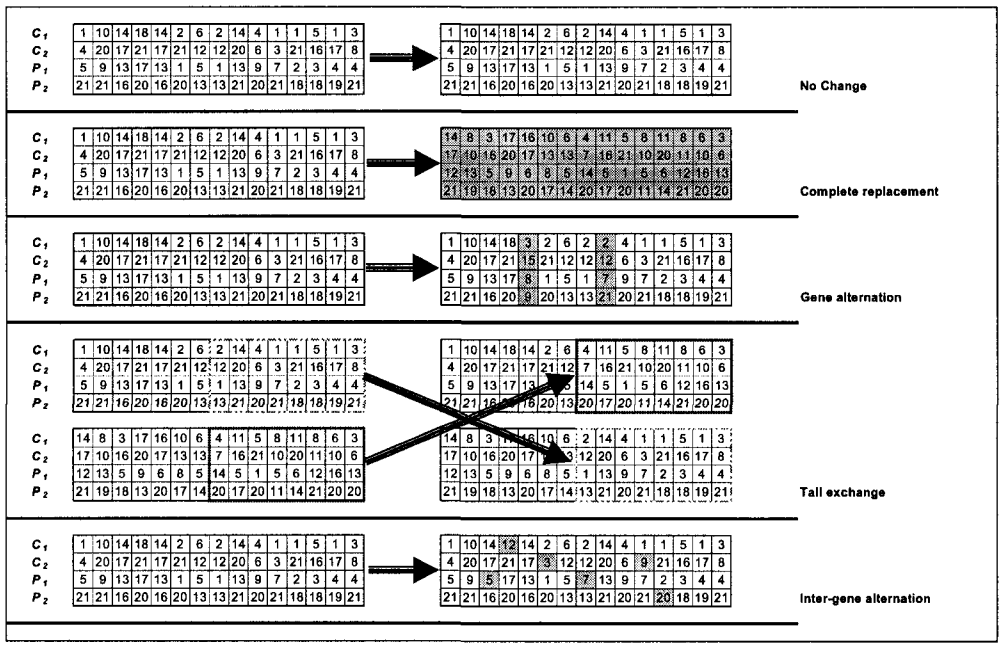

Figure C-1: Illustration of regeneration mechanisms. Numbers correspond to electrode numbers. Each survey (chromosome) has 15 4-electrode arrays.

To demonstrate the application of a genetic algorithm optimization to the selection of an optimal ERT array, we will search for the 15-array survey that gives the best representation of the electrical conductivity of the subsurface. One initial guess will be the locally optimized set, determined using the approach of *Furman et al.* (2002). The

contribution of this initial guess to the convergence rate will be examined. All other initial guesses will be comprised of random selections of electrodes.

We use a chromosome pool of fixed size, N. Five adaptive mechanisms, described below, generate N_1, N_2, N_3, N_4, and N_5 chromosomes at each generation, where $N_1+N_2+N_3+N_4+N_5 = N$. In general, the size of the chromosome pool as well as the size of each of the sub-groups may be changed at each generation. However, for simplicity, we use fixed values of $N_1 = N_2 = N_3 = N_4 = N_5 = 20$.

The first group of N_1 chromosomes is the group that shows the highest performance at any iteration (generation), which is also called the "elite" group. This group plays a crucial part in the GA, as members of this group are used to create some of the mutants that will enter the chromosome pool in the next generation. In evolutionary terms, these strong chromosomes are the only members to reproduce. The inclusion of such a group in the GA is called elitism. In this paper, chromosomes are chosen from the N_1 group, on a random basis. This (i.e. the random selection) allows the variation in the size of the different groups, as well as preventing oscillations near a local optimum.

The first adaptive mechanism is the random generation of new chromosomes. This generation of new initial guesses is one of the unique characteristics of GA that distinguishes it from many other optimization techniques. In this paper, we generate N_2 new chromosomes at each generation (i.e. iteration), replacing N_2 chromosomes from the previous generation.

All other mechanisms are essentially perturbations of existing chromosomes. This alternation of existing chromosomes is another aspect of GA that differs from other simple search methods. In order to speed convergence, chromosomes of group N_1 are used as bases for these alternations.

The second adaptive mechanism is complete gene perturbation. In each of the chromosomes in the N_3 group some N_3P ($N_3^P = 2$ in our example) genes (ERT arrays) are replaced by other randomly generated arrays. This keeps the majority of each of the best performing survey sets and changes only a few of the arrays composing it.

The third adaptive mechanism is the creation of new chromosomes through marriage. Two different parent chromosomes, typically (in this paper strictly) from the highest ranking group, N_1, are both broken at the same arbitrary point, and the four pieces are merged into two new chromosomes by switching the two "tails" of the original chromosomes. In this way, N_4 new chromosomes are generated at each iteration. In general any part of the chromosomes may be switched, however, we limit the mechanism in this paper to tail switching.

The fourth adaptive mechanism is alteration of internal parts of the gene. Unlike previous mechanisms, where a complete gene was replaced, here only a few electrodes in some of the genes composing a chromosome are changed. In each of the chromosomes in the N_5 group some N_5P ($N_5^P = 2$ in our example) electrodes are replaced by other randomly generated electrodes. Through this mechanism, N_5 chromosomes are generated at each iteration.

Evolution towards an optimal survey

After adapting, the GA evolves towards an optimal survey. The best N_1 surveys (chromosomes) are kept in the process. The other $(N_2 + N_3 + N_4 + N_5)$ surveys are rejected, and replaced by N_2 entirely new N_2 surveys; N_3 perturbations of the best N_1 surveys; N_4 surveys which are inter-duplications of the best N_1 chromosomes; and N_5 inter-gene alternations, as described above.

The process is repeated until a certain number of iterations (generations) have passed, or until no change is observed in the top ranked survey. Then, the top ranked survey is selected as the optimal survey set. In cases where the theoretical optimal value of the performance is known (but not the structure of the optimal solution), a convergence criteria may be defined.

The convergence rate of the algorithm depends on some arbitrary factors, such as the rate at which new arrays and new surveys enter the set, but also on the wisdom in the selection of these arrays (i.e. how well the adaptive mechanisms perform with regard to the specific problem). Statistical description of the distribution of sensitivity within each survey set may allow for a wiser selection of arrays, especially regarding which existing chromosomes (survey sets) are used to create new chromosomes. Analysis of the performance of the GA is, however, beyond the scope of this paper, and we limit ourselves here to demonstration of the applicability of GA to the identification of optimal ERT surveys.

Table C-1: parameters and notation

Parameter	Description
A	Total number of arrays in a survey
a	Array index
C	Current electrode
E	Array offset with regard to all perturbations
e	Array offset with regard to a perturbation
J	Total number of perturbations
j	Perturbation index
N_e	Number of electrodes
N	Total number of chromosomes in pool
N_1	Chromosomes in group 1 ("elite")
N_2	Chromosomes in group 2
N_3	Chromosomes in group 3
N_4	Chromosomes in group 4
N_5	Chromosomes in group 5
N_3^P	Number of array alternations in group 3
N_5^P	Number of electrode alternations in group 5
P	Potential electrode
S	Sensitivity
S^{max}	Maximal sensitivity
Z	Performance
α	Perturbation weighting factor
β	Offset weight
σ	Sensitivity standard deviation

Results and discussion

We present here the application of the ERT optimization scheme. Presented are results for the different types of objective functions (i.e. equations [6] and [9]), for a small demonstrative survey, and for small full-scale surveys. We also present the use of few parameters to allow control over the resultant sensitivity distribution.

Consider an ERT survey that consists of 21 electrodes, designed to determine the average subsurface EC with no consideration of the distribution of sensitivity ($\beta = 1$). Electrodes are placed along a line with 1 m separations between the electrodes. Assuming that we have no information regarding the EC distribution in the subsurface, we evenly distribute 28 perturbations in a triangular region of the subsurface beneath the electrodes (see Figure C-2). Note that all results may be scaled by the electrode separation.

For the optimization process we use a chromosome pool of $N = 100$ chromosomes, with N_1, N_2, N_3, N_4, and N_5 each equal to 20. Each chromosome includes $A = 15$ genes. We use 25,000 iterations (generations) in each run.

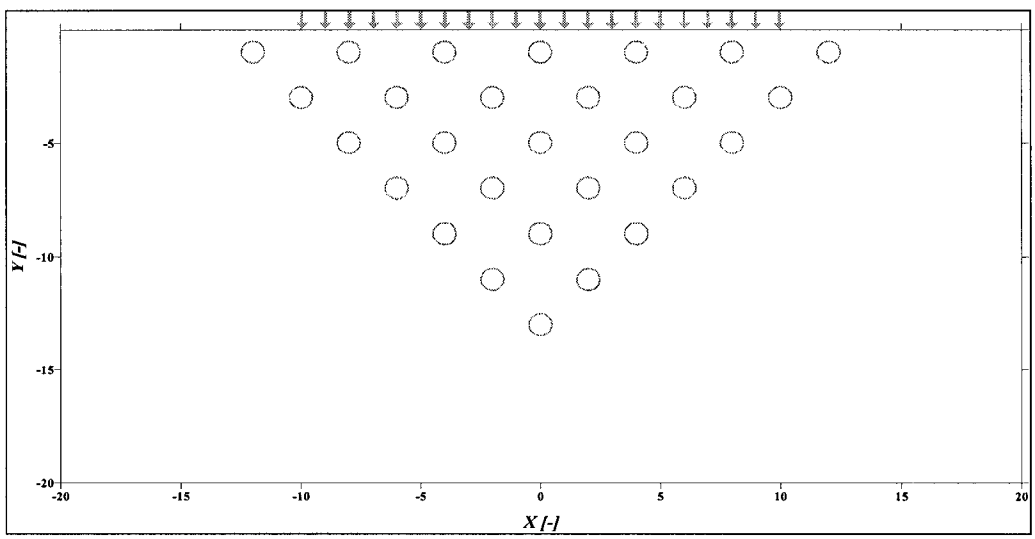

Figure C-2: locations of perturbations relative to locations of electrodes.

Twenty-one electrodes generate a gene space of 35,910 arrays. The total number of 15-array surveys that can be composed with these electrodes is approximately $2 \cdot 10^{68}$. It is

clear, then, that a systematic search for the optimal solution is not possible. Our algorithm only searches a maximum of $2.5 \cdot 10^6$ sets, which is a very small percentage of all possible sets. For the case of $\beta = 1$ and uniform α, the optimal survey can be identified directly by choosing the 15 arrays with the maximal average sensitivity. That is, the sensitivity of each array to all perturbations is calculated and averaged over all perturbations. Next, arrays are sorted by their average sensitivities, and the highest ranked arrays are selected.

Figure C-3 shows the evolution of the optimal survey performance through successive generations for several runs. As the algorithm relies on random number generation (e.g. for gene alternation), each run is unique and cannot be repeated. Therefore, each value or graph presented here is a single realization of the optimization process. The performance of the true optimal survey is $Z = 0.004568$ (shown as dash line in Figure C-3). In some realizations, the convergence towards the optimal solution may be immediate. It is important to note that the GA can not a priori guarantee reaching the global optimum within a certain number of generations. But, as shown in Figure C-3, the routine reaches the vicinity of the optimal solution within a relatively small number of sets searched compared to the solution space size.

To investigate the sensitivity of the optimization to the initial set of chromosomes, we considered an initial guess of a survey set composed of the arrays that show the highest sensitivity to individual perturbations. As suggested by *Furman et al.* (2002), a survey composed of such locally optimal arrays shows higher performance than those composed

of a single array type. As the number of perturbations used in the optimization process is not necessarily equal to the number of arrays in a survey, we randomly pick locally optimal arrays into an initial guess (chromosome). This random nature of array selection may make the initial guess non-realistic, composed of repeats of the same array; nevertheless, it is useful for computational reasons. The optimization routine ensures that the final optimal survey is a realistic one by rejecting non realistic solutions.

In Figure C-3 three more realizations that include a locally optimal initial guess are also presented. Note that the initial advantage of those surveys diminishes during optimization.

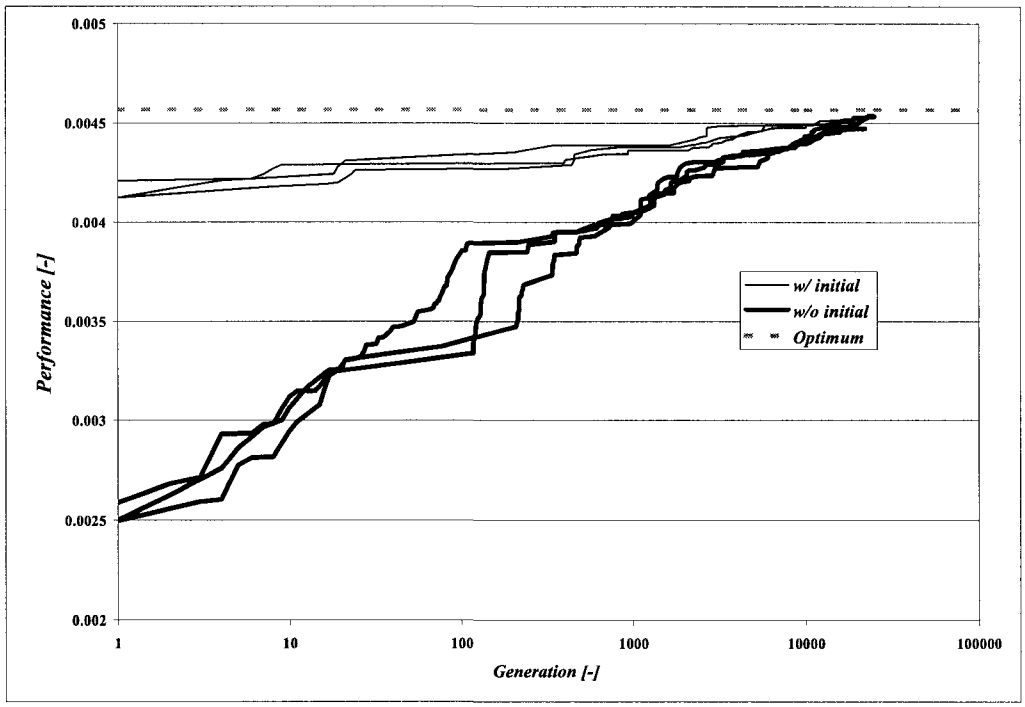

Figure C-3: six different realizations of the basic GA solution with $\beta = 1$.

Initially, the GAs rapidly approaches the optimum (Note that generations are plotted in log scale). Further iterations introduce relatively limited improvement. The incorporation of a wise initial starting point leads to slightly more rapid initial converge, but the final solution (i.e. after 25,000 iterations) is not improved. This suggests that the GA optimization is not sensitive to the initial guess. However, since the incorporation of initial guess is very cheap in terms of computational effort, there is no reason not to include it in the algorithm.

An important point for practical applications is the computation of time required for optimization. Although the exact number of processor operations ("flops") was not

measured, the following computational times were recorded for the runs presented in Figure C-3:

Setup (mainly calculation of the array sensitivities for all arrays and all perturbations) requires about 1 minute.

GA (iterations) requires about 3 minutes.

All calculations were all made on an Intel Pentium 4 machine with a processor speed of 2.4 GHz, and with 512 MB of RAM. Note that the computational effort for the first stage is more or less of order N_e^4, where N_e is the number of electrodes (computational effort is a linear function of the number of arrays that can be made of N_e electrodes, which is of order N_e^4). Computational effort increases approximately linearly with the number of perturbations.

Figure C-4 (top) presents the sensitivity map corresponding to a pseudo-optimal solution (i.e. that was obtained after 25,000 generations) for the 15-array survey with $\beta = 1$. As seen, the sensitivity is distributed relatively homogeneously in the region where the perturbations are located, but very little sensitivity is associated with the deeper perturbations (6 deepest perturbations are within the 90% cumulative sensitivity region).

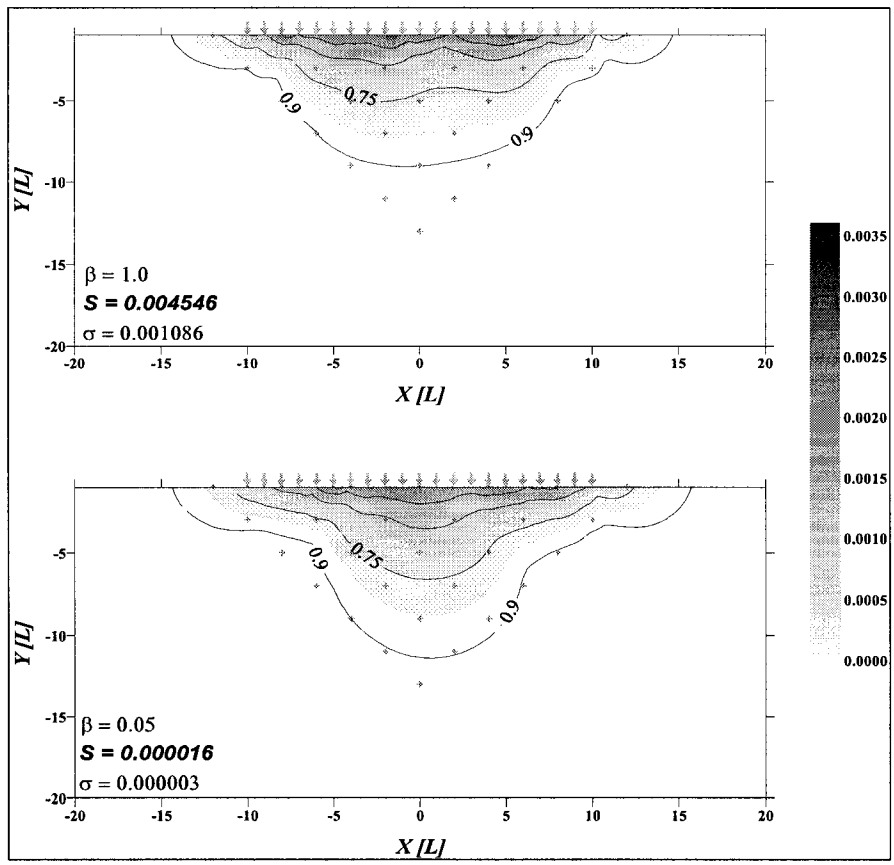

Figure C-4: sensitivity maps for optimal survey for $\beta = 1$ (top) and $\beta = 0.05$ (bottom). Locations of electrodes and perturbations are marked.

Effect of β value

So far we have presented results taking into consideration only the sensitivity (i.e. $\beta = 1$). Although controlled primarily by the distribution of the perturbations in the subsurface, the optimal solution in this case will prefer the shallower perturbations as these are of higher sensitivity. By applying a non-zero weight to the standard deviation of the offset, σ, we make the distribution of the offset (and hence the sensitivity) more homogeneous.

Figure C-4 (bottom) presents the sensitivity distributions of the 15-array optimal surveys using $\beta = 0.05$. Both cases (i.e. $\beta = 1$ and $\beta = 0.05$) are presented "per measurement" (i.e. values are normalized by the number of arrays). Both solutions are presented after 25,000 GA iterations. Note that as only 25,000 GA iterations were used, the solutions are not as smooth as a global solution (e.g. Figure C-5) looks. Increasing the number of generations used would reduce this effect.

The sensitivity distribution for the case of $\beta = 0.05$ is clearly more homogeneous as expressed by the standard deviation ($3 \cdot 10^{-6}$ for $\beta = 0.05$ compared with $4.5 \cdot 10^{-3}$ for $\beta = 1$), and as can be seen clearly by comparing the 0.9 cumulative sensitivity line in both panes of Figure C-4. The fractions of the domain that contain the most sensitive 25, 50, 75, and 90% of the cumulative sensitivity are 1.0, 2.8, 7.6, and 17.9%, respectively, for the $\beta = 1$ case, and 1.1, 3.2, 8.7, and 20.4% for the $\beta = 0.05$ case. The increase in sample areas due to the use of standard deviation weight is not huge, however it provide increased sensitivity mostly in the deep regions of the subsurface, leading to deeper investigation ability (in higher accuracy) of ERT.

The immediate conclusion is that the use of $\beta = 1$ (i.e. optimization for average sensitivity only) may result in a survey that is relatively shallow in penetration. This depends also on the spatial distribution of the perturbations in the subsurface.

While the use of non-zero weight increases the uniformity of the sensitivity, it also reduces the absolute value of the sensitivity. Maximal values of sensitivity for the $\beta = 1$

case are about $S = 0.0035$, while for the $\beta = 0.05$ case the maximal values are around $S = 0.0025$ (about 28% reduction).

Use of offset in objective function

As discussed before, the objective function of the optimization problem may be simplified by the use of the normalized offset instead of the sensitivity. In such cases, the optimal solution may be obtained directly by calculating the average normalized offset of each individual array (although this requires large computational effort, it still is manageable even for large electrode sets, as shown by the above estimations of computational time). Results presented in Figure C-5 and in Table C-2 make use of the offset in the objective function (equation [9]).

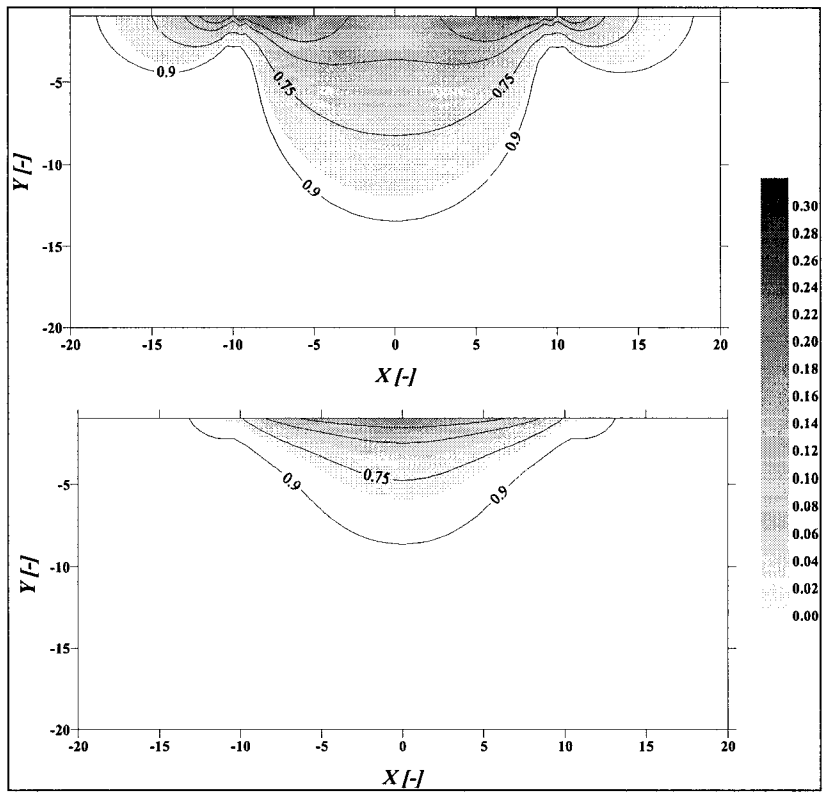

Figure C-5: sensitivity distributions for optimal (top) and Wenner (bottom) surveys

Commonly only one of three array types is used to form a survey: Wenner, Schlumberger, or double dipole. We compare here the spatial sensitivities and sample areas of these surveys, as defined by *Furman et al.* (2003), when analyzed for the same 28 perturbations used here. We also include the other survey presented by *Furman et al.* (2003), namely the partially overlapping survey with an offset of one.

For more direct comparison, we compare optimal surveys comprised of the same number of arrays as each of the other survey types (i.e. 63 for Wenner, 217 for Schlumberger, etc.). All results are obtained using equation [9] as the objective function.

None of the typically used survey types has a performance close to that of the optimal survey (Table C-2). The partially overlapping survey is an improvement compared to the classic surveys, but is still far from optimal.

Table C-2: performance of typical surveys

Survey	# of arrays	Performance	Optimal performance
Wenner	63	0.116	0.565
Schlumberger	217	0.107	0.538
Double dipole	297	0.019	0.530
Partially overlapping	171	0.249	0.544

While performance is a quantitative measure, it is hard to directly relate it to survey sensitivity. Therefore, we compare directly the sensitivity distributions and sample areas for optimal and typical surveys. Figure C-5 compares the spatial sensitivity distribution of the optimal survey to that of a Wenner survey. Shown are integrated sensitivity (i.e. summed over all arrays), and its distribution within the domain. For comparison with other surveys see *Furman et al.* (2003) [note that figures of *Furman et al.* (2003) are normalized by the number of arrays in each survey].

The sensitivity values are higher for the optimal solution than for the Wenner survey. The 25, 50, 75, and 90 percents sample areas of the optimal survey are much larger than those of the Wenner survey (2.2%, 6.8%, 15.8%, and 30.9%, respectively, for the optimal case, compared with 1.1%, 3.2%, 8.6%, and 20.4%, respectively, for the Wenner survey). This indicates that the sensitivity distribution of the optimal survey is more uniform than

of the Wenner survey (see *Furman et al.*, 2002), and that the sensitivity is higher throughout the domain.

Looking into the types of arrays composing the optimal survey (Figure C-5 and Table C-2) emphasize the idea that an optimal survey is not to be composed of a single array type as are classic surveys. For the case of 63 arrays in a survey, and with $\beta = 1$, the optimal set is composed of 18 Wenner-Schlumberger-like arrays (i.e. CPPC configuration, where C indicates a current electrode, and P indicates a potential electrode), 15 inverse Schlumberger-like arrays (i.e. PCCP configuration), and 30 partially overlapping arrays (i.e. CPCP or PCPC configuration). About the same ratio of array types is kept for wide range of survey sizes. None of the arrays composing the optimal survey is a double-dipole array (i.e. CCPP or PPCC configuration). The first double dipole array comes to the optimal set only if 14,559 arrays or more were used to compose a survey.

For all solutions presented in Figure C-5 and in Table C-2, almost all electrodes are used, but outer electrodes are used more often, leading to clear preference of the large arrays. Small arrays show an offset close to one for all deep perturbations. As a result, the optimal survey uses only the outer electrodes. This may be an advantage in terms of cabling and electrode mobilization. However, we speculate that it is likely that measurements that do not use wide variation of electrode spacings will not lead to a unique, or stable, inversion of EC distribution. Partially, this is because background noise may make measurements similar, leading to linearly dependent equations making the inverse solution highly under-specified.

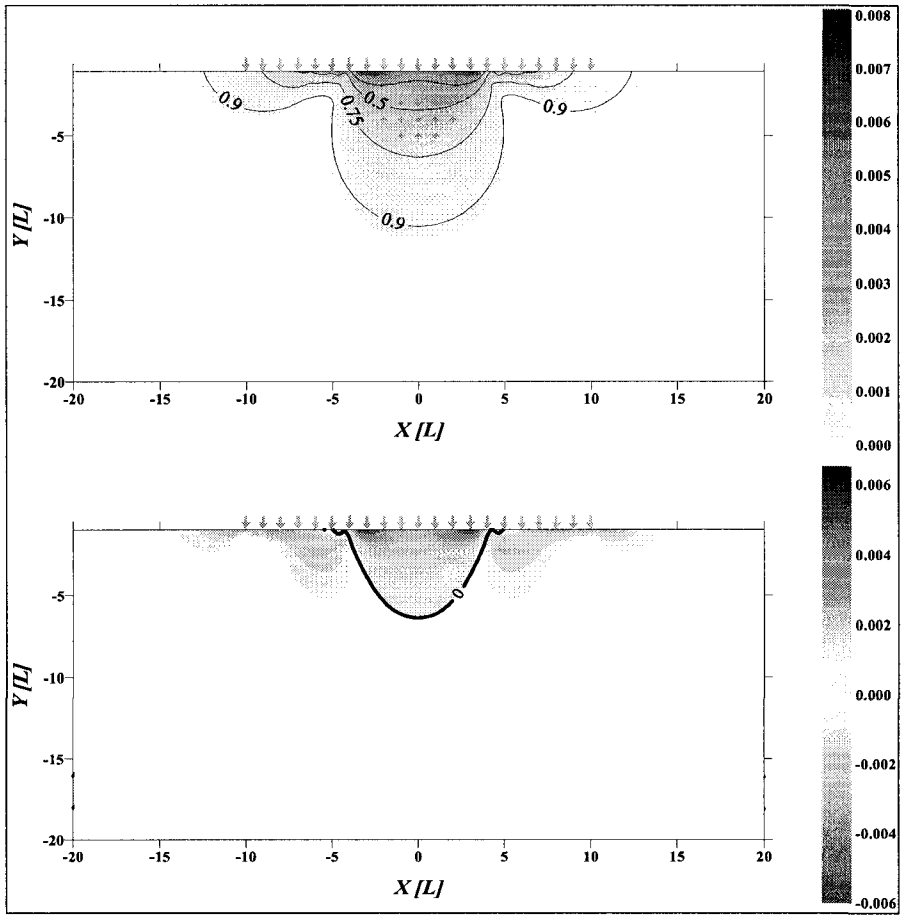

Figure C-6: Sensitivity distribution for targeted survey (top), and difference between the targeted and non-targeted (Figure C-5, top) cases (bottom). Locations of Electrodes and perturbations for targeted case are marked in both panes. Zero sensitivity change line is highlighted at bottom pane.

Spatial distribution of perturbations

One way to control the distribution of sensitivity is the use of the standard deviation of the sensitivity in the objective function. This is, however, a very limited method, which

allow mostly the enforcement of a homogeneous sensitivity distribution. In some cases, an ERT survey may be conducted to obtained information from a specific region of the subsurface. Examples may vary from archeological surveys, with prior knowledge of target depth, to the tracking of infiltration wetting front, where the approximate depth of the wetting front with time may be easily estimated. By specifying perturbation locations in the optimization process according to the desired regions in the subsurface where data is to be gathered, the ERT survey may be specifically targeted.

Consider as an example the design of a survey tailored to gather information from a smaller region than the original triangle presented in Figure C-2. Figure C-6 (top) presents the sensitivity map created using the optimal 15-electrode survey (using equation [9] as the objective function). Also marked are the locations of the 11 perturbations that we use to designate the target region for this case. To demonstrate the effect of targeting survey sensitivity, the spatial sensitivity of the targeted survey (Figure C-6, top) can be compared with the optimized spatial sensitivity based on a homogeneous distribution of perturbations (Figure C-5, top). The difference in sensitivities is shown in Figure C-6, bottom. Blue regions have increased sensitivity for the targeted case, and red regions have reduced sensitivity.

Figure C-6 is somewhat similar to Figure C-5 (top), except for the scale. The main difference is that the targets span over a shorter portion of the electrodes, forcing smaller arrays to enter the optimal set and therefore creating a more homogeneous distribution of the sensitivity near the surface (above the target). It is clear, however, that the use of

target perturbations created focusing of the sensitivity to that region. Note the sensitivity values that range between approximately 0.003 to 0.005 in the targeted case, compared with approximately 0.0015 to 0.0025 for the same region in Figure C-5 (top). As seen in Figure C-6 (bottom), the increase of sensitivity in the vicinity of the targeted perturbations comes mostly at the expense of sensitivity in outer regions.

Conclusions

A simple yet powerful approach is presented for the optimal selection of arrays to comprise a time-limited ERT survey. An objective function is defined for the optimal allocation of electrodes to achieve maximum cumulative survey sensitivity, based on perturbation placed in the subsurface. A more complex objective function can be used to consider both the distribution of the sensitivity and the maximum cumulative sensitivity to design a survey with a more uniform measurement sensitivity. For some cases this optimality criterion may be used directly. For cases where no direct solution is available, a simple genetic algorithm optimization is suggested. The convergence of this algorithm towards the optimal solution is tested for a few simple cases. It is shown that the algorithm converges to within 10% of the optimal value (in cases for which the optimum is known) within about 10,000 iterations. The use of a wise initial guess for the GA is showed to have impact on the initial convergence of the GA, but it does not necessarily improve the final solution. Computational effort and computational times are presented,

suggesting the method can be applied using modern computation to optimize surveys in real time during monitoring subsurface transient processes.

The optimal survey is composed of mixture of arrays of different types. One clear result is that double dipole arrays are seldom part of the optimal solution. In cases where the objective function looks only into the largest average sensitivity, clear preference for wide arrays is observed.

Two alternatives are suggested for the control of the distribution of the sensitivity. The first make use of a normalized form of the offset of an array from the perturbation's maximal sensitivity, resulting in a simplified objective function. The second alternative (which can also be combined with the first) makes use of a targeted allocation of perturbations to achieve a desired sensitivity distribution. The second approach opens the way to targeted ERT survey designs. This use of smart allocation of perturbations allows for the specific tailoring of an ERT survey according to survey goals, which may change with time when monitoring temporally changing field conditions.

Acknowledgments

This research was funded in part by SAHRA (Sustainability of Semi-Arid Hydrology and Riparian Areas) under the STC program of the National Science Foundation, agreement EAR-9876800. This research was also supported in part by Western Research Project W-188.

References

Advanced Geophysics Inc. (AGI), Austin, TX (found at www.agiusa.com, accessed Sep. 2002).

Archie, G.E. 1942. The electric resistivity log as an aid in determining some reservoir characteristics. *Trans. Am. Inst. Min. Metall. Pet. Eng.,* 146: 54-62.

Barker, R., J. Moore, 1998. The application of time-lapse electrical tomography in groundwater studies, *The Leading Edge*, pp. 1454-1458.

Buselli, G., K. Lu, 2001. Groundwater contamination monitoring with multichannel electrical and electromagnetic methods, *Journal of Applied Geophysics*, 48: 11-23.

Coley, D.A., 1999. An introduction to genetic algorithms for scientists and engineers, *World Scientific.*

Dahlin, T., M.H. Loke, 1998. Resolution of 2D Wenner resistivity imaging as assessed by numerical modeling, *Journal of Applied Geophysics*, 3: 237-249.

Dahlin, T., 2000. Short note on electrode charge-up effects in DC resistivity data acquisition using multi-electrode arrays, *Geophysical prospecting*, 48: 181-187.

Edlefsen, N.E., and A.B.C. Anderson. 1941. The four-electrode resistance method for measuring soil-moisture content under field conditions. *Soil Science*, 51: 367-376.

Furman, A., A.W. Warrick, T.P.A. Ferré, 2002a. Electrical Potential Distributions in Response to Applied Current in a Heterogeneous Subsurface: Solution for Circular Inclusions, *Vadose Zone Journal*, 1: 273-280.

Furman, A., T.P.A. Ferré, A.W. Warrick, 2003. A Sensitivity Analysis of Electrical-Resistance-Tomography Array Types Using Analytical Element Modeling, *Vadose Zone Journal*, 2: 416-423.

Grifiths, D.H., R.D. Barker, 1993. Two-dimensional resistivity imaging and modeling in areas of complex geology, *Journal of Applied Geophysics*, vol. 29, pp. 211-226.

Holland, J.H., 1975. Adaptation in natural and artificial systems, *Univ. of Michigan press*, Ann Arbor.

Ritz, M., H. Robain, E. Pevago, Y. Albouy, C. Camerlynck, M. Descloitres, A. Mariko, 1999. Improvement to resistivity pseudosection modeling by removal of near-surface inhomogeneity effects: application to a soil system in south Cameroon, *Geophysical Prospecting*, 47: 85-101.

Savic, D.A., G.A. Walters, 1997. Genetic algorithms for least-cost design of water distribution systems, J. of Water Resources Planing and Management, 123: 67-77.

Storz, H., W. Storz, F. Jacobs, 2000. Electrical resistivity tomography to investigate geological structure of the earth's upper crust, *Geophysical Prospecting*, 48: 455-471.

Sun, N-Z. 1994. Inverse problems in groundwater modeling, *Kluwer Academic Publishers*, pp. 337.

Wang, M., C. Zheng, 1998. Ground water management optimization using genetic algorithms and simulated annealing: Formulation and comparison, *Journal of the American Water Resources Association*, 34(3): 519-530.

Wardlaw, R.,M. Sharif, 1999. Evaluation of Genetic Algorithms for Optimal Reservoir System Operation, *Journal of Water Resources Planning and Management*, 125(1): 25-33.

Yadav, G.S., P.N. Singh, K.M. Srivastava, 1997. Fast method of resistivity sounding for shallow groundwater investigations, *Journal of Applied Geophysics*, 36: 45-52.

Zhou, W., B. Beck, A. Adams, 2002. Selection of electrode array to map sinkhole risk areas in karst terrenes using electrical resistivity tomography, *Proceedings of SAGEEP 2002*, EEGS, Las Vegas.

APPENDIX D: LAPLACE-TRANSFORM ANALYTIC ELEMENT SOLUTION OF TRANSIENT FLOW IN POROUS MEDIA

Alex Furman, Shlomo P. Neuman

Accepted for publication in Advances in Water Resources (Sept. 2003)

Abstract

A Laplace-transform analytic element method (LT-AEM) is described for the solution of transient flow problems in porous media. Following Laplace transformation of the original flow problem, the analytic element method (AEM) is used to solve the resultant time-independent modified Helmholtz equations, and the solution is inverted numerically back into the time domain. The solution is entirely general, retaining the mathematical elegance and computational efficiency of the AEM while being amenable to parallel computation. It is especially well suited for problems in which a solution is required at a limited number of points in space-time, and for problems involving materials with sharply contrasting hydraulic properties. We illustrate the LT-AEM on transient flow through a uniform confined aquifer with a circular inclusion of contrasting hydraulic conductivity and specific storage. Our results compare well with published analytical solutions in the special case of radial flow.

Introduction

The analytic element method (AEM) was developed in its present form by *Strack* (1989) and his students starting in the 1970s. Examples of important applications include the National Groundwater Model of The Netherlands and the Metropolitan Groundwater

Model of Minneapolis/Saint Paul in Minnesota (*De Lang and Strack*, 1999) as well as a model of regional groundwater flow around Yucca Mountain in Nevada (*Bakker et al.*, 1999). Recent advances (e.g. (*Janković and Barnes*, 1999; *Barnes and Janković*, 1999) allow simulating highly heterogeneous subsurface flow conditions with a large number of circular (or spherical) inhomogeneities. The method's efficiency and accuracy in handling conditions near material interfaces makes it attractive for application to unsaturated flow around a circular Gardner inclusion (*Warrick and Knight*, 2002) and the flow of electrical current through nonhomogeneous materials (*Furman et al.*, 2002). The AEM has also been used in the context of solute transport and inverse (parameter estimation) problems (e.g. *Janković*, 2002). A recent review of the method and its application was presented by *Strack* (2003).

The AEM consists of superimposing analytic solutions corresponding to various individual features of the flow domain. Detailed descriptions of the AEM and its theoretical basis can be found in the books of *Strack* (1989) and *Haitjema* (1995). To date, the theory and its applications were limited largely to steady state. Attempts to develop transient versions of the AEM have required sacrificing some of its most attractive features. *Haitjema and Strack* (1985) accounted for transient effects by discretizing the flow domain into triangular finite elements (i.e. to represent storage) and using finite differences in time (see also *Janković and Barnes, 2000; Janković et al.*, 2001), thereby eliminating one of the AEM's major advantages (of avoiding numerical discretization). *Zaadnoordijk* (1988) and *Zaadnoordijk and Strack* (1993) developed transient analytic elements for point, line and area sources and for point and line doublets.

Lack of convergence to steady state prompted *Zaadnoordijk* (1988) to develop a correction element in the form of ring source. According to *Zaadnoordijk* (1998), this was motivated by the fact that the AEM, and some analytic solutions such as that of *Theis* (1935), apply to infinite domains. The approach of *Zaadnoordijk* (1988) requires adding transient elements each time that well discharge or other sink or source terms change in magnitude, rendering it cumbersome in realistic applications. The method is presently limited to a far narrower class of problems than is the traditional steady state AEM. Recent work along similar lines was published by *Bakker et al.* (2002) and *Bakker* (2003).

We present a Laplace-transform analytic element method (LT-AEM) for the solution of transient flow problems in porous media that is entirely general and retains both the mathematical elegance and the computational efficiency of the AEM, in Laplace space, while being amenable to parallel computation. Our method relies on Laplace transformation of the original flow problem, analytic element solution of the resultant time-independent modified Helmholtz equation, and numerical inversion of the Laplace transformed solution. The Laplace-transform analytic element method (LT-AEM) is especially well suited for problems in which a solution is required at a limited number of points in space-time, and for problems involving materials with sharply contrasting hydraulic properties. We demonstrate the method by solving the problem of transient flow to a well through a uniform confined aquifer with a circular inclusion of contrasting hydraulic conductivity and specific storage, and compare it with published analytical solutions for the special case of radial flow.

Mathematical solution

General approach

The Laplace transform of any time-dependent function *f(t)* is (e.g. *Bateman*, 1954; *Gradshteyn and Ryzhik*, 2000)

$$[1] \qquad L\left[f(t)\right] = \overline{f}(p) = \int_0^\infty f(t) e^{-pt} dt$$

where $p > 0$ is a parameter having inverse time dimension. The corresponding inverse Laplace transform is

$$[2] \qquad L^{-1}\left[\overline{f}(p)\right] = f(t) = \frac{1}{2\pi i} \int_{\gamma - i\infty}^{\gamma + i\infty} \overline{f}(p) e^{pt} dp$$

where γ is a real number chosen to be larger than the real value of any singularity in $\overline{f}(p)$ and $i = \sqrt{-1}$ is an imaginary number.

The first step in LT-AEM is to apply Laplace transformation to the partial differential equation (PDE) and related boundary and/or interface conditions. This results in time-independent PDE and boundary/interface conditions that incorporate the initial conditions and depend on the Laplace parameter p. The latter is solved by an AEM approach and the result back transformed into the time domain using numerical Laplace inversion. We use an algorithm developed by *Crump* (1976) and perfected by *De Hoog et al.* (1982), which yields time-domain solutions corresponding to discrete values of p. As these solutions are independent of each other, they are amenable to parallel computation.

Two dimensional application

Consider two-dimensional transient confined flow governed by the linear diffusion equation

$$[3] \qquad \frac{\partial^2 \Phi}{\partial x^2} + \frac{\partial^2 \Phi}{\partial y^2} = \frac{1}{\alpha} \frac{\partial \Phi}{\partial t}$$

where $\Phi = Kh$ is discharge potential, K is hydraulic conductivity, h is hydraulic head, $\alpha = K/S_s$ is hydraulic diffusivity and S_s is specific storage. For application to unconfined aquifers one would have to adopt the Dupuit assumption, linearize the corresponding Bousinesq equation, and redefine the discharge potential and hydraulic diffusivity as $\Phi = Kh^2/2$ and $\alpha = Kh_{av} / S_Y$ where h_{av} is vertically averaged head or water table elevation relative to the aquifer bottom and S_Y is specific yield. It is important to note that non-linear problems are difficult to transform into the Laplace domain and require linearization to be solvable via the AEM. Taking the Laplace transform of [3] yields

$$[4] \qquad \frac{\partial^2 \overline{\Phi}}{\partial x^2} + \frac{\partial^2 \overline{\Phi}}{\partial y^2} = \frac{1}{\alpha}\left[p\overline{\Phi} - \Phi_0 \right]$$

where $\overline{\Phi}$ is the Laplace transform of Φ and Φ_0 is the initial discharge potential. For simplicity we set $\Phi_0 \equiv 0$ so that [4] becomes the modified Helmholtz equation. In the case of nonzero Φ_0 the solution in Laplace space would be the sum of two components, one

forming the solution of the modified Helmholtz equation with $\Phi_0 \equiv 0$, and one forming the solution of a Poisson equation with a nonzero source term Φ_0.

The AEM typically deals with infinite domains without external boundaries. In the future, it may be desirable to allow the incorporation of external boundaries in AEM. Both external and internal boundary conditions (e.g. interfaces between regions of different hydraulic conductivities) must, if they exist, be subjected to Laplace transformation.

We present below two elements in connection with the LT-AEM: point source and a circular inhomogeneity. The two elements are developed in different ways which are equally valid. The point source is developed entirely in the time domain and the solution is transformed to the Laplace domain. The circular inhomogeneity is developed entirely in the Laplace domain.

It is important to understand that for a wider application of the LT-AEM than that presented here, additional element types need to be developed. A solution for a line sink may be obtained following *Bakker and Strack* (2003).

Point source

In a two-dimensional plane, the discharge potential due to an instantaneous point source of strength q at the origin, occurring at time τ and satisfying the linear diffusion equation [3], is (*Carslaw and Jaeger*, 1959, eq. [10.3.1])

$$[5] \qquad \Phi = \frac{q}{4\pi\alpha(t-\tau)} e^{-\frac{r^2}{4\alpha(t-\tau)}}$$

where r is radial distance from the origin. Source strength is defined as the volume of water V injected per unit specific storage, $q = V / S_s$. The incremental potential due to a source of infinitesimal strength $dq(\tau) = c(\tau)d\tau$, where $c(\tau)$ is a finite time rate, is then given by

$$[6] \qquad d\Phi = \frac{c(\tau)d\tau}{4\pi\alpha(t-\tau)} e^{-\frac{r^2}{4\alpha(t-\tau)}}$$

Considering that $c = Q / S_s$ where Q is the volumetric rate of water injection and integrating yields

$$[7] \qquad \Phi = \frac{1}{4\pi}\int_0^t \frac{Q(\tau)}{(t-\tau)} e^{-\frac{r^2}{4\alpha(t-\tau)}} d\tau$$

This is a convolution integral whose Laplace transform is (*Bateman*, 1954, eq. [20], pp. 131)

$$[8] \qquad \overline{\Phi} = \frac{\overline{Q}(\tau)}{2\pi} \mathrm{K}_0\left(r\sqrt{\frac{p}{\alpha}}\right)$$

where K_0 is a modified Bessel function of second kind and zero order. Equation [8] is a solution of the modified Helmholtz equation in radial coordinates,

$$[9] \qquad \frac{\partial^2\overline{\Phi}}{\partial r^2} + \frac{1}{r}\frac{\partial\overline{\Phi}}{\partial r} - \frac{p}{\alpha}\overline{\Phi} = 0$$

In the special case where injection occurs at a constant rate Q_p starting at time τ,

$$[10] \qquad Q(t \mid \tau) = Q_p H(t-\tau)$$

where H is the unit step (Heaviside) function. Taking Laplace transform gives (*Gradshteyn and Ryzhik*, 2000, eq. [93], p. 1107)

$$[11] \qquad \bar{Q}(p \mid \tau) = Q_p \frac{e^{-p\tau}}{p}$$

Substituting into [8] yields

$$[12] \qquad \bar{\Phi} = \frac{Q_p e^{-p\tau}}{2\pi p} \mathrm{K}_0\left(r\sqrt{\frac{p}{\alpha}}\right)$$

which agrees with a solution presented by *De Glee* (1930) and *Jacob* (1946).

Circular inhomogeneity

To account for a circular inhomogeneity, we apply separation of variables to the modified Helmholtz equation

$$[13] \qquad \bar{\Phi} = \sum_{n=0}^{\infty} R_n(r)\Psi_n(\psi)$$

where r is radial distance from the center of the inhomogeneity and ψ is a polar angle measured counterclockwise from the positive x axis. The corresponding solution is (*Moon and Spencer*, 1961, page 15)

$$[14] \qquad R_n(r) = A_n \mathrm{J_n}\left(i\sqrt{\frac{p}{\alpha}}r\right) + B_n \mathrm{Y_n}\left(i\sqrt{\frac{p}{\alpha}}r\right)$$

$$[15] \qquad \Psi_n(\psi) = C_n \sin(n\psi) + D_n \cos(n\psi)$$

where A, B, C, and D are coefficients and $\mathrm{J_n}$ and $\mathrm{Y_n}$ are Bessel functions of the first and second kind and order n, respectively. The latter can be replaced by modified Bessel functions upon eliminating the complex parameter, i, from their arguments. The complete form is then

$$[16] \qquad \overline{\Phi} = \sum_{n=0}^{\infty} A_n^* \mathrm{I_n}(\lambda r)\sin(n\psi) + B_n^* \mathrm{I_n}(\lambda r)\cos(n\psi) + C_n^* \mathrm{K_n}(\lambda r)\sin(n\psi) + D_n^* \mathrm{K_n}(\lambda r)\cos(n\psi)$$

where the superscript * indicates coefficient that are not the same as those used in equations [14] and [15]. Equation [16] is written twice, for the interior and for the exterior of the inhomogeneity. The behavior of Bessel functions at $r = 0$ and $r = \infty$ omits some of the product coefficients, resulting in expressions written as

$$[17] \qquad \overline{\Phi}^{+}(r,\psi) = \sum_{n=0}^{\infty} \frac{\mathrm{K_n}\left(r\sqrt{\frac{p}{\alpha}}\right)\left[a_n \cos(n\psi) + b_n \sin(n\psi)\right]}{\mathrm{K_n}\left(r_0\sqrt{\frac{p}{\alpha}}\right)}$$

in the exterior of the inclusion and as

$$[18] \qquad \overline{\Phi}^{-}(r,\psi) = \sum_{n=0}^{\infty} \frac{\mathrm{I_n}\left(r\sqrt{\frac{p}{\alpha}}\right)\left[c_n \cos(n\psi) + d_n \sin(n\psi)\right]}{\mathrm{I_n}\left(r_0\sqrt{\frac{p}{\alpha}}\right)}$$

in the interior, where r_0 is the radius of the inclusion; a, b, c and d are coefficients; and $\mathrm{I_n}$ and $\mathrm{K_n}$ are modified Bessel functions of the first and second kind and order n, respectively. Normalization is not necessary but useful for matching purposes (i.e. in the matching phase $r = r_0$, and hence the ratio of the Bessel functions is unity and need not be computed). Truncating the series at $n = N - 1$ leaves a finite number of $4N$ coefficients. Of these, two (b_0 and d_0) need not to be computed as they do not contribute to the function. These are determined by insuring that the solution satisfies continuity of head and normal flux

$$[19] \qquad \frac{\overline{\Phi}^{+}(r_0,\psi) + \overline{\Phi}_B}{K^{+}} = \frac{\overline{\Phi}^{-}(r_0,\psi) + \overline{\Phi}_B}{K^{-}}$$

$$[20] \qquad \left.\frac{\partial \overline{\Phi}^{+}}{\partial r}\right|_{(r_0,\psi)} = \left.\frac{\partial \overline{\Phi}^{-}}{\partial r}\right|_{(r_0,\psi)}$$

at $M > 4N$ (*Barnes and Janković*, 1999; *Janković and Barnes*, 1999; *Strack*, 2003) discrete nodal points on the interface, where the subscript B designates background discharge potential that is not due to the circular inhomogeneity.

In traditional AEM, one either maintains exact continuity of flux and approximate continuity of heads across interfaces between inhomogeneities (e.g. *Barnes and Janković*, 1999) or the reverse (*Warrick and Knight*, 2002). Our approach requires approximating both to within an error that is explored numerically later. The corresponding over-determined system of discrete equations,

$$[21] \quad \frac{1}{K^+}\sum_{n=0}^{N-1}\left[a_n\cos(n\psi)+b_n\sin(n\psi)\right]+\frac{\bar{\Phi}_B}{K^+}=\frac{1}{K^-}\sum_{n=0}^{N-1}\left[c_n\cos(n\psi)+d_n\sin(n\psi)\right]+\frac{\bar{\Phi}_B}{K^-}$$

$$[22] \quad \sum_{n=0}^{N-1}\frac{\partial \mathrm{K_n}(r)}{\partial r}\left[a_n\cos(n\psi)+b_n\sin(n\psi)\right]=\sum_{n=0}^{N-1}\frac{\partial \mathrm{I_n}(r)}{\partial r}\left[c_n\cos(n\psi)+d_n\sin(n\psi)\right]$$

where

$$[23] \quad \frac{\partial \mathrm{I_n}(r)}{\partial r}=\begin{cases}\mathrm{I_1}(r) & n=0\\ \frac{1}{2}\left[\mathrm{I_{n-1}}(r)+\mathrm{I_{n+1}}(r)\right] & n\neq 0\end{cases}$$

$$[24] \quad \frac{\partial \mathrm{K_n}(r)}{\partial r}=\begin{cases}-\mathrm{K_1}(r) & n=0\\ -\frac{1}{2}\left[\mathrm{K_{n-1}}(r)+\mathrm{K_{n+1}}(r)\right] & n\neq 0\end{cases}$$

is solved by least squares or any other suitable optimization method.

Inverse Laplace transform

To invert the Laplace solution we used a *Matlab* (2002) code due to *Hollenbeck* (1998) based on the algorithm of *De Hoog et al.* (1982). We modified the algorithm slightly to allow computing the AEM parameters in Laplace space only once for each discrete value of p. These parameters can then be used efficiently to compute the discharge potential at an arbitrarily large number of points in real space corresponding to each p. Though solutions at various p values are easily computed in parallel (further enhancing computational efficiency), we have not done so in the examples presented here.

Numerical Implementation

We illustrate the LT-AEM on transient flow through a uniform confined aquifer with a circular inclusion of contrasting transmissivity and storativity, and compare our results with published analytical solutions in the special case of radial flow. Some estimates of computational efficiency are also given.

Single circular inhomogeneity and single well

We consider a two-dimensional flow domain of unit thickness and infinite lateral extent. The domain has a uniform hydraulic diffusivity $\alpha_0 = 10^4$ (hydraulic conductivity $K_0 = 1$ and specific storage $S_{s0} = 0.0001$) except for a circular inclusion of radius $r_0 = 1$ centered

about $(x_c, y_c) = (2, 2)$ that may have a different hydraulic diffusivity α_1 (hydraulic conductivity K_1 and specific storage S_{s1}). The discharge potential throughout the domain is initially uniform. At time $t = 0$, a well located at $(x_w, y_w) = (0, 0)$ starts injecting water at a constant rate of $Q = 1$. All quantities are given in arbitrary consistent length and time units.

The potential due to the well is described by [12]. The potential in the interior of the circular inhomogeneity is given by [16] and in its exterior by [17]. We solve the corresponding transient flow problem (equations [21] and [22]) using $N - 1 = 20$ terms in each series and $M = 100$ nodal points spaced evenly along the circumference of the inclusion. Values of M and N were selected to be large enough based on the authors experience in similar problems (*Furman et al.*, 2002). Since we deal with a relatively simple problem, corresponding values of are due only to the well and computed solely using equation [12].

Contours of equal head are shown in Figure D-1 at four different times following the onset of injection when $\alpha_1 = 10^6$ ($K_1 = 100$ and $S_{s1} = 0.0001$). Detailed contours in the inclusion and its immediate vicinity at $t = 1$ when $\alpha_1 = 10^5$ ($K_1 = 10$ and $S_{s1} = 0.0001$) are shown in Figure D-2. Properties were selected so as to achieve visual clarity of relevant effects.

As the conductivity of the inclusion is higher than that of the surrounding material, the former acts as a focusing lens causing flow to converge toward it and diverge away from it, as evident from the lower gradients inside the inclusion.

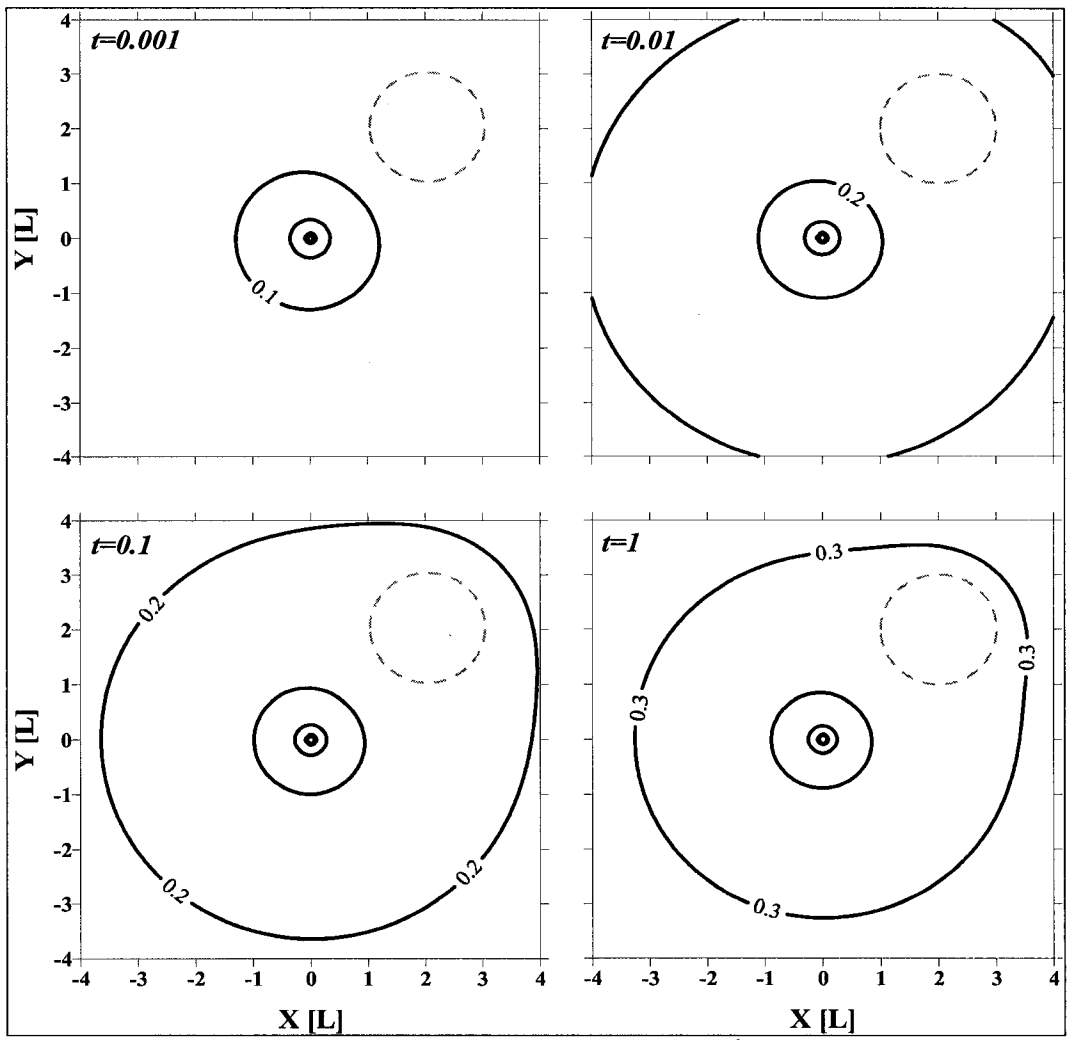

Figure D-1: Time evolution of head around well when $\alpha_1 = 10^6$ ($K_1 = 100$ and $S_s = 0.0001$).

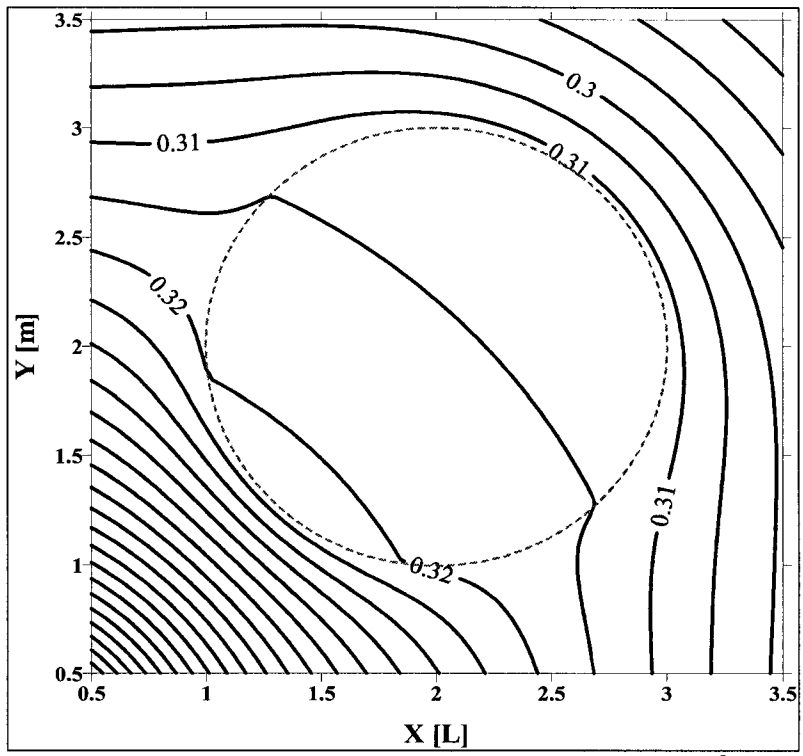

Figure D-2: Head contours in inclusion and vicinity at $t = 1$ when $\alpha_I = 10^5$ ($K_I = 10$ and $S_s = 0.0001$).

The effect of changing the hydraulic conductivity of the inclusion on head distribution at $t = 1$ for the original case (i.e. $S_s = 0.0001$) is presented in Figure D-3. When $K_I < K_0$ the inclusion acts as a scattering lens, causing approaching flow to diverge and receding flow to converge. Hence, a conductive inclusion transmits the well signal faster and a resistant inclusion more slowly than would a uniform medium.

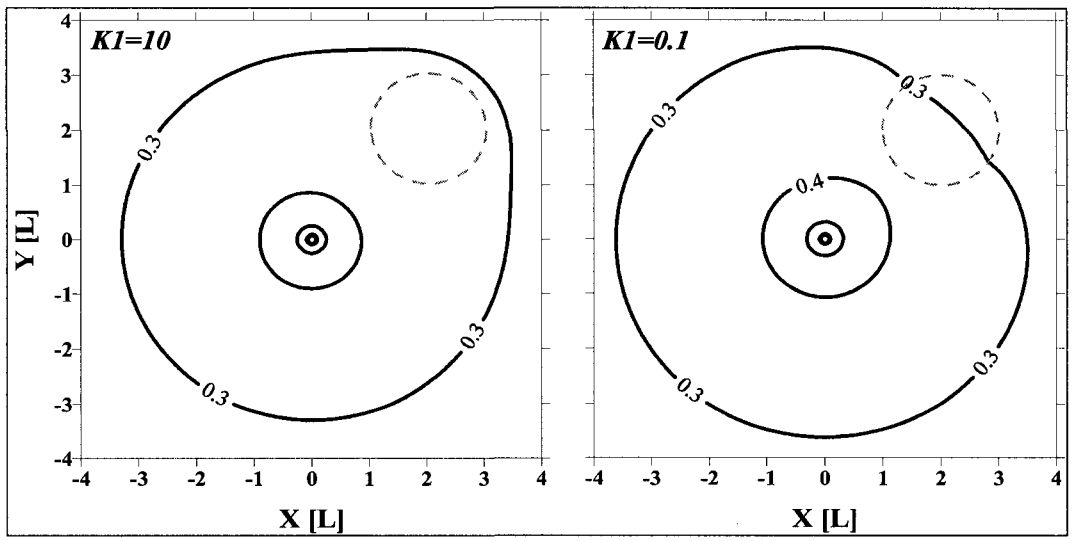

Figure D-3: Effect of inclusion conductivity on head contours at t = 1 for S_s = 0.0001.

Figure D-4 shows what happens at $t = 1$ when specific storage throughout the system (both background and inclusion) is reduced by a factor of 10, keeping the original hydraulic conductivity (i.e. $K_0 = 1$, $K_1 = 100$). Whereas the head values increase (the injection signal propagates faster than it did before), the shape of the head contours remains virtually unaffected, except for minor changes in the vicinity of the inclusion. Keeping the original value of $S_s = 0.0001$ in the domain but increasing the specific storage of the inclusion by a factor of 100 results in modified head contours as depicted in Figure D-5. The effect is limited largely to the inclusion and its immediate surroundings.

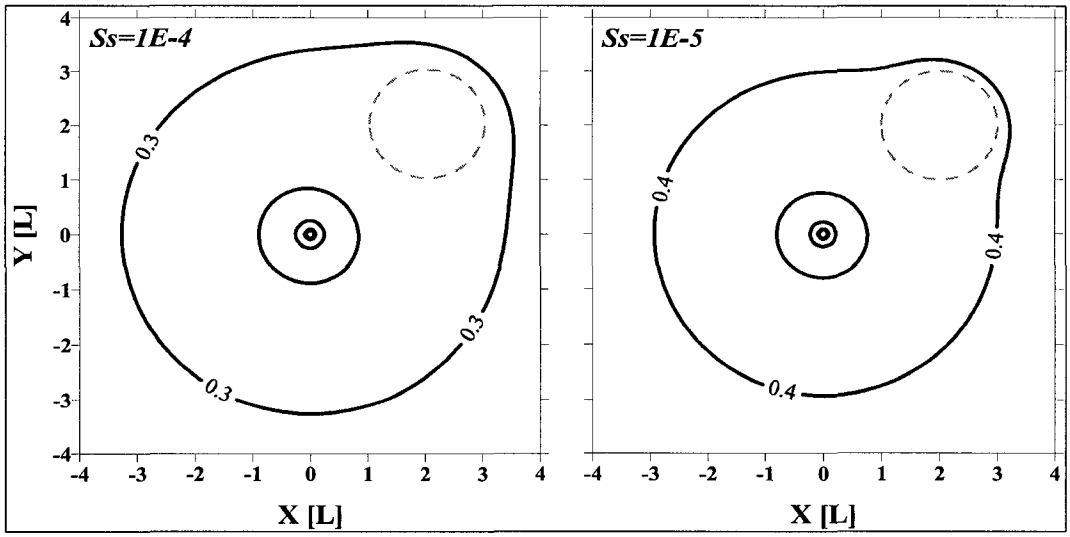

Figure D-4: Effect of specific storage on head contours at t = 1 for K_0 = 1 and K_1 = 100.

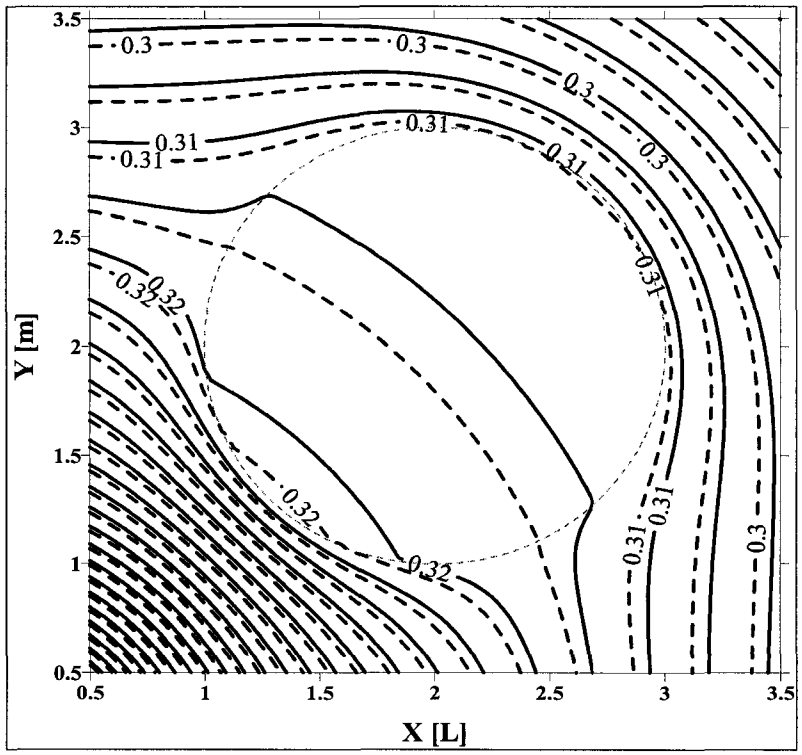

Figure D-5: Head contours at t = 1 resulting from background specific storage S_s = 0.0001 (solid) and 100-fold increase in specific storage of inclusion (dashed) when K_0 = 1, K_1 = 100.

Comparison with Analytical Solutions

Sternberg (1969, see appendix) published an analytical solution for transient flow to a fully penetrating well at the center of a circular inclusion in an otherwise uniform confined aquifer. The well has finite radius and pumps at a constant rate Q. To derive his solution, Sternberg used an approximate inverse Laplace transform.

Since our LT-AEM solution treats the well as a point sink of zero radius, we compare it in Figure D-6 with *Sternberg's* (1969) finite radius solution by setting $r_w = 10^{-4}$. The well pumps at a rate $Q = 1$ from the center of a circular inclusion of radius r0 = 1, hydraulic conductivity and specific storage $S_s = 0.001$. The surrounding aquifer has hydraulic conductivity $K_0 = 1$ and a similar specific storage. Figure D-6 compares the two solutions at $t = 1$ for the homogeneous case [H] where $K_1 = 1$, a high-conductivity inclusion [+] with $K_1 = 2$, and a low conductivity inclusion [-] with $K_1 = 0.5$. A comparison to the *Theis* (1935) solution, computed using an approximation in *Abramowitz and Stegun* (1964, equation [5.1.53]), is included for reference (Figure D-7).

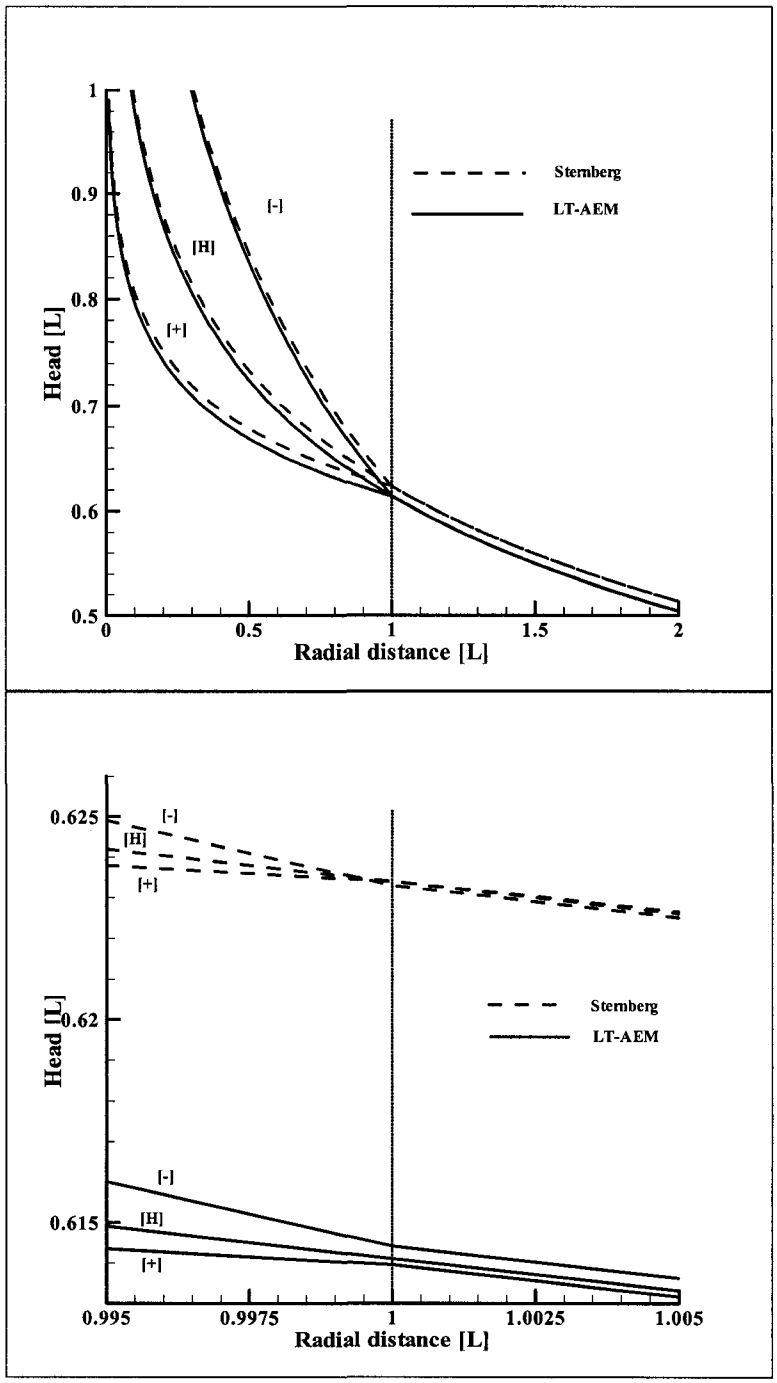

Figure D-6: Comparison with Sternberg's (1969) analytical solution for pumping well at center of circular inhomogeneity. [H] represents homogeneous aquifer, [+] inclusion with elevated conductivity and [-] with reduced conductivity. Lower pane shows details around interface.

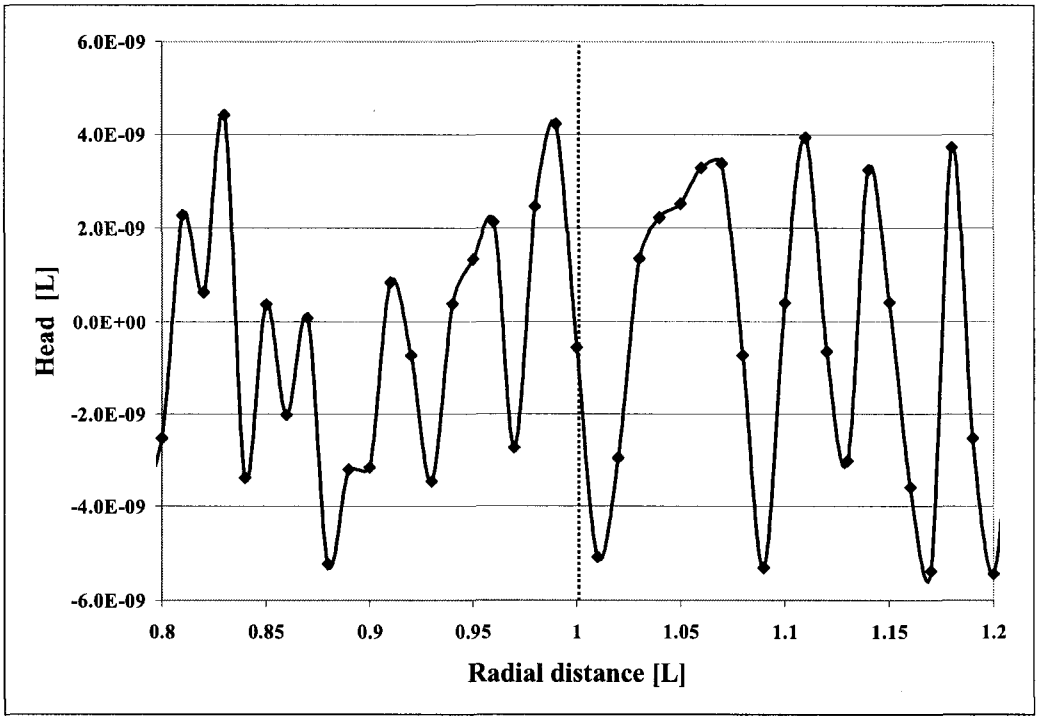

Figure D-7: Difference between Theis solution and the LT-AEM for a homogeneous case. Black diamonds indicate locations where values were computed.

The LT-AEM solution practically coincides with the *Theis* (1935) solution in the homogeneous case (the maximum difference between the two solutions being of order 10^{-9}). *Sternberg's* (1969) solution lies close but consistently above the LT-AEM solution. We attribute the slight difference between these two solutions to *Sternberg's* reliance on the approximate analytical inverse Laplace transform of *Schapery* (1961). Whereas *Sternberg's* solution yields a unique head in the surrounding aquifer for all three cases,

the LT-AEM solution shows that the effect of a high- or low-conductivity inclusion persists beyond its outer radius (see right pane of Figure D-6).

Computational efficiency

All computations were performed using *Matlab* (2002, version 6.1) on an Intel Pentium 4 computer with processor speed of 2 GHz and 1 GB of RAM. The total time required to compute (and print, on a point-by-point basis) 1681 values to plot a pane (e.g. Figure D-5) was approximately 450 s. Of this, approximately 100 s were used to estimate coefficients and 350 s to compute and print head contours. One should be able to render the computation much more efficient by (a) using a lower level programming language, (b) parallelizing and (c) optimizing the LT-AEM algorithm and code.

Error analysis

As mentioned earlier, flux and head compatibility conditions are approximated across the inhomogeneity interface. This is in contrast with the approach used for inhomogeneities in the steady state case (e.g. *Barnes and Janković*, 1999; *Warrick and Knight*, 2002), where one of these conditions (either flux or head) can be satisfied automatically. To estimate the error involved in our formulation, and to provide a measure of its accuracy, we plot in Figure D-8 heads and fluxes at the interface and corresponding jumps in these quantities across the interface for $p = 1$. All other parameters are those used in Figure D-

1. As seen, the differences between the internal and the external quantities are smaller by factors of 10^{11} to 10^{14} than the quantities themselves, indicating high accuracy.

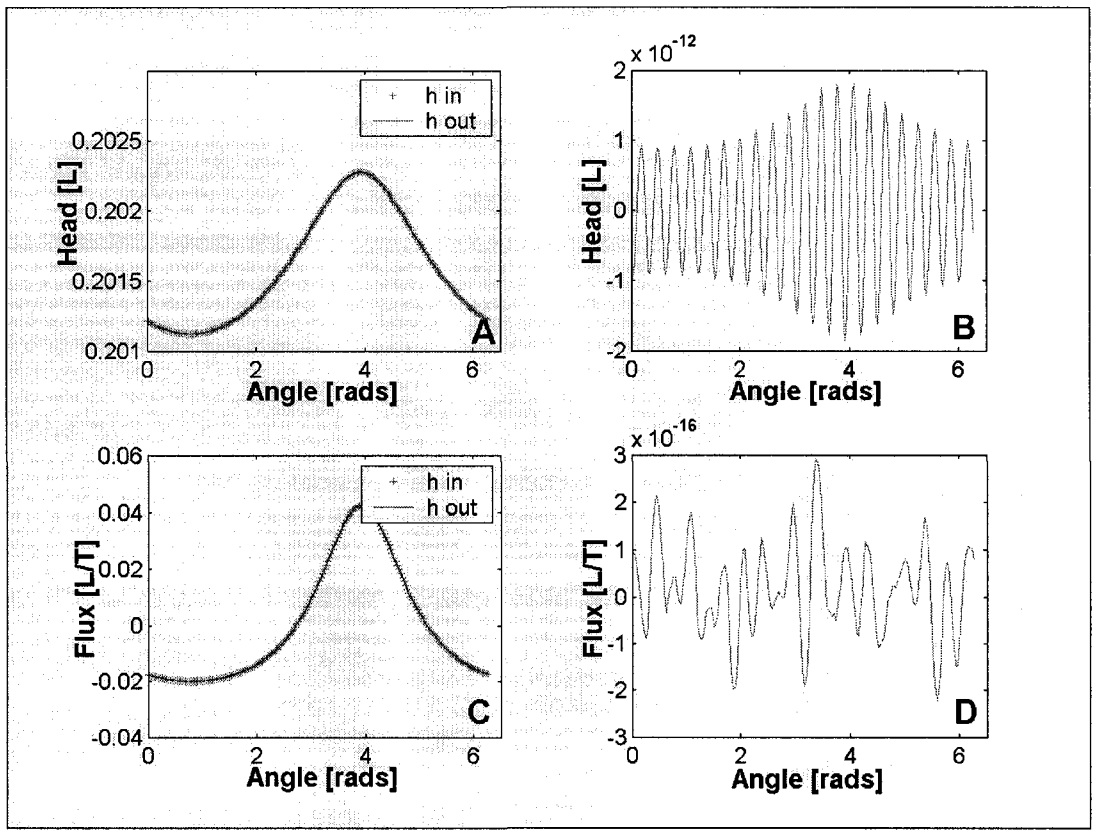

Figure D-8: A) Heads, and fluxes (C) for p = 1 along the inhomogeneity boundary; B) head, and flux (D) differences (in – out) for p = 1 across the inhomogeneity. Properties are consistent with Figure D-1.

The accuracy of the method depends also on the accuracy of the inverse Laplace transform. Limited evaluation of the method's accuracy was conducted by *Crump* [9] and *De Hoog et al.* (1982). While direct evaluation of this error is not done here, the accuracy

of the method may be evaluated by comparing the homogeneous solution (i.e. when inhomogeneity is identical in properties to the background) with the *Theis* (1935) solution, as presented in Figure D-7. Again, the high accuracy of the LT-AEM solution is notable.

Summary

A Laplace transform analytic element method (LT-AEM) was described and illustrated for the solution of transient flow problems in porous media. The solution is entirely general, retaining the mathematical elegance (in the Laplace domain) and computational efficiency of the AEM while being amenable to parallel computation. It is especially well suited for problems in which a solution is required at a limited number of points in space-time, and for problems involving materials with sharply contrasting hydraulic properties. We have illustrated the LT-AEM on transient flow through a uniform confined aquifer with circular inclusion of contrasting hydraulic conductivity and specific storage. Our results compare well with published analytical solutions in the special case of radial flow. A remaining challenge is to derive analytical expressions for additional two- and three-dimensional elements such as line sinks, doublets, dipoles and polygons or other shapes satisfying the modified Helmholtz equation that arises from LT-AEM. A first step in this direction may be the development of expressions for line sinks following the approach of *Bakker and Strack* (2003) in the framework of steady state flow in semi-confined and multiaquifer systems.

Acknowledgments

We thank Mark Bakker, Henk M. Haitjema and Willem J. Zaadnoordijk for their assistance in our background research for this paper. We also thank the four anonymous reviewers for their insightful comments, which contributed significantly to the quality of this paper.

Appendix

Sternberg (1969) presents a solution for a fully penetrating well of finite radius r_w, pumping at a constant rate Q at the center of a circular inclusion of radius r_0, in an infinite confined aquifer. Inside the inclusion

$$[\text{A-1}] \quad h(r,t) = \frac{-Q\sqrt{2t\alpha_1}}{2\pi r_w T_0}\left[\frac{\mathrm{I}_0(d)+\mathrm{I}_1(c)\mathrm{K}_0(d)/\mathrm{K}_1(c)}{A\cdot\mathrm{K}_1(c)+\mathrm{I}_1(c)} - \frac{\mathrm{K}_0(d)}{\mathrm{K}_1(c)}\right]$$

and outside of it

$$[\text{A-2}] \quad h(r,t) = \frac{-Q\sqrt{2t\alpha_1}}{2\pi r_w T_0}\left[\frac{\mathrm{I}_0(a)+\mathrm{I}_1(c)\mathrm{K}_0(a)/\mathrm{K}_1(c)}{A\cdot\mathrm{K}_1(c)+\mathrm{I}_1(d)} - \frac{\mathrm{K}_0(d)}{\mathrm{K}_1(c)}\right]\frac{\mathrm{K}_0(e)}{\mathrm{K}_0(b)}$$

where the coefficients

$$[\text{A-3}] \quad a = \sqrt{r_0^2/2t\alpha_1}$$

$$[\text{A-4}] \quad b = \sqrt{r_0^2/2t\alpha_0}$$

$$[\text{A-5}] \quad c = \sqrt{r_w^2/2t\alpha_1}$$

[A-6] $$d = \sqrt{r^2/2t\alpha_1}$$

[A-7] $$e = \sqrt{r^2/2t\alpha_0}$$

[A-8] $$A = \frac{\theta \mathrm{K}_0(b)\mathrm{I}_1(a) + \mathrm{K}_1(b)\mathrm{I}_0(a)}{\mathrm{K}_0(a)\mathrm{K}_1(b) + \theta \mathrm{K}_1(a)\mathrm{K}_0(b)}$$

[A-9] $$\theta = \frac{K_1}{K_0}\sqrt{\frac{\alpha_1}{\alpha_0}}$$

References

Abramowitz, M., I.A. Stegun (editors), 1964. Handbook of mathematical functions, *National Bureau of Standards*.

Bakker, M., 2003. Transient analytic elements for periodic Dupuit-Forchheimer flow, submitted for publication in to *Advances in Water Resources*.

Bakker, M., A.I. Anderson, T.N. Olsthoorn, O.D.L. Strack, 1999. Regional groundwater modeling of the Yucca mountains site using analytic elements, *J. of Hydrology*, 226 (3-4): 167-178.

Bakker, M., V. Kelson, W.J. Zaadnoordijk, 2002. The TIM project, http://www.engr.uga.edu/~mbakker/tim.html, accessed Dec. 2002.

Bakker, M., O.D.L. Strack, 2003. Analytic elements for multi aquifer flow, *J. of Hydrology*, 271: 119-129.

Barnes, R., I. Janković, 1999. Two-dimensional flow through large number of circular inhomogeneities, *J. of Hydrology*, 226: 204-210.

Bateman, H., 1954. Tables of integral transforms, Volume 1, *McGraw-Hill.*

Carslaw, H.S., J.C. Jaeger, 1959. Conduction of heat in solids, second edition, *Clarendon Press, Oxford.*

Crump, K.S., 1976. Numerical inversion of Laplace transforms using a Fourier series approximation, *J. of the Association for Computing Machinery*, 23(1): 89-96.

De Glee, G.J., 1930. Over groundwaterstromingeen bij wateronttrekking door middel van putten. Thesis. J. Waltmena, *Delft* (The Neterlands), 175 pp.

De Hoog, F. R., J. H. Knight, and A. N. Stokes, 1982. An improved method for numerical inversion of Laplace transforms. *S.I.A.M. J. Scientific and Statistical Computation*, 3: 357-366.

De Lange, W.J., O.D.L. Strack. 1999. Introductory comments, *J. of Hydrology*, 226 (3-4): 127.

Furman, A., A.W. Warrick, T.P.A. Ferré, 2002. Electrical Potential Distributions in Response to Applied Current in a Heterogeneous Subsurface: Solution for Circular Inclusions, *Vadose Zone Journal*, 1: 273-280.

Gradshteyn, I.S., I.M. Ryzhik, 2000. Table of integrals, series, and products, Sixth edition, *Academic Press*.

Haitjema, H.M., 1995. Analytic element modeling of groundwater flow. *Academic Press*.

Haitjema, H.M., O.D.L. Strack, 1985. An initial study of thermal energy storage in unconfined aquifers, Final report to *Battelle Pacific-Northwest laboratory*.

Hollenbeck, K.J., 1998. INVLAP.M: A matlab function for numerical inversion of Laplace transforms by the De Hoog algorithm, available at http://www.isva.dtu.dk/staff/karl/invlap.htm, accessed Dec. 2002.

Jacob, C.E., 1946. Radial flow in a leaky artesian aquifer, *Transactions, American Geophysical Union*, 27(11): 198-205.

Janković, I., 2002. http://www.civil.buffalo.edu/Faculty/jankovic.html, accessed Dec. 2002.

Janković, I., R. Barnes, 1999. Three-dimensional flow through large number of spheroidal inhomogeneities, *J. of Hydrology*, 226: 224-233.

Janković, I., R. Barnes, 2000. Analytic-based Solution for Three-dimensional Transient Groundwater Flow Near Partially Penetrating Wells Under Unconfined Conditions, *2000 AGU Fall Meeting, San Francisco, CA*.

Janković, I., R.J. Barnes, R. Soule, 2001. Local Modelling of Groundwater Flow Using Analytic Element Method Three-dimensional Transient Unconfined Groundwater Flow With Partially Penetrating Wells and Ellipsoidal Inhomogeneities, *2001 AGU Fall Meeting, San Francisco, CA*.

Matlab, 2002. Version 6.1 user manual, *The Mathworks*.

Moon, P., D.E. Spencer, 1961. Field theory handbook, *Springer-Verlag*.

Schapery, R.A., 1961. Approximate method of transform inversion for viscoelastic stress analysis. *Proceedings of the fourth U.S. National Congress of Applied Mathematics*, pp. 1075-1085.

Strack, O.D.L., 1989. Groundwater mechanics. *Prentice-Hall*.

Strack, O.D.L., 2003. Theory and applications of the analytic element method, Review of *Geophysics*, 41(2), doi:10.1029/2002RG000111.

Sternberg, Y.M., 1969. Flow to wells in the presence of radial discontinuities, *Groundwater*, 7: 17-20.

Theis, C.V., 1935. The relation between the lowering of the piezometric surface and the rate and duration of discharge of a well using groundwater storage, *Transactions, American Geophysical Union*, 2: 519-524.

Warrick, A.W., J.H. Knight, 2002. Two-dimensional unsaturated flow through circular inclusion, *Water Resources Research*, 38(7), DOI 10.1029/2001WR001041.

Zaadnoordijk, W.J., 1988. Analytic elements for transient groundwater flow. PhD thesis, *University of Minnesota.*

Zaadnoordijk, W.J., 1998. Transition from Theis wells to steady Thiem wells. *Hydrological Sciences J.*, 43(6): 859-873.

Zaadnoordijk, W.J., O.D.L. Strack, 1993. Area sinks in the analytic element method for transient groundwater flow. *Water Resources Research*, 29(12): 4121-4129.